

DISCLAIMER

This report was prepared as an account of work sponsored by an agency of the United States Government. Neither the United States Government nor any agency thereof, nor any of their employees, makes any warranty, express or implied, or assumes any legal liability or responsibility for the accuracy, completeness, or usefulness of any information, apparatus, product, or process disclosed, or represents that its use would not infringe privately owned rights. Reference herein to any specific commercial product, process, or service by trade name, trademark, manufacturer, or otherwise does not necessarily constitute or imply its endorsement, recommendation, or favoring by the United States Government or any agency thereof. The views and opinions of authors expressed herein do not necessarily state or reflect those of the United States Government or any agency thereof.

UCLA/PPG--1171

TI88 017301

PISCES and ALT II: Jülich PSI Papers

UCLA-PPG-1171

August, 1988

Contributors

UCLA, Institute of Plasma Fusion and Research:

R. W. Conn, Y. Hirooka, B. LaBombard, R. Moyer, D. M. Goebel, W. K. Leung, R. E. Nygren, W. J. Corbett, R. Lehmer, Y. Ra, G. Tynan,

Association EURATOM-KFA, FRG:

K. H. Dippel, K. H. Finken, A. Hardtke, W. Kohlhaas, G. Wolf, the TEXTOR Team

Association EURATOM-Belgian State, Brussels, Belgium: the ICRH Team
P. Vandenplas, M. Messian, G. Van Oost R. Weynants,

Associazione EURATOM, Frascati, Italy: E. Franconi

Nagoya University, Nagoya, Japan: A. Miyahara, A. Sagara

Sandia National Laboratories, Albuquerque, NM:

W. B. Gauster, J. A. Koski, R. T. McGrath, J. G. Watkins

Sandia National Laboratories, Livermore, CA:

M. E. Malinowski,

MASTER



OFFICE OF THE DIRECTOR
INSTITUTE OF PLASMA AND FUSION RESEARCH
405 HILGARD AVENUE
LOS ANGELES, CALIFORNIA 90024-1600

(213) 825-4544

August 8, 1988

Dear Colleague:

This publication comprises papers from the PISCES and Alt-II Programs at UCLA which were presented at the International Plasma Surface Interactions Meeting held in Jülich, FRG on May 2-6, 1988. In response to requests for further information, we have prepared this compilation which includes the PSI papers, abstracts of a few other recent papers which provide greater breadth and depth, and a list of publications from the PISCES and Alt-II.

The meeting provided an opportunity to present several papers that represent current directions in our experimental programs. The considerable interest shown in our work on materials plasma edge physics was gratifying to us.

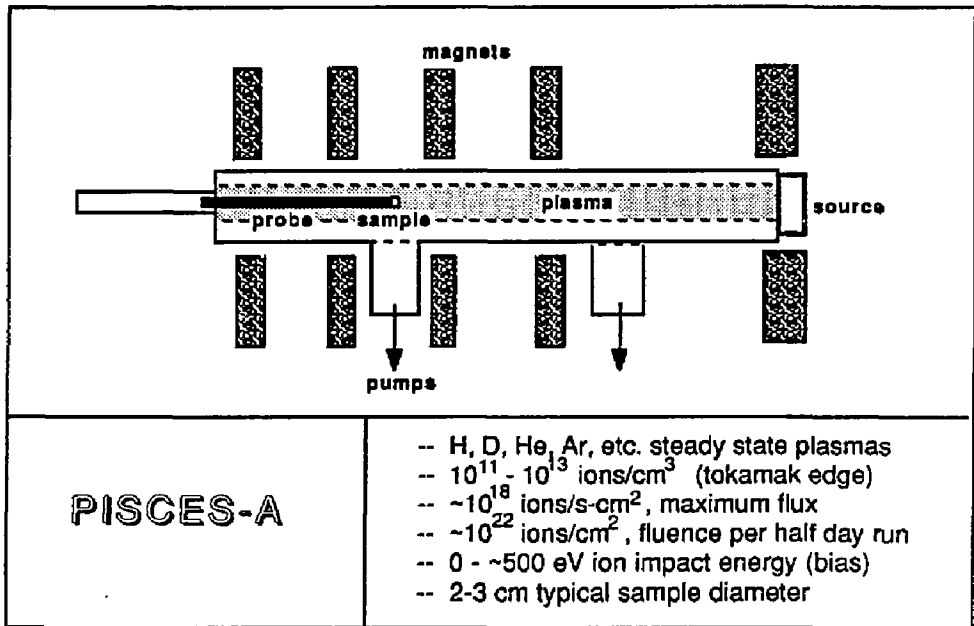
Sincerely,

A handwritten signature in cursive script that reads "Bob Conn".

Robert W. Conn

PISCES FACILITY -- UCLA

The PISCES research laboratory at UCLA is devoted to work on plasma edge physics, materials behavior and plasma-materials interactions in fusion devices. The laboratory's first plasma device, PISCES-A, has operated since 1984. A second device, PISCES-B, will begin operation in 1988. Each device has the capability to generate continuous plasma covering the range, $n = 10^{11}$ - 10^{13} cm⁻³, $T_e = 3$ -30 eV and heat fluxes on samples up to 100-200 W/cm². These plasma conditions are similar to the plasma at the edge of a large tokamak.



For more information about the PISCES Program, please contact:

Prof. Robert W. Conn (213) 825-1613
University of California, Los Angeles
6291 Boelter Hall
Los Angeles, California 90024-1597

PISCES -- Top View

1 meter

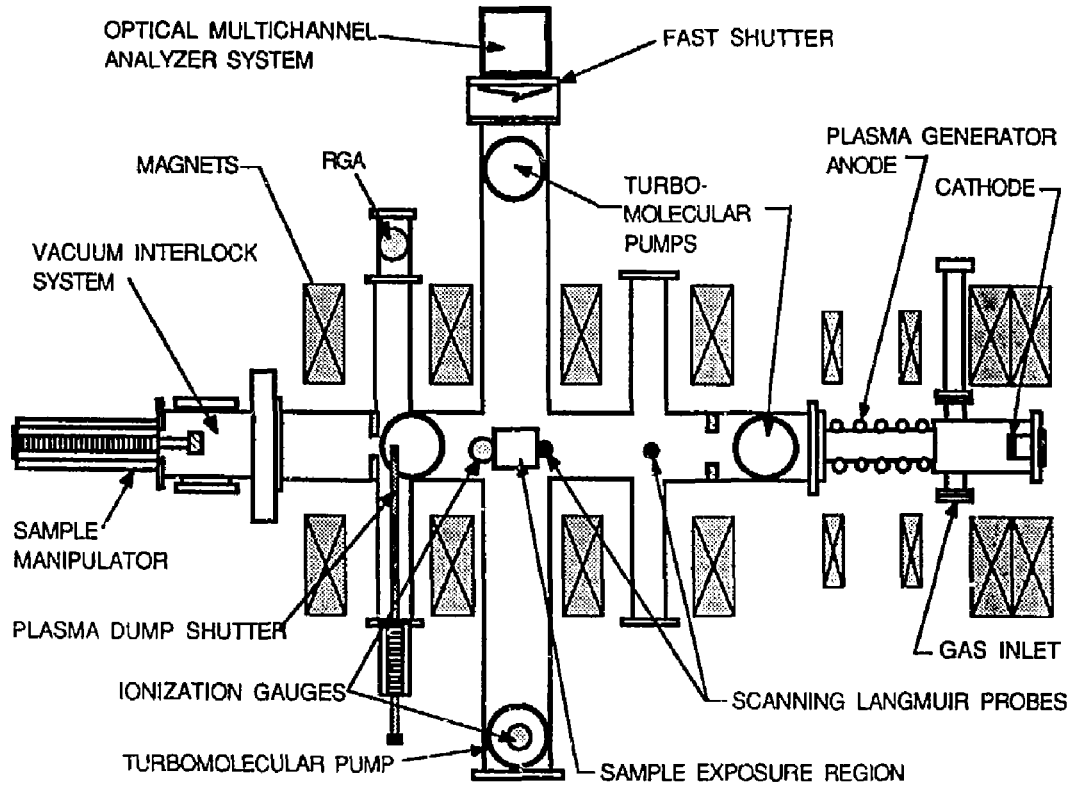


TABLE OF CONTENTS

1. "Deuterium pumping and erosion behavior of selected graphite materials under high flux plasma bombardment in PISCES"
Y. Hirooka, R.W. Conn, D.M. Goebel, B. LaBombard, R. Lehmer, W.K. Leung, R.E. Nygren, Y. Ra
2. "Erosion and redeposition behavior of selected NET-candidate materials under high-flux hydrogen, deuterium plasma bombardment in PISCES"
E. Franconi, Y. Hirooka, R.W. Conn, W.K. Leung, B. LaBombard, R.E. Nygren
3. "Presheath profiles in simulated tokamak edge plasmas"
B. LaBombard, R.W. Conn, Y. Hirooka, R. Lehmer, W.K. Leung, R.E. Nygren, Y. Ra, G. Tynan
4. "Boundary asymmetries and plasma flow to the ALT-II toroidal belt pump limiter"
W.J. Corbett, D.M. Goebel, R.W. Conn, R.T. McGrath, K.H. Dippel, K.H. Finken
5. "ALT-II toroidal belt pump limiter performance in TEXTOR"
D.M. Goebel, R.W. Conn, W.J. Corbet, K.H. Dippel, K.H. Finken, W.B. Gauster, A. Hardtke, J.A. Koski, W. Kohlhaas, R.T. McGrath, M.E. Malinowski, A. Miyahara, R. Moyer, A. Sagara, J.G. Watkins, G. Wolf, the TEXTOR Team, and the ICRH Team
6. "An in-situ spectroscopic erosion yield measurement with applications to sputtering and surface morphology alterations"
W.K. Leung, Y. Hirooka, R.W. Conn, D.M. Goebel, B. LaBombard, R.E. Nygren
7. Abstracts
8. Publication List

Deuterium Pumping and Erosion Behavior of Selected Graphite Materials
under High Flux Plasma Bombardment in PISCES

Y.Hirooka, R.W.Conn, D.M.Goebel, B.LaBombard,
R.Lehmer, W.K.Leung, R.E.Nygren, Y.Ra

Institute of Plasma and Fusion Research
Department of Mechanical, Aerospace and Nuclear Engineering
University of California, Los Angeles
Los Angeles, CA 90024, USA

ABSTRACT

Deuterium plasma recycling and chemical erosion behavior of selected graphite materials have been investigated using the PISCES-A facility. These materials include: Pyro-graphite; 2D-graphite weave; 4D-graphite weave; and POCO-graphite. Deuterium plasma bombardment conditions are: fluxes around 7×10^{17} ions $s^{-1}cm^{-2}$; exposure time in the range from 10 to 100 s; bombarding energy of 300 eV; and graphite temperatures between 20 and 120°C. To reduce deuterium plasma recycling, several approaches have been investigated. Erosion due to high-fluence helium plasma conditioning significantly increases the surface porosity of POCO-graphite and 4D-graphite weave whereas little changes for 2D-graphite weave and Pyro-graphite. The increased pore openings and refreshed in-pore surface sites are found to reduce the deuterium plasma recycling and chemical erosion rates at transient stages. The steady state recycling rates for these graphite materials can be also correlated to the surface porosity. Surface topographical modification by machined-grooves noticeably reduces the steady state deuterium recycling rate and the impurity emission from the surface. These surface topography effects are attributed to co-deposition of reemitted deuterium, chemically sputtered hydrocarbon and physically sputtered carbon under deuterium plasma bombardment. The co-deposited film is found to have a characteristic surface morphology with dendritic microstructures.

1. INTRODUCTION

Recycling of hydrogen isotopes from plasma-facing components in a magnetic fusion device is widely recognized as a crucial issue affecting the fueling scenario and the on-site tritium inventory. Particularly, wall pumping effects to reduce fuel particle recycling by graphite components such as a limiter and divertor plate have been recently observed in major tokamaks: TFTR [1]; JET [2]; DIII-D [3]; and TEXTOR [4] and have generated considerable interest. Except for the case of JET, the surface conditioning of these plasma-facing components plays a crucial role in obtaining the wall pumping effect.

In our previous work [5], the helium or argon plasma-activation processes (He, Ar-PAP) were established as new surface conditioning techniques for low-density, isotropic graphite materials. The activated graphite surface showed a sponge-like morphology with significantly increased open pores and a large surface gas adsorption capacity. Using activated graphite, the first non-tokamak wall pumping experiments were conducted for a short plasma exposure duration of 20s to simulate fusion devices operating in the short pulse mode. The increased surface porosity and gas adsorptivity due to He-PAP were found to enhance retention of hydrogen plasma particles and hence provided a significant plasma pumping effect at temperatures between 20 and 480°C.

Here, one must notice that these wall pumping effects are observed only up to the point when the plasma-facing surface becomes saturated with fuel particles. These saturable pumping effect thus will not contribute significantly to the control of the particle balance in future long-pulse fusion devices such as TIBER [6]. For possible applications in the future devices, reinforced graphite materials such as C-C composites are currently under development. Yet little is understood about the hydrogen recycling behavior of these new materials.

In the present work, several possibilities to reduce particle recycling both at the transient stages and at the steady state have been investigated using the PISCES-A facility [7]: (1) helium plasma conditioning to increase surface porosity; and (2) surface topographical modification to induce particle retrapping. Used for this purpose are selected graphite materials including: Pyro-graphite (Pfizer); 2D-graphite weave (BF-Goodrich); 4D- graphite weave (FMI); and POCO-graphite (grade: HPD-1).

2. EXPERIMENTAL

After ultrasonic cleaning in acetone, a disk target of graphite with a diameter of 4.5 cm and with a thickness of 6 mm was placed in steady-state helium and deuterium plasmas in the PISCES-A facility. The plasma diameter was set around 6 cm. The temperature of the graphite target during plasma exposure was measured both by a thermocouple and an infra-red pyrometer. The plasma density and the electron temperature were measured using a Langmuir probe positioned in front of the target. A 1.3m monochromator with an optical multi-channel analyzer (OMA) was aligned in such a way that plasma radiations (e.g. D-alpha) could be monitored, particularly near the specimen surface. Details of the PISCES-A facility and materials experiments in this facility can be found elsewhere [7,8].

The graphite target was first activated in a helium plasma at temperatures around 800°C (He-PAP) and was then exposed to a deuterium plasma for recycling measurements with calibrated D-alpha spectroscopy. The deuterium plasma exposure time was varied from 10 to 100 s. Simultaneously with recycling measurements, chemical erosion behavior due to deuterium plasma bombardment was monitored using a differentially pumped residual gas analyzer (RGA).

Plasma bombardment conditions are generally: flux in the range from 5×10^{17} to 1×10^{18} ions $s^{-1} cm^{-2}$; bombarding energies of 100 and 300 eV for helium and deuterium plasmas, respectively; plasma density of the order of $10^{11} cm^{-3}$; electron temperature in the range from 5 to 15 eV; and neutral pressure of the order of 10^{-5} - 10^{-4} torr. Here, the bombarding energy is controlled by applying a negative DC-bias to the target in addition to the floating potential because the intrinsic ion energy in the PISCES plasma is about a few electron volts. The magnetic field is perpendicular to the target surface and is about 800 gauss. Under these conditions, the ion gyro-radii are 2 to 3 mm. The thickness of the sheath region is around 10 μm . Therefore, ions accelerated by the total sheath potential (floating potential plus negative bias) will strike on the surface at the approximately normal incidence.

During plasma bombardment, important experimental parameters: ion saturation current from the Langmuir probe (i.e. plasma bombardment flux to the target surface); D-alpha intensity; signals from RGA; and target temperature were monitored at sampling rates of 1-10 Hz. To avoid complicated effects associated with redeposition, the plasma parameters were controlled to generate conditions in the erosion regime [8] for both physically sputtered carbon and chemically sputtered hydrocarbons (e.g. CD_4).

4. RESULTS AND DISCUSSION

4-1. Basic considerations

In the present work, the deuterium recycling behavior is analyzed using calibrated D-alpha spectroscopy. The plasma density is below 10^{13} cm^{-3} , the brightness of D-alpha light, B , is related to plasma parameters through the relation [9]:

$$B = k n_e n_D \langle \sigma v \rangle \quad (1)$$

where k is the calibration constant, n_e is the plasma density, n_D is the density of atomic deuterium and $\langle \sigma v \rangle$ is the rate coefficient for the reaction: $D + e^- \Rightarrow D^+ + 2e^-$. The rate coefficient is calculated from Lotz's formula [10]. One can evaluate n_D from eq.(1) using the plasma density and electron temperature from Langmuir probe measurements. Also, n_D is considered as an approximate indicator of the density of molecular deuterium reemitted from the surface.

Here, we define the recycling coefficient, R , as

$$R \equiv K n_D / \Gamma_{\text{ion}}, \quad (2)$$

where K is the unit conversion constant to make R dimensionless, and Γ_{ion} is the flux. It is important to mention here that the effects of the start-up machine time constant and/or fluctuations of the flux on the recycling coefficient are cancelled by definition.

4-2. Effects of He-plasma conditioning on the surface morphology

The graphite target was first bombarded with a helium plasma to a fluence of the order of $10^{21} \text{ ions/cm}^2$ at a bombarding energy of 100 eV and at elevated temperatures around 800°C (i.e. He-PAP). The basal plane of Pyro-graphite and the weave plane of 2D-graphite weave were exposed to the helium plasma. The surface morphology after He-PAP was observed with scanning electron microscopy (SEM).

The results of SEM observations are shown in Fig. 1. Sponge-like surface morphologies with significantly increased pore openings are found for POCO-graphite and

4D-graphite weave. (Not shown here are the surface morphologies of these materials before He-PAP: the surface pores are blanked off by machining dusts or weekly bound particles.) One can notice that POCO-graphite exhibits relatively small but high density pores whereas the opposite is true for 4D-graphite weave. The sponge-like surface morphology observed for POCO-graphite is found to be similar to that observed for graphite limiter tiles used in TFTR for a long term (≈ 2 years). In our previous work [5], the surface roughness of POCO-graphite after He-PAP was estimated to be about 345 from molecular adsorption measurements. From the observed surface morphology, one may expect a similar or somewhat smaller surface roughness factor for activated 4D-graphite weave. For Pyro-graphite and 2D-graphite weave, in contrast, no obvious surface pore openings are observed.

4-3. Recycling and erosion behavior of graphite materials

In this series of experiments, a graphite target specimen was mounted on a water-cooled copper manipulator. One can consider this setup as simulation of an actively water-cooled plasma-facing component. The plasma exposure time was about 10s. The activated graphite target was bombarded with a deuterium plasma at a bombarding energy of 300 eV. The flux was set at 7×10^{17} ions $s^{-1} cm^{-2}$. Using the particle reflection coefficient of 0.16 obtained from TRIM code [11], the net incoming flux is calculated to be 6×10^{17} ions $s^{-1} cm^{-2}$. Due to the heat flux of $0.3 MW/m^2$, the target temperature rises up to temperatures around $70^\circ C$, as shown in Fig. 2-a. These conditions are believed to be relevant to those for plasma interactions with graphite bumper limiters in TFTR [12].

Typical results of recycling measurements for 4D-graphite weave are shown in Fig. 2-b and those for other materials are summarized in Table 1. The activated surface has yielded a significantly reduced recycling coefficient, relative to the pre-saturated surface. (The pre-saturated surface is defined as the surface previously subjected to He-PAP followed by high-fluence deuterium plasma bombardment [5].) The recycling curve for the activated surface merges the curve for the pre-saturated surface after about 30 second deuterium plasma exposure. Not shown here is the recycling coefficient from the surface before He-PAP, which is essentially the same as the one for Pyro-graphite but is fluence dependent because of the gradual opening of pores under plasma bombardment. The

recycling coefficient for the pre-saturated surface tends to peak first and then gradually decrease to the steady state level, presumably due to ion-impact desorption. The pre-saturated surface can be easily reactivated by helium plasma bombardment to a fluence of the order of 10^{19} ions/cm².

It is important to mention here that deuterium recycling apparently reaches a steady state after transient stages of pumping even as the surface temperature changes. Generally, retention of hydrogen isotopes in graphite decreases with increasing surface temperature, and significant thermal desorption is often seen to start at temperatures around 250°C [13]. However, the temperature at the end of plasma exposure is still low enough to retain deuterium.

Notice in Table 1 that the recycling coefficients for activated materials at the steady state are found to decrease with increasing surface porosity (see Fig. 1). This clearly indicates that increased surface pore openings and refreshed in-pore surface adsorption sites by He-PAP play an important role in determining the effective deuterium retention capacity. Also, the recycling coefficients for the pre-saturated surfaces remains below unity. This can be attributed to an in-pore storage mechanism that deuterium temporarily resides in pores under plasma bombardment. (Details of the in-pore storage mechanism will be discussed in the next section.) Deuterium, once stored in pores of the pre-saturated surface, may be released after plasma bombardment.

In Fig 2-c, the signal from RGA set for CD₄ is seen to track with the recycling coefficient. Generally, steady state chemical erosion of graphite requires surface saturation with implanted hydrogen isotopes [14]. Consistently, the activated surface with an increased deuterium retention capacity is observed to exhibit significantly retarded erosion behavior to reach the steady state, relative to the pre-saturated surface. It follows that one can avoid hydrocarbon formation by He-PAP in fusion devices having short plasma discharge durations of 2 - 3 sec. A similar result was obtained in our previous work using an in-situ spectroscopic technique [5].

One finds in Table 1 that Pyro-graphite has yielded a higher CD₄ signals than other materials. This may be due either to the fact that the temperature of Pyro-graphite is higher than those for other materials or to the fact that the flat and pore-free surface does not provide any in-pore storage effects. Unfortunately, these possibilities can not be differentiated at present.

4.4. Plasma effects on recycling behavior

From these observations, one postulates that the surface pore openings increase penetration of particles arriving from the plasma and then activated in-pore surface adsorption sites trap these particles after kinematical slowdown due to collisions with the in-pore walls. To understand this process, one must consider the plasma effects: both ions and neutrals are arriving at the surface. Here, deuterium ions are accelerated to the bombarding energy set at 300 eV. The neutrals include molecular deuterium with thermal energies and atomic deuterium with energies ranging a few to 10 eV due to dissociation due to atomic processes (e.g. Frank-Condon process [15]).

Generally, molecular deuterium will not significantly contribute to the surface adsorption process because of its inertness to graphite. Atomic neutrals can be directly transported into pores to an appreciable depth before they come to rest upon adsorption because the particle and energy reflection coefficients maximize at energies around a few electron volts [15]. In contrast, deuterium ions can not directly penetrate deep into pores, as they are, because of the gyration effect (see section 2). However, they will eventually saturate a local area on the in-pore wall and then eject neutral deuterium by ion-impact desorption. Neutral deuterium generated by the ion-impact desorption process generally has energies of a few electron volts and will behave similarly to that transported directly from the plasma. Unfortunately, it is difficult to differentiate these effects individually.

One may extend these arguments to the case when in-pore surface adsorption sites are pre-occupied with deuterium. This case corresponds to the pre-saturated surface. Under deuterium plasma bombardment, atomic deuterium may penetrate even deeper *without being trapped due to adsorption and may not be transported outward unless effective backscattering occurs*. This effect can be seen reproducibly so long as the surface is porous. Untrapped deuterium will be released, presumably as molecules after the plasma bombardment is stopped or when the flux decreases abruptly. The in-pore storage effect seen for the pre-saturated surface is believed to be explained by this mechanism. The in-pore storage mechanism might in part contribute the wall pumping effect observed in JET [2].

Here, it is important to note that deuterium trapped in the in-pore surface space will be replaced easily with other molecules having more stable adsorption characteristics, for example, with water vapor molecules upon air-exposure. From these arguments, thermal desorption experiments after plasma bombardment may not yield consistent spectra.

4-5. Effect of surface grooves on recycling behavior

As seen in section 4-3, POCO-graphite with the sponge-like surface morphology has yielded the lowest steady state recycling coefficient. As an attempt to further reduce the recycling coefficient by particle retrapping, a POCO-graphite target was topographically modified with machined-grooves. The grooved surface was first subjected to He-PAP and then to deuterium plasma bombardment under similar conditions to those described in the previous section. The deuterium plasma exposure time is extended to 100s to ensure the effect of surface grooves. Towards the end of the extended plasma exposure, the surface temperature rises up to about 120°C, as shown in Fig. 3-a. The groove dimensions are roughly: 4.5 mm deep and 1.5 mm apart. Due to these grooves, the geometrical surface area is increased by a factor of 2.5.

The deuterium recycling behavior of the pre-saturated surfaces with and without machined-grooves is shown in Fig. 3-b. Notice that the surface with machined-grooves yields about 20-25% reduction of the recycling coefficient at the steady state. No saturation behavior is observed. In addition, radiation intensities from CD-band at 4311Å and from C-I at 9095Å measured at the steady state were found to be reduced by about 10% and 15%, respectively. At temperatures around 700°C, similar reduction in recycling of deuterium as well as sputter-induced impurities was also seen, but to a lesser degree. These findings indicate that reemitted deuterium, chemically sputtered hydrocarbon and physically sputtered carbon are continuously co-deposited in the groove structure.

In fact, a yellowish film, indicative of hydrogenated carbon [16], is found on the bottom half surface of the groove partitioning walls and on the groove bottom area. This localized film formation indicates that sputter-emitted carbon from the plasma-front part of the groove partitioning wall dominates the burial process of recycling particles in the bottom part. Since the grooved gap distance is comparable with the gyro-radii of plasma particles (see section 2), most of the ions will strike on the groove partitioning wall mainly in the plasma-front part at a bombarding energy of 300 eV. These energetic deuterium ions will hinder the formation of the co-deposited film. This postulation is consistent with the localized formation of the co-deposited film towards the groove bottom.

Shown in Fig. 4 are the surface morphologies of the groove partitioning wall. A similar but somewhat less porous sponge-like morphology is observed in the plasma-front side (see Fig. 4-a) to that observed for the flat graphite surface after He-PAP (see Fig. 1-a). However, the yellowish co-deposited layer exhibits a completely different surface

morphology with no obvious porosity (Fig. 4-b). Also, notice characteristic dendritic growth of dens-packed microstructures. Unfortunately, no data are available for analysis of incorporated deuterium in the co-deposited film to date.

Here, one must bear in mind that the co-deposition effect will lead to an increase of the on-site tritium inventory in fusion devices. In TFTR, a significant amount of deuterium (of the order of 10^{17} - 10^{18} D/cm²) has been recently found in the gap space between graphite tiles (a few milli meters) and has been attributed to a similar co-deposition effect [17]. However, the deuterium concentration decreases exponentially with increasing distance from the plasma-facing side of the tile. The opposite is true in the present observation. The co-deposited surface in TFTR might serve as a substrate for redepositing particles with relatively low energies and hence one sees only the geometry effect on the reach of the particle in-flow. In contrast, the plasma-front side of the partitioning walls of the groove structure used here acts as the sputter target to supply carbon to bury recycling particles by being bombarded with the deuterium plasma at 300 eV. As a result, the localized co-deposition is observed towards the bottom of grooves.

As demonstrated here, the first attempt to reduce particle recycling by the topographical surface modification has been successful. The partitioning wall of the groove structure is found to act in part as a sputter target to supply carbon to bury recycling particles and to serve in part as a substrate of the co-deposited film under deuterium plasma bombardment. Since obviously the burial probability depends on the in-groove residential time of the particle for a given condition, one might attribute the reduction of deuterium recycling to the plasma effects in such a way that low energy neutrals reside longer than bombarding ions (or neutrals after the first few collisions with the partitioning walls). Further improvement of the groove arrangement is possible. Details will be published separately.

5. CONCLUSIONS AND IMPLICATIONS TO RECYCLING IN FUSION DEVICES

Several possibilities have been investigated, intending to reduce particle recycling from selected graphite materials under high-flux deuterium plasma bombardment. The significance of the plasma effects is pointed out as the crucial issue in understanding the particle recycling behavior.

The increased surface pore openings and refreshed adsorption sites by He-PAP are found to enhance retention of deuterium. This effect leads to a significant reduction of particle recycling and chemical erosion under deuterium plasma bombardment. Also, increasing the surface porosity by appropriate materials selection can reduce the steady state recycling rate due to the in-pore storage mechanism. Due to physical and chemical sputtering, high-fluence hydrogen plasma bombardment will naturally provide the sponge-like surface to low-density, isotropic graphite [18]. Thus, one can expect reduced recycling in fusion devices for the plasma-facing components made of isotropic graphite materials, e.g. POCO-graphite in TFTR, CL5890PL in JET, as the confinement and conditioning plasma discharges are repeated.

Non-saturable deuterium plasma pumping as well as reduced emission of sputter-induced impurity have been observed for a machine-grooved surface. This effect is attributed to continuous co-deposition of particles in the groove space. The co-deposited film is found to have a characteristic surface morphology with dendritic microstructures. The concept of topography-induced co-deposition can be applied to the control of fuel particle recycling as well as impurities in fusion devices, via adjustment to edge-plasma parameters and local magnetic field configuration. Yet the effect of continuous co-deposition on the tritium inventory is crucial. Incorporated tritium might be recovered through thermal decomposition of the co-deposited films. Details are still unclear. Further investigation is necessary to clarify this point.

ACKNOWLEDGEMENT

The authors would like to express sincere gratitude to R.A.Causey, B.L.Doyle, A.Pospieszczyk, W.R.Wampler and K.L.Wilson for illuminating discussions. Special thanks go to K.Andrews, J.Elverum and T.Sketchley for technical support. This work is supported by the Office of Fusion Energy, US Department of Energy under contract #DE-AT03-84ER52104.

REFERENCES

- [1] K.W.Hill, V.Arunasalm, M.G.Bell et.al., Proc.IAEA 11th Int.Conf.on Plasma Physics and Controlled Fusion Research, Kyoto, p. 207 (1986).
- [2] S.A.Cohen, J.Ehrenberg, T.T.C.Jones et.al., 'Particle balance and wall pumping in tokamaks', JET Rep. JET-P(87)39.
- [3] G.L.Jackson, T.E.Evance, M.Ali Mardavi et.al., APS Fall Meeting, San Diego, (1987).
- [4] D.M.Goebel, R.W.Conn, W.J.Corbett et.al., These proceedings.
- [5] Y.Hirooka, W.K.Leung, R.W.Conn et.al., J.Vac.Sci. & Technol.-A (in press).
- [6] TIBER-team, J.D.Lee (ed.), 'TIBER-II/ETR Final Design Report', Vols. II & III, LLNL Rep. #UCID-21150 (1987).
- [7] D.M.Goebel, G.A.Campbell and R.W.Conn, J.Nucl.Mater. 111&112(1984) 457.
- [8] Y.Hirooka, D.M.Goebel, R.W.Conn et.al., J.Nucl.Mater. 141-143(1986)193.
- [9] E.S.Marmar, J.Nucl.Mater. 76&77(1978)59.
- [10] W.Lotz, Zeitschrift fur Physik 216(1968)241.
- [11] J.P.Biersack and L.G.Haggmark, Nucl.Instr.& Meth. 121(1980)257.
- [12] D.B.Heifetz, M.I.Baskes, H.F.Dylla and M.Ulrickson, J.Nucl.Mater. 145-147(1987)326.
- [13] K.L.Wilson and W.L.Hsu, J.Nucl.Mater. 145-147(1987)121.
- [14] C.M.Braganza, S.K.Erents and G.M.McCracken, J.Nucl.Mater.75(1978)220.
- [15] D.E.Post and R.Behrisch (ed.), 'Physics of Plasma-Wall Interactions in Controlled Fusion', NATO ASI-series vol. 131, Plenum Press (1986).
- [16] For example, H.Tsai and D.B.Bogy, J.Vac.Sci.& Technol.-A 5(1987)3287.
- [17] W.R.Wampler, B.L.Doyle, S.Lee et.al., J.Vac.Sci.& Technol.-A (in press) Paper presented at 34th AVS National Symposium (1987).
- [18] D.M.Goebel, Y.Hirooka, R.W.Conn et.al., J.Nucl.Mater. 145-147(1987)61.

Table 1 Summary of recycling coefficients and methane yields at the steady state*.

Material	Recycling coefficient*	CD ₄ signal**	Temperature(°C)
<u>POCO-graphite</u>			
Pre-saturated	0.75(0.85***)	0.69	65
Activated	0.72	0.65	60
<u>4D-graphite weave</u>			
Pre-saturated	0.85(1.0***)	0.64	69
Activated	0.8	0.65	65
<u>2D-graphite weave</u>			
Pre-saturated	0.96(1.0***)	0.65	72
Activated	0.94	0.62	65
<u>Pyro-graphite</u>			
Pre-saturated	1.0(1.0***)	0.72	81
Activated	1.0	0.70	87

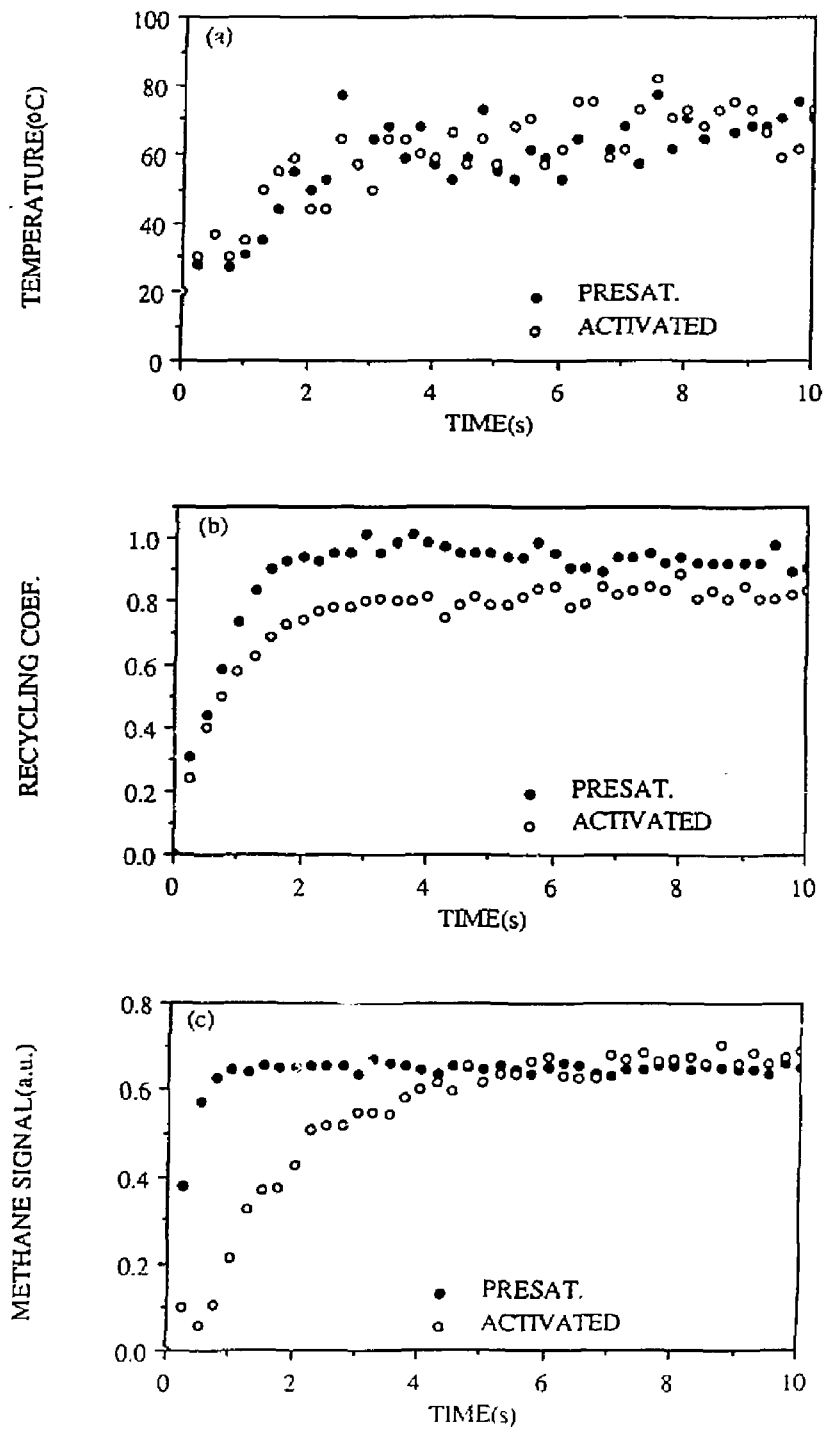
* The recycling coefficient is taken at $t = 10s$ and normalized to that for Pyro-graphite as a pore-free reference material (see Fig. 1).

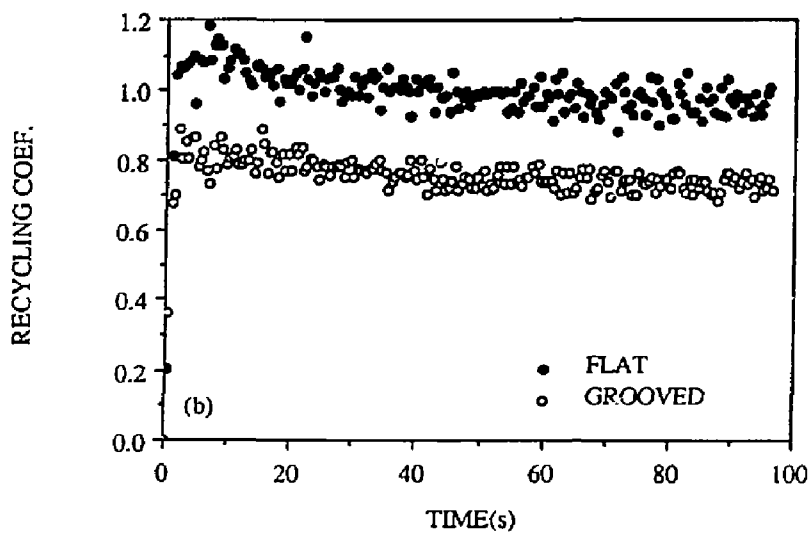
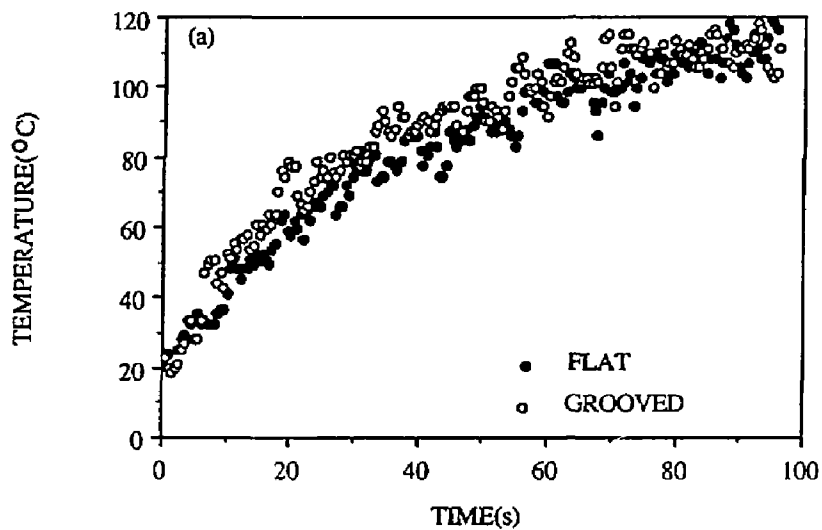
** The signal intensity for CD₄ is normalized to that at 600°C (not reported here).

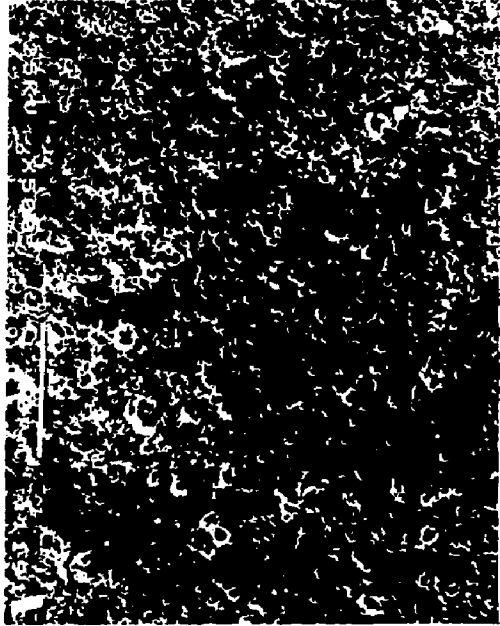
*** The recycling coefficient peak due to ion-impact desorption (see text).

FIGURE CAPTIONS

- FIG. 1; Surface morphologies of graphite materials after He-PAP: (a) POCO-graphite; (b) 4D-graphite weave; (c) 2D-graphite weave; and (d) Pyro-graphite. Notice that the surface porosity decreases in order: POCO-graphite, 4D-graphite weave, 2D graphite weave, and Pyro-graphite.
- FIG. 2; Typical data from recycling and erosion measurements for plasma-activated and pre-saturated 4D-graphite weave: (a) temperature; (b) recycling coefficient; and (c) methane signal from RGA, each as a function of time. The recycling coefficients shown here are normalized to the steady state value for Pyro-graphite as a pore-free reference material (see Fig. 1).
- FIG. 3; Deuterium recycling behavior of the pre-saturated POCO-graphite targets with a flat surface and with the grooved surface: (a) temperature; and (b) recycling coefficient, each as a function of time. The recycling coefficients shown here are normalized to the steady state value observed for the flat surface.
- FIG. 4; Surface morphologies of the partitioning wall (a) the plasma-front side with no obvious co-deposited films; and (b) the groove bottom side with the co-deposited film. This particular target was subjected to deuterium plasma bombardment to a fluence of the order of 10^{21} ions/cm² at 300 eV.



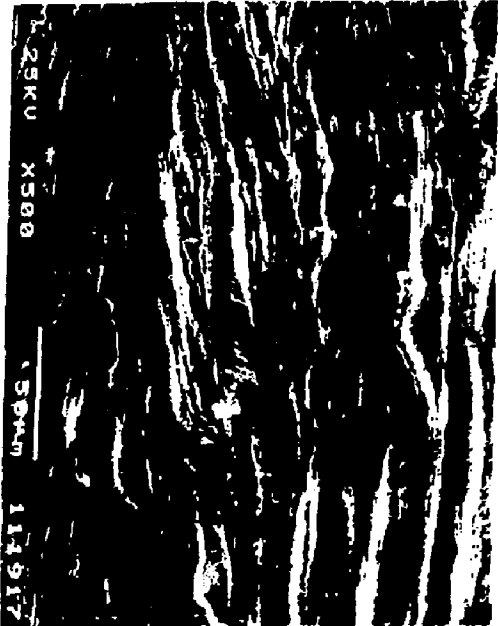




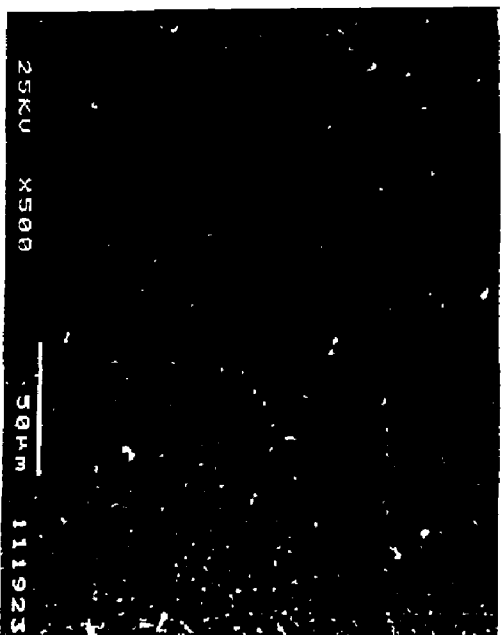
(a)



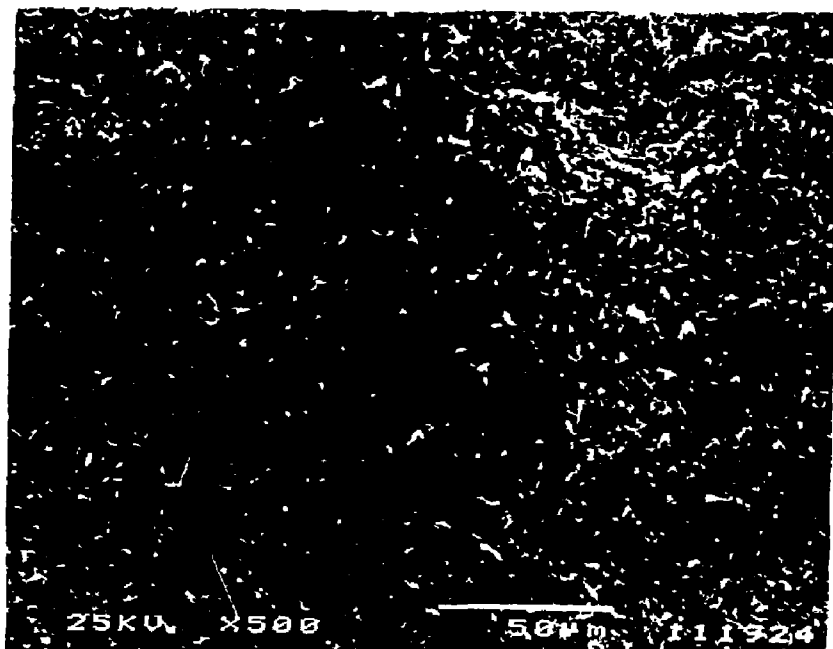
(b)



(c)



(d)



(a)



(b)

**PRESHEATH PROFILES IN SIMULATED
TOKAMAK EDGE PLASMAS**

**B. LaBombard, R.W. Conn, Y. Hirooka, R. Lehmer,
W.K. Leung, R.E. Nygren, Y.Ra., G. Tynan**

UCLA-PPG-1147

April, 1988

**Department of Mechanical, Aerospace and Nuclear Engineering
Institute of Plasma and Fusion Research
University of California, Los Angeles, CA, 90024, U.S.A.**

PRESHEATH PROFILES IN SIMULATED TOKAMAK EDGE PLASMAS

B. LABOMBARD, R.W. CONN, Y. HIROOKA, R. LEHMER,
W.K. LEUNG, R.E. NYGREN, Y. RA, G. TYNAN

Institute of Plasma and Fusion Research
Department of Mechanical, Aerospace and Nuclear Engineering
University of California, Los Angeles
Los Angeles, CA 90024, USA

The PISCES plasma surface interaction facility at UCLA generates plasmas with characteristics similar to those found in the edge plasmas of tokamaks ($n = 10^{11}$ - 10^{13} cm⁻³, $T_e = 3$ - 30 eV). Steady state magnetized plasmas produced by this device are used to study plasma-wall interaction phenomena which are relevant to tokamak devices. We report here progress on some detailed investigations of the presheath region that extends from a wall surface into these "simulated tokamak" edge plasma discharges along magnetic field lines.

A number of edge plasma diagnostics have been specially developed for this work and are now becoming fully operational including a fast-scanning multiple Langmuir/Emissive/Mach probe system and a CID camera imaging system. Both systems allow detailed diagnoses of a $10 \times 10 \times 10$ cm³ region of magnetized plasma in contact with a wall surface. Measurements of plasma density, electron temperature, floating potential, space potential, and bulk plasma flow velocities have been obtained in hydrogen, helium, and argon plasmas with densities ranging from 10^{12} to 10^{13} cm⁻³, electron temperatures from 5 to 15 eV, and axial magnetic fields of 0.2 to 1.4 kG. Plasma density profiles along the magnetic field typically show a characteristic factor of 2 decrease towards the wall surface. A plasma potential variation in the near presheath zone of order $0.5 \times T_e$ is measured, consistent the bulk plasma flow approaching the ion sound speed near the wall surface as inferred from a simple "free fall" model. A Boltzmann model for the presheath density profile accurately tracks the density profile measured both by the Mach probe and by spectroscopic means. Flow profiles are used as a consistency check on various magnetized Mach probe theories. Results suggest that cross-field transport of parallel momentum through ion viscosity is relatively unimportant in PISCES discharges. In discharges that have a non-thermal "hot" electron component with a number density of a few percent or more of the "colder" bulk electrons, axial profiles of space potential and floating potential indicate that the overall electron distribution function at the wall surface is "hotter". This is found to be consistent with an "energy filtering" model in which a fraction of the colder, bulk electrons is reflected by the presheath potential drop while the "hotter" electrons are able to reach the sheath edge near the wall surface.

1. Introduction

The presheath zone is loosely defined as the quasineutral plasma region extending from the sheath near a wall surface into the bulk plasma. In a magnetic field, the presheath zone extends large distances along magnetic field lines and is populated by plasma through cross-field transport and/or ionization processes. Thus, an entire tokamak scrape-off layer can be considered as a large magnetized presheath plasma zone. Electric fields within the presheath are responsible for accelerating the ion species from rest within the bulk plasma to sound speed velocities at the sheath edge thereby satisfying the Bohm criterion.

A detailed understanding of presheath physics is important not only for assessing the overall impact of plasma/wall interactions on a tokamak discharge but also in diagnosing the tokamak edge plasma itself. Local wall erosion/redeposition rates depend critically on the presheath electric fields and plasma flows which can sweep ionized impurities back onto wall surfaces. The interpretation of data collected by an electric probe in such a flowing plasma relies on an accurate model of not only the plasma presheath zone in which it is immersed but also the small presheath zone that is induced by the probe surface itself.

The PISCES plasma surface interaction facility at UCLA [1,2] provides a means for studying tokamak-like edge plasma-wall interaction phenomena from both the materials and plasma physics points. We report in this paper on the progress of some basic plasma physics experiments in PISCES aimed at diagnosing in detail a magnetized presheath region of a "simulated tokamak" plasma-wall interaction zone. The goals of these experiments are threefold: 1) to characterize the presheath zone, providing a more accurate interpretation of plasma-wall interaction experiments, 2) to assemble an experimental data base to enable a test of various theoretical plasma physics models of the presheath zone in "tokamak-like" plasmas, and 3) to test the interpretation of electric probe diagnostics in a flowing plasma. This paper focuses primarily on progress made in achieving the first goal. Work towards the latter two goals is ongoing and will be reported in future publications [3].

2. Experimental Arrangement

The PISCES facility produces plasma by a PIG discharge using a hot LaB_6 cathode disc. Details of the plasma source operation and construction can be found in the references [1,2,4]. The disc cathode and cylindrical anode are placed at one end of a vacuum chamber which is coaxial with a series of magnetic field coils at Helmholtz spacing. The axial magnetic field provides radial

plasma confinement and maps from a hot cathode disc onto an electrically floating end plate (fig. 1). Electrons emitted from the hot LaB_6 disk are accelerated by the cathode-plasma sheath drop and injected along magnetic field lines with energies in the range of 60 to 150 eV. The sheath at the electrically floating end plate reflects most of the electrons back to the cathode and allows these particles to efficiently ionize the background fill gas (5×10^{-5} to 5×10^{-3} torr) even though their mean free path can be much longer than the column length. Steady-state plasmas with densities in the range of 10^{11} to 10^{13} cm^{-3} and electron temperatures of 3 to 30 eV are readily achieved in a 6 to 10 cm diameter cylindrical column of approximately 100 cm in length. Similar to a tokamak edge plasma, these plasmas exhibit fully "turbulent" dynamics, namely, broadband fluctuation spectra and cross-field particle diffusion coefficients that are characteristic of the Bohm level. In the standard operation, material samples are immersed in the plasma column for testing through a modified end plate, as shown in fig. 1.

The arrangement for the presheath plasma profile measurements reported here is also shown in fig. 1. A test sample is inserted into the plasma and allowed to electrically "float", drawing no net current from the plasma. A zone of plasma of approximately $10 \times 10 \times 10$ cm^3 in front of the material test sample is investigated by three principal diagnostics: a fast-scanning pneumatically driven probe; a stationary water-cooled Langmuir probe; and a solid state CID (charge injected device) camera. Since the Debye length is typically much less than 100 μm , these three diagnostics record conditions in the quasineutral presheath plasma zone in front of the material sample.

A fast-scanning probe system capable of employing a wide variety of electrical probe techniques and geometries has been specially built to diagnose PISCES plasmas [5]. A pneumatic cylinder is used to drive a single or multiple probe tip across the plasma column and back (15 cm stroke) in less than 400 msec. This enables a vertical profile to be taken in one "shot" and at the same time limits the total energy deposited on the probe to safe levels during the high density plasmas that can be achieved in PISCES (power fluxes > 400 W/cm^2). A differentially-pumped sliding seal allows the probe to be positioned for a fast vertical scan at various axial distances from the sample surface. By vertically scanning the plasma column through its centerline at uniformly spaced axial locations, a complete map of plasma parameters in the near presheath of the material sample can be assembled.

A unique probe tip that functions simultaneously as a two-sided Langmuir probe (or "Mach probe") and as an emissive probe was constructed for these and other experiments in PISCES. The probe tip simply consists of a 4.8 mm diameter 4-hole extruded alumina rod with a specially sculptured end (fig. 2). Two 1mm diameter molybdenum wires of approximately 2.5 mm of exposed length collect particles on opposing sides of an alumina separator. The 45° angle on the

alumina allows the probe to be operated as a unidirectional probe or as a bidirectional probe, depending on its orientation with respect to the magnetic field. For the presheath measurements reported here, the probe was operated as a bidirectional or "Mach probe" with the "up-stream" probe facing towards the LaB_6 cathode along magnetic field lines and the "down-stream" probe facing the material test sample. Both probes were continuously biased in ion saturation at -140 volts. Ion saturation current data were numerically smoothed over a 10 msec time window to reduce "noise" due to density fluctuations (typically $\delta n/n = 0.3$ to 0.5).

A 0.25 mm diameter 1% thoriated tungsten wire loop was inserted into the remaining two holes of the alumina and employed as a thermionic electron emitter. Typically, the tungsten filament was preheated by an AC current for approximately 0.5 sec before the probe initiated its fast vertical scan. The filament was maintained in a mode of strong electron emission ($T > 2000$ °C) throughout the inward travel of the probe. Power was turned off to the filament on the return stroke and the entire probe assembly was allowed to cool between scans. The "floating" voltage of the filament was recorded and interpreted as the local plasma potential in the case when the filament strongly emitted electrons and as the usual plasma floating potential in the case when the filament was turned off during a scan. A stationary, water-cooled Langmuir probe could also be inserted into the plasma stream and was typically used to cross-check data from the fast-scanning probe or to record a complete Langmuir characteristic at a fixed spatial position.

An image intensified CID camera was used during these experiments to record line-integrated brightness profiles of $\text{H}\alpha$ (6563 Å) emission as well as to record a picture of the experimental arrangement on video tape for later reference (fig.1). Since the mean free paths of both atomic and molecular hydrogen in PISCES plasmas are typically much larger than the plasma radius, a relatively uniform hydrogen neutral density can be maintained within the diagnosed presheath region. In non-hydrogen discharges this was accomplished by "bleeding in" trace amounts of hydrogen into the feed gas. Under these conditions, the variation in $\text{H}\alpha$ emissivity along a given magnetic field line was expected to track the local electron density variation in the presheath as long as the electron temperature was constant.

In order to obtain the local $\text{H}\alpha$ emissivity as a function of both plasma radius and distance along magnetic field lines, video images were digitized and an Abel inversion was performed on the cylindrically symmetric brightness data. Profiles of $\text{H}\alpha$ emissivity were then compared to density profiles measured independently by the fast-scanning probe. This was used as a cross-check on the probe data to assure that the insertion of the probe did not significantly perturb the presheath plasma profiles.

3. Results

3.1 Presheath Density and Potential Profiles

Fig. 3 shows a typical mapping of plasma density and potential in the presheath plasma zone from a series of fast probe scans. These data were obtained in a helium discharge with the following parameters: helium fill pressure (measured near the material sample) $P_{\text{He}} = 4 \times 10^{-3}$ torr, electron temperature on axis $T_e = 12$ eV, and axial magnetic field $B = 1.4$ kG. The mapping was obtained by scanning the fast probe twice in the vertical (x) direction at each of 22 regularly spaced positions in the horizontal (z) direction. The two vertical scans at each horizontal position allowed the emissive probe to alternately record floating potential profiles as a cold filament and plasma potential profiles as a hot, strongly emitting filament. The Mach probe was operated in ion saturation mode for all scans.

The density reported in fig. 3(a) was estimated by simply averaging the ion saturation currents collected on the up-stream and down-stream facing probes and assuming that the electron temperature had a spatially uniform value of 12 eV. This technique effectively treats the two probes as one larger probe. The electron temperature was measured by momentarily inserting a water-cooled Langmuir probe at an axial position of $z = 4$ cm. Since the vertical electron temperature profile is not unfolded from the data in fig. 3, the density variation in the vertical direction should not be taken as completely accurate. However, in this discharge the electron temperature is found to be very nearly constant along the magnetic field. Consequently, the relative variation in density along the z axis in fig. 3(a) is reliable. Note that there is nearly a factor of two drop in the density over an 8 cm distance along the magnetic field lines that intercept the material sample.

Plasma potential contours shown in fig. 3(b) were deduced from the potential acquired by the hot tungsten filament. At filament temperatures near 2000°C , the thermionic electron flux can approach and exceed the random electron flux in the plasma. Under these conditions, the potential of the filament tends to "float" to a value that is close to the local plasma potential. Power to the filament was adjusted so as to achieve this condition of strong electron emission by incrementally increasing the AC voltage on the filament until the potential profile recorded by the probe no longer changed.

Fig. 3(b) shows that vertical plasma potential profiles exhibit a minimum on the central axis of the plasma column ($x=0$). The steepest gradients in potential occur in the vertical direction. Radial electric fields on the order of 12 volts/cm are estimated from this potential variation. In the axial direction, there is evidence of a weaker potential variation along field lines intercepted by the material sample. This is the presheath electric field induced by the presence of the material sample.

A potential variation on the axis of approximately 6 volts occurs over a distance of 8 cm, consistent with the expected order of magnitude for the presheath potential variation of $0.5xT_e$.

Due to the anode/cathode geometry which is used to form the PISCES plasma (see fig. 1), a strong radial electric field is always present. The radial electric field in PISCES plasmas appears to adjust itself for a given axial magnetic field so as to maintain azimuthal $E \times B$ rotation speeds that are from 0.1 to 1.0 times the ion sound speed. Such strong azimuthal rotation velocities are believed to contribute to the plasma turbulence and Bohm-like cross-field transport fluxes observed in PISCES. However, this azimuthal velocity profile also complicates the interpretation of any Langmuir probe measurements which are not made on the central axis of rotation. Indeed, the vertical density asymmetry shown in fig. 3(a) can be simply attributed to a data interpretation problem stemming from the effect of the azimuthal $E \times B$ rotation. In these plasmas the $E \times B$ azimuthal flow was directed into the top half of fig. 3(a) and out the bottom half. Referring to fig. 2, one can see that the "sculptured" probe tip was orientated in such a way as to face into this flow during the upper half of its vertical scan and away from the flow during the bottom half of its scan. As a result, a relatively higher ion saturation flux could be collected while the probe was in the upper half of the scan. The true vertical density profile is therefore better represented by an average of the upper and lower half values of fig. 3(a). In any event, the remainder of this paper focuses on axial profiles along $x=0$ where the effect of this $E \times B$ rotation on data interpretation is expected to be minimal.

Ion saturation currents recorded on the up-stream facing probe were found to typically exceed those recorded on the down-stream facing probe by a factor of two or more, suggesting the presence of a strong parallel plasma flow directed towards the material sample. Even with the Mach probe rotated 180° with respect to the magnetic field, the same ratio of up-stream facing to down-stream facing flux was obtained indicating that this ratio was not simply due to a difference in probe collection areas. Nevertheless, rather than attempt to account for a parallel plasma flow in computing the local density, an equivalent "no flow" plasma density is computed from standard planar probe theory. In this way, the data could be displayed independent of the errors that might be introduced by trying to model the effect of the flow.

"Densities" deduced from the flux on the up-stream facing probe, the flux on the down-stream facing probe, and an average of these two fluxes, assuming no plasma flow, are plotted versus axial position in fig. 4. Also plotted in fig. 4 are an $H\alpha$ emissivity profile inferred from the CID camera, and a plasma density profile inferred from a Boltzmann law, $n(x) = n_0 \exp\{(\Phi(x) - \Phi_0)/T_e\}$, using the measured values of the plasma potential and electron temperature. Since the latter two profiles do not yield an absolute value for the plasma density, they are both normalized to the "average" density profile obtained from the Mach probe at an axial position of 8 cm. Helium

plasma conditions for this data set were: $P_{He} = 2 \times 10^{-3}$ torr, $T_e = 8$ eV, and $B = 0.8$ kG. A hydrogen partial pressure of $P_{H_2} = 4 \times 10^{-5}$ torr was added in order to allow H_{α} profiles to be recorded in this plasma.

A number of important points are illustrated in fig. 4. Since the emissive probe measures the plasma potential by effectively cancelling the net random electron flux to the probe, bulk plasma flow velocities on the order of the ion sound speed should not influence this measurement. Consequently, the density profile inferred from the Boltzmann law can be taken as the true presheath plasma density variation. The "average" density from the Mach probe fits the Boltzmann density profile very well, somewhat justifying the ad hoc technique of averaging the up-stream and down-stream ion saturation currents. Normalization of the Boltzmann density profile to the up-stream "density" or down-stream "density" profiles do not yield such a good fit.

The H_{α} emissivity profile also tracks the "average" density from the Mach probe. Again, normalization of the H_{α} emissivity profile to the up-stream "density" or down-stream "density" profiles only yields a poorer fit. The H_{α} emissivity profile was recorded without any probes inserted into the plasma. Thus, it indicates that the presheath plasma density profiles are not significantly perturbed by the insertion of the fast probe.

Finally, these experiments point out that caution should be exercised in deducing the local plasma density from a directional Langmuir probe in the presence of a plasma flow. Without information from the down-stream facing probe, one could easily overestimate plasma densities by 50% or more, by incorrectly assuming that the plasma flow speed is zero.

3.2 Presheath Plasma Flows

A number of models have been considered in an attempt to predict plasma flow velocities from magnetized Mach probe measurements [6-9]. In these models, the plasma flow velocity along magnetic field lines, expressed in Mach number (M), is related to the ratio (R) of plasma flux collected on the up-stream facing probe over the flux collected on the down-stream facing probe. This functional relationship, $M = f(R)$, varies significantly from model to model and depends on the physics that is emphasized in each.

Fig. 5 shows Mach number profiles computed from three different models considered by Stangeby [7], Harbour and Proudfoot [6], and Hutchinson [8], using the probe data that was shown in fig. 4. Positive Mach numbers refer to parallel plasma flow velocities directed towards the material sample. Also shown in fig.5 are Mach numbers based on a "free fall" velocity of ions

accelerated by the presheath potential drop. These "free fall" profiles were derived from the simple conservation of energy formula,

$$M(x) = \sqrt{M_0^2 + \frac{2(\Phi_0 - \Phi(x))}{T_e}} \quad (1)$$

using the measured values for the presheath potential profile. The initial velocities for each "free fall", M_0 , were chosen to coincide with the velocities predicted from each of the three models at $z = 8$ cm.

Although eq. (1) is not rigorously correct, it predicts the maximum change in plasma flow velocity for a given potential drop within the presheath region (assuming ion pressure effects are negligible). Effects such as ionization, charge exchange, cross-field particle transport, and viscosity only serve to reduce this flow speed by effectively adding drag. Fig. 5 shows that, independent of the initial velocity of the flow at $z = 8$ cm, the "free fall" Mach number approaches 1 near the material sample surface. This is consistent with the Bohm criterion which requires that the flow be greater than or equal to Mach 1 at the wall surface. It also justifies the use of a "free fall" model to approximate the plasma flow profile since the introduction of any appreciable drag effects would not allow the flow to achieve Mach 1 at the wall.

A Mach number profile deduced from the measured flux ratio, R , and the Stangeby model [7] compares most favorably with the "free fall" velocity profile. The Harbour and Proudfoot [6] and Hutchinson [8] models predict much lower flow speeds everywhere and seem to suffer from the rather severe problem of not achieving a Mach 1 flow near the material sample surface. This is particularly true of the Hutchinson model and may indicate that cross-field parallel momentum transfer due to ion viscosity is relatively unimportant in these discharges [9]. In fact, one expects that the "correct" model should predict Mach numbers greater than 1 at the wall surface using the measured flux data. As the Mach probe gets very close to the wall, the flux tube from which the down-stream facing probe collects particles becomes cut-off by the wall. As a result, less flux should be collected by this probe near the wall surface and hence erroneously large flux ratios recorded there. Mach numbers deduced from these overestimated flux ratios near the wall surface should therefore be higher than actual Mach numbers. Nevertheless, only the Stangeby model is found to exhibit this trend, estimating Mach numbers greater than 1 at the wall.

To be consistent in the analysis of Mach probe data, one needs to account for the local flow velocity in determining the local plasma density. Fig. 6 plots the density profile data displayed in fig. 4, corrected for the plasma flows inferred from each of the three models. All three models

predict lower plasma densities near the material sample than is inferred from the Boltzmann law. However, this may simply be a consequence of the down-stream facing probe collecting less particles as its flux tube becomes interrupted by the sample surface. Since the density profile is found to be predicted equally well by all three models, no further information about the applicability of these models for the analysis of PISCES plasmas is obtained.

3.3 Non-Maxwellian Electron Effects

The power input to PISCES discharges originates from "primary electrons" injected from the hot LaB₆ cathode. Under the some conditions, the plasma-cathode sheath potential drop can be as high as 150 volts. If at the same time the plasma density is low, thermalization of these high energy electrons becomes poor and the electron distribution function displays a non-thermal high energy component. From analysis of Langmuir probe characteristics, it is found that these non-thermal electron distribution functions can be accurately described by a two temperature distribution model. The "cold" or bulk component of the electrons typically makes up 90% or more of the electron population while the "hot" component, with an equivalent temperature in the range of 30 to 60 eV, makes up the balance of the electron population.

One consequence of a two temperature electron distribution function in PISCES is that the presheath density profile is coupled to the potential profile through a modified Boltzmann law,

$$n(x) = n_0^{\text{cold}} \exp\{(\Phi(x) - \Phi_0)/T_e^{\text{cold}}\} + n_0^{\text{hot}} \exp\{(\Phi(x) - \Phi_0)/T_e^{\text{hot}}\} \quad (2)$$

The effect of a presheath potential drop of 0.5 to 0.7 times the bulk or "cold" electron temperature is to reduce the density of the cold electron component near the wall to approximately half its value far from the wall surface. On the other hand, the hot component is relatively unaffected by the potential change and maintains a nearly constant density up to the sheath edge at the wall surface. Thus, even in these non-Maxwellian discharges, analysis of density profiles using an isothermal Boltzmann law (section 3.1) is still approximately valid. However, the effective temperature of the electrons near the wall surface can be "hotter" than the electrons farther upstream.

Data plotted in fig. 7 shows evidence of a "hotter" electron population near the material sample surface. These data were obtained from the same discharge that was displayed in fig. 3. Langmuir probe characteristics taken at $z = 4$ cm indicated a "hot" electron density fraction of approximately 10% of the bulk with an effective temperature of 30 eV ("cold" component

temperature was 12 eV). Two potential profiles from the emissive probe are plotted in fig. 7, one when the filament was cold and one when the filament was hot and strongly emitting electrons. The potential of the cold filament can be simply interpreted as the plasma "floating potential" while the potential of the hot filament is expected to approximate the local plasma space potential. In a plasma with Maxwellian electrons at temperature T_e and cold ions ($T_i \ll T_e$), the space potential (Φ) and floating potential (V_f) are simply related by

$$T_e = \alpha (\Phi - V_f) \quad (3)$$

where α takes into account the ratio of ion sound speed to electron thermal speed as well as secondary electron emission effects (also geometry effects when the ion Larmor radius is larger than the probe wire diameter as in the case of the emissive probe). For illustration, an electron temperature profile deduced from eq. (3) is also plotted in fig.7. In order to avoid choosing a value for α , the profile is normalized to the electron temperature ("cold" component) inferred by the Langmuir probe at $z = 4$ cm. This figure clearly shows that the electron population near the material surface is more energetic, causing a depression in the local floating potential relative to the space potential. Of course under these circumstances, T_e is not properly deduced from eq. (3) and one must work with the actual local distribution function to determine its energy content.

4. Discussion

Throughout the analysis in this paper two critical assumptions have been made about the operation of the fast scanning Mach probe, namely, 1) that the probe was large compared to the ion Larmor radius so that a planar probe theory could be applied and 2) that the perturbation length of the probe was short relative to the presheath scale length in the experiment.

Since the magnetic field strength is relatively low in PISCES, it is recognized that the validity of the first assumption can become marginal even at low ion temperatures. As a result, helium discharges were chosen over hydrogen discharges so as to avoid molecular dissociation processes which can input energy to the ions. From doppler broadening measurements of He^{II} emission, He^+ ions are estimated to have temperatures between 0.5 and 1.2 eV over a wide variety of discharge parameters [10] (uncorrected for any additional broadening effects due to viewing a rotating plasma). He^+ is expected to be the dominant ion species since the rate of He^{++} formation from He^+ is almost two orders of magnitude lower than the rate of He^+ formation from He^0 for

the plasma and neutral conditions in PISCES. At a magnetic field of 0.6 kG, 0.5 eV He⁺ ions have Larmor radii that are comparable to the Mach probe radius. For this reason, data shown in figs. 3 and 7 were taken in 1.4 kG discharges while the remaining figures show data taken in 0.8 kG discharges. The presheath profiles recorded by the Mach probe were found to be nearly identical for both magnetic field strengths. The only notable difference between runs in 0.8 kG and 1.4 kG was that the current ratio (R) recorded nearest to the material sample was higher for the latter case. This suggests that the perturbation length of the Mach probe can become long enough to interfere with the material sample.

Assuming a Bohm cross-field diffusion rate, the characteristic perturbation length of the Mach probe along the magnetic field ($L \approx a^2 Cs / D$) is estimated to be approximately 1 cm for 0.8 kG and 2 cm for 1.4 kG B-fields. In this respect, the data taken at 0.8 kG is more reliable. A 1 cm perturbation length implies that the data shown in figs. 4-6 are the result of "averaging" plasma parameters over a 1 to 2 cm axial extent. Since the presheath extends well beyond 8 cm and has a fairly linear profile, the effect of this spatial "averaging" should not impact the overall results obtained by the Mach probe. However, at distances of less than 2 cm away from the material sample surface, one expects that Mach probe data should record a profile that departs from the expected trend. Such a departure near the surface is suggested by the data in fig. 5 (Stangeby model predicting Mach # > 1) and fig. 6.

5. Summary

A number of edge plasma diagnostics have been developed to perform some basic plasma physics experiments in the PISCES facility associated with the formation of a magnetized presheath region near a wall surface. Presheath density, potential, and flow profiles have been deduced under a variety of plasma conditions. Some key observations that have been made from these experiments thus far include:

(1) Density profiles are found to exhibit a characteristic factor of 2 decrease along magnetic field lines that intercept a wall surface, consistent with the generally accepted model for the presheath zone.

(2) Plasma potential variations of order $0.5 \times T_e$ are detected in the near presheath region, consistent with density profiles inferred from a Boltzmann law and cross-checked with both "Mach probe" measurements and H α emissivity profiles.

(3) Plasma flow velocities inferred from "free fall" acceleration of ions using the measured potential profiles are checked against models which predict flow velocities from Mach probe data.

In all cases the "free fall" model yields flow velocities consistent with a Mach 1 boundary condition at the wall surface. However, Mach probe models differ in their predictions of the flow speed. The Stangeby model [7] is found to best fit presheath flow profiles in PISCES plasmas, suggesting that viscosity effects do not play a dominant role [9].

(4) Presheath profiles with a non-Maxwellian electron population are investigated. Low energy electrons are reflected by the presheath potential drop leading to the detection of a "hotter" electron population at the sheath edge near the wall surface.

Acknowledgements

The authors gratefully acknowledge the invaluable contributions from the PISCES technical staff, especially T. Sketchley, G. Gunner, and J. Elverum for assistance in hardware and electronics, and K. Andrews and K. Sheedy for computer and data acquisition systems support. Special thanks are extended to K. Chung for both his stimulating discussions and his assistance in evaluating Mach numbers and densities from the various Mach probe models. This work is supported by the U.S. Department of Energy Contract No. DE-FG03-86ER52134.

References

- [1] D.M. Goebel, D.M., G.A. Campbell, G., R.W. Conn, J. Nucl. Mater. **121** (1984) 277.
- [2] D.M. Goebel, and R.W. Conn, J. Nucl. Mater. **128 & 129** (1984) 249.
- [3] Partly in collaboration with I. Hutchinson, B. Lipschultz, and K. Chung at the Massachusetts Institute of Technology, Cambridge Massachusetts, USA.
- [4] D. M. Goebel, Y. Hirooka, and T.A. Sketchley, Rev. Sci. Instr. **56** (1985) 1717.
- [5] B. LaBombard, R.W. Conn, R. Lehmer, W.K. Leung, Bull. Amer. Phys. Soc. **32** (1987) 1941.
- [6] Average of the particle and fluid models considered by P.J. Harbour and G. Proudfoot in analyzing Mach probe data from DITE. See G. Proudfoot, P.J. Harbour, J. Allen, A.

Lewis, J. Nucl. Mater. **128 & 129** (1984) 180 and P.J. Harbour, G. Proudfoot, J. Nucl. Mater. **121** (1984) 222.

- [7] P.C. Stangeby, Phys. Fluids **27** (1984) 2699.
- [8] I.H. Hutchinson, Phys. Fluids **30** (1987) 3777.
- [9] I.H. Hutchinson, preprint; to be published in Phys. Rev. A.
- [10] A. Pospieszczyk, private communication.

Figure Captions

- Fig. 1 - Experimental arrangement for presheath experiments in the PISCES Plasma Surface Interaction Facility. A PIG discharge is maintained between a hot LaB_6 cathode and a cylindrical anode. 10 cm diameter cylindrical plasmas of 100 cm length are confined radially by a 0.2 - 1.4 kG axial magnetic field and guided onto a material test sample. A $10 \times 10 \times 10 \text{ cm}^3$ zone of plasma in contact with the material sample is investigated in detail by three diagnostics: a fast-scanning probe, a fixed Langmuir probe, and a CID camera.
- Fig. 2 - Detail view of fast-scanning probe tip. The probe functions as a two-sided or Mach probe as well as an emissive probe. 1 mm diameter molybdenum wires collect particles on opposing sides of 4-hole alumina insulator. A loop of thoriated tungsten projects beyond the molybdenum wires, collecting plasma from both directions along the B-field. The loop is resistively heated into strong electron emission over a 1 to 2 sec pulse. The probe tip is pneumatically driven across the plasma in 400 msec.
- Fig. 3 - Contour plots of density and potential from the fast-scanning probe. Density profiles exhibit almost a factor of 2 decrease upon approaching the material sample surface along magnetic field lines. The vertical (x) density asymmetry is interpreted as an "artifact" due to a strong azimuthal $E \times B$ rotation. The potential profile exhibits large radial E-fields and records a near presheath potential variation of approximately $0.5 \times T_e$ along the central axis.
- Fig. 4 - A comparison of density profiles along the central axis from three diagnostics. Three density profiles are inferred from the Mach probe assuming no plasma flow: density from the up-stream facing probe, density from the down-stream facing probe, and an average of these. For comparison, a density profile was computed from the Boltzmann law using the measured potential profile and electron temperature. This profile is shown, normalized to the average density from the Mach probe at $z=8 \text{ cm}$. A density profile inferred from the local $H\alpha$ emissivity is also plotted with a similar normalization. The consistency in these profiles lends confidence to the experiment and shows the the probe did not perturb the plasma profiles in which it measured. The magnitude of density error bars are suggested by the scatter in these data.

Fig. 5 - Comparison of Mach number profiles deduced from three models. The ratio of up-stream facing flux to down-stream facing flux was used to compute parallel flow speeds from three Mach probe models. For comparison, the "free fall" velocity of ions accelerated by the presheath potential variation is also plotted. The initial velocity of this "free fall" is chosen to coincide with each of the three models at $z=8$ cm. The Stangeby model [7] is found to fit the velocity profile data best and suggests that viscosity does not play a significant role in these discharges [9].

Fig. 6 - Density profiles computed from three Mach probe models, including a correction for plasma flow. For comparison, density profiles computed from a Boltzmann law are overlaid. These profiles are normalized at $z=8$ cm. All models predict a lower density at the material sample surface than predicted by the Boltzmann law. This may be a consequence of the Mach probe's flux tube interfering with the material surface.

Fig. 7 - Plasma potential and floating potential profiles showing non-Maxwellian electron effects. Local electron temperatures computed from the difference in space and floating potentials indicates a "hotter" electron population near the material sample surface in some discharges. The "cold" electron population is reflected by the presheath potential drop while the "hot" population is able to reach the sheath edge at the sample surface.

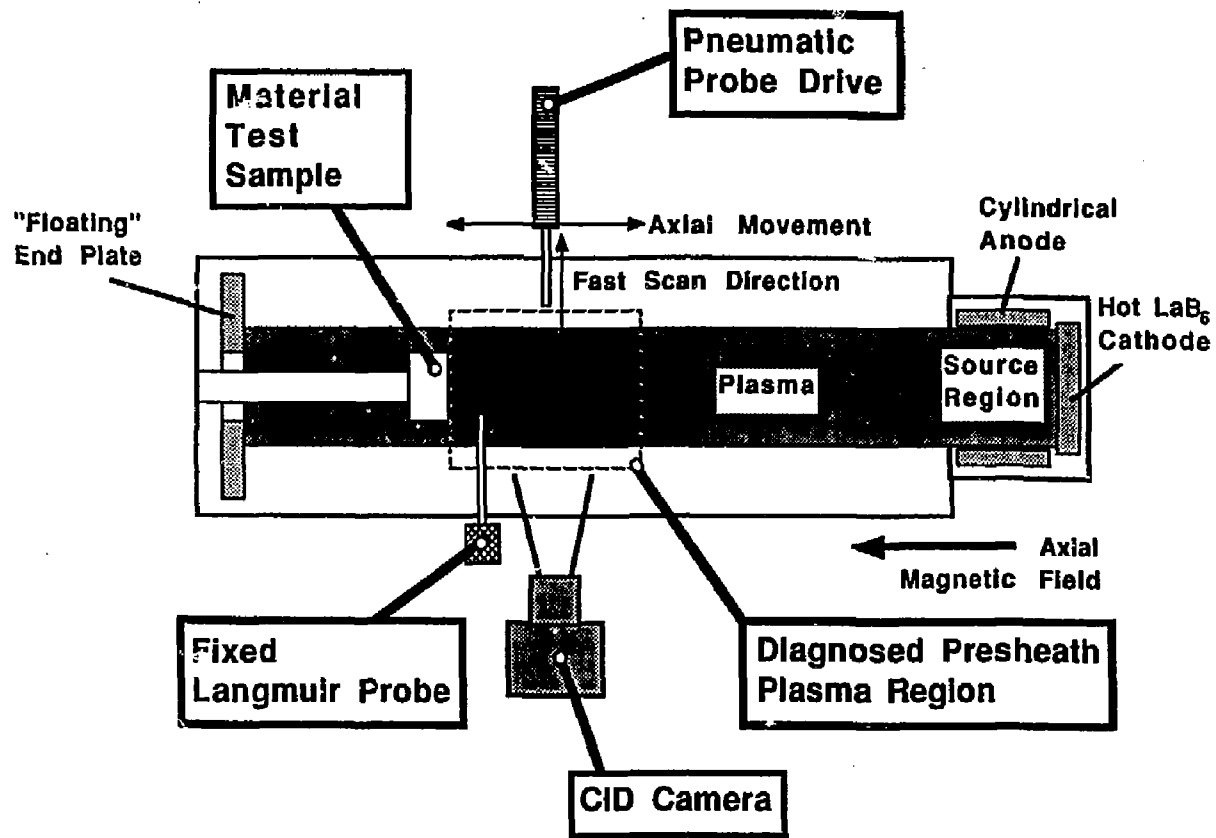


FIGURE 1

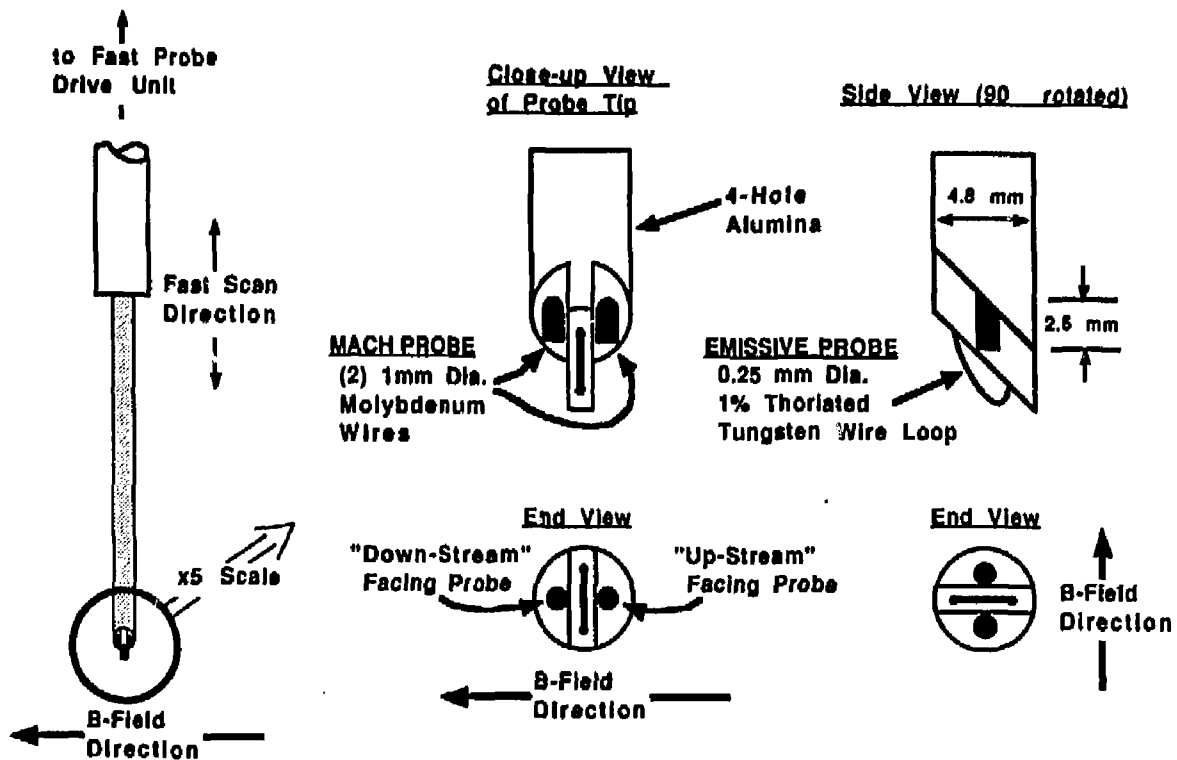
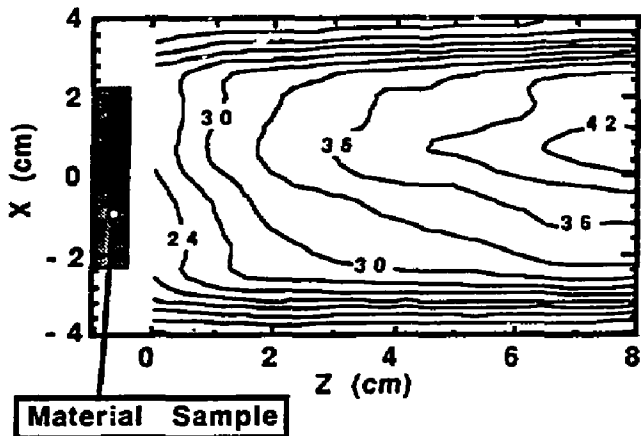


FIGURE 2

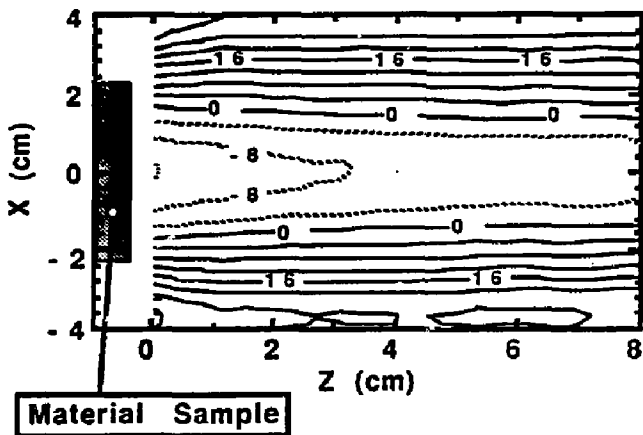
a) **Density Contours**
($3 \times 10^{11} \text{ cm}^{-3}$ per contour)

Maximum = $4.4 \times 10^{12} \text{ cm}^{-3}$



b) **Plasma Potential Contours**
(4 volts per contour)

Maximum = 33 volts Minimum = -12 volts



← Magnetic Field →

FIGURE 3

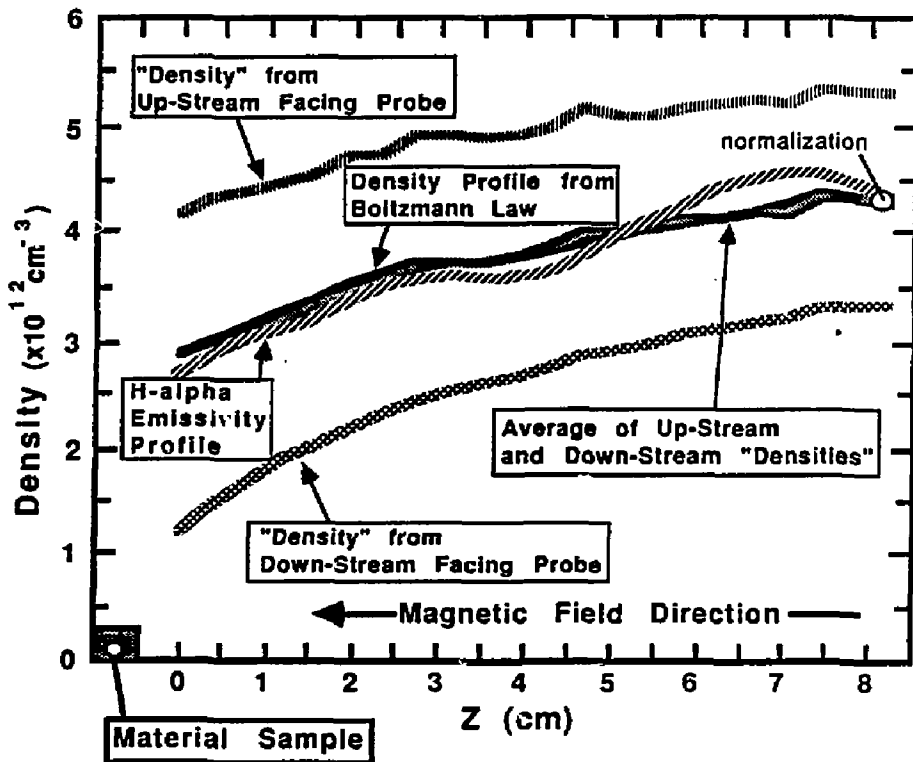


FIGURE 4

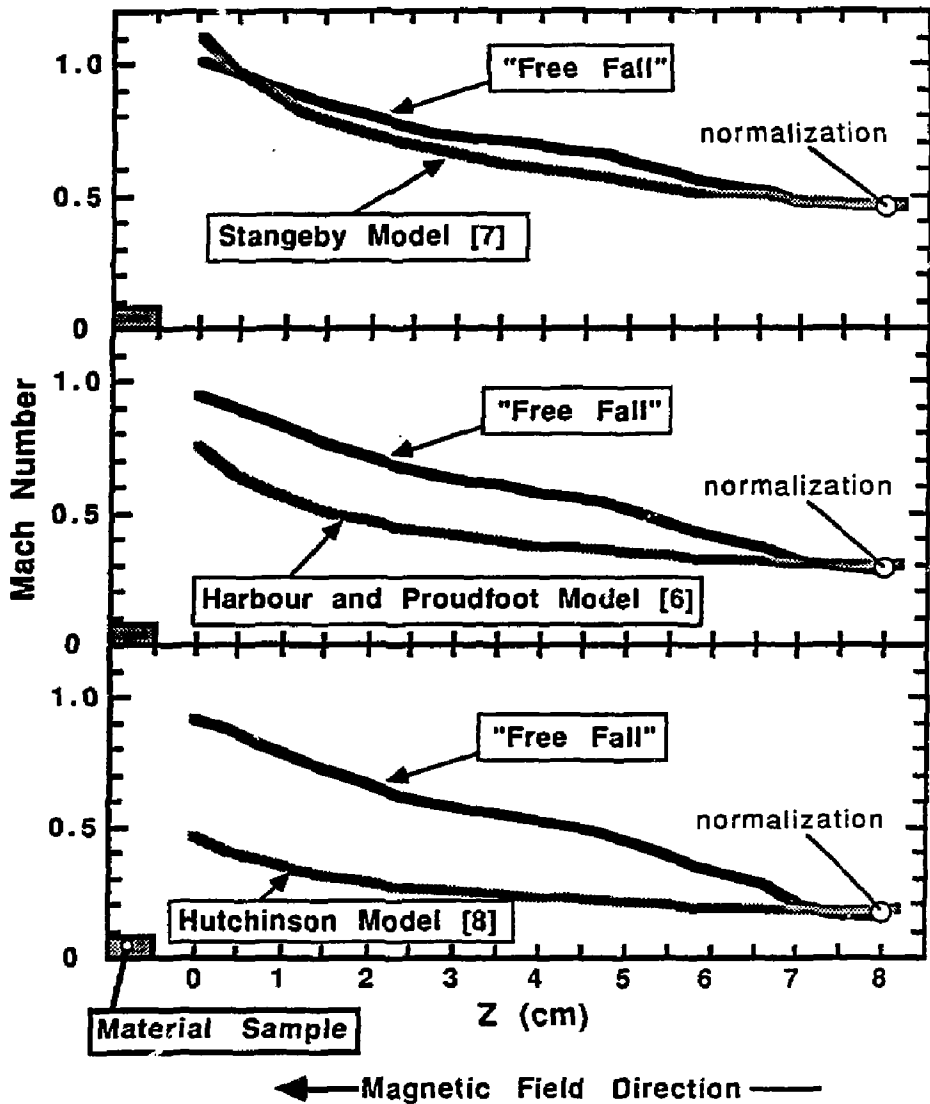


FIGURE 5

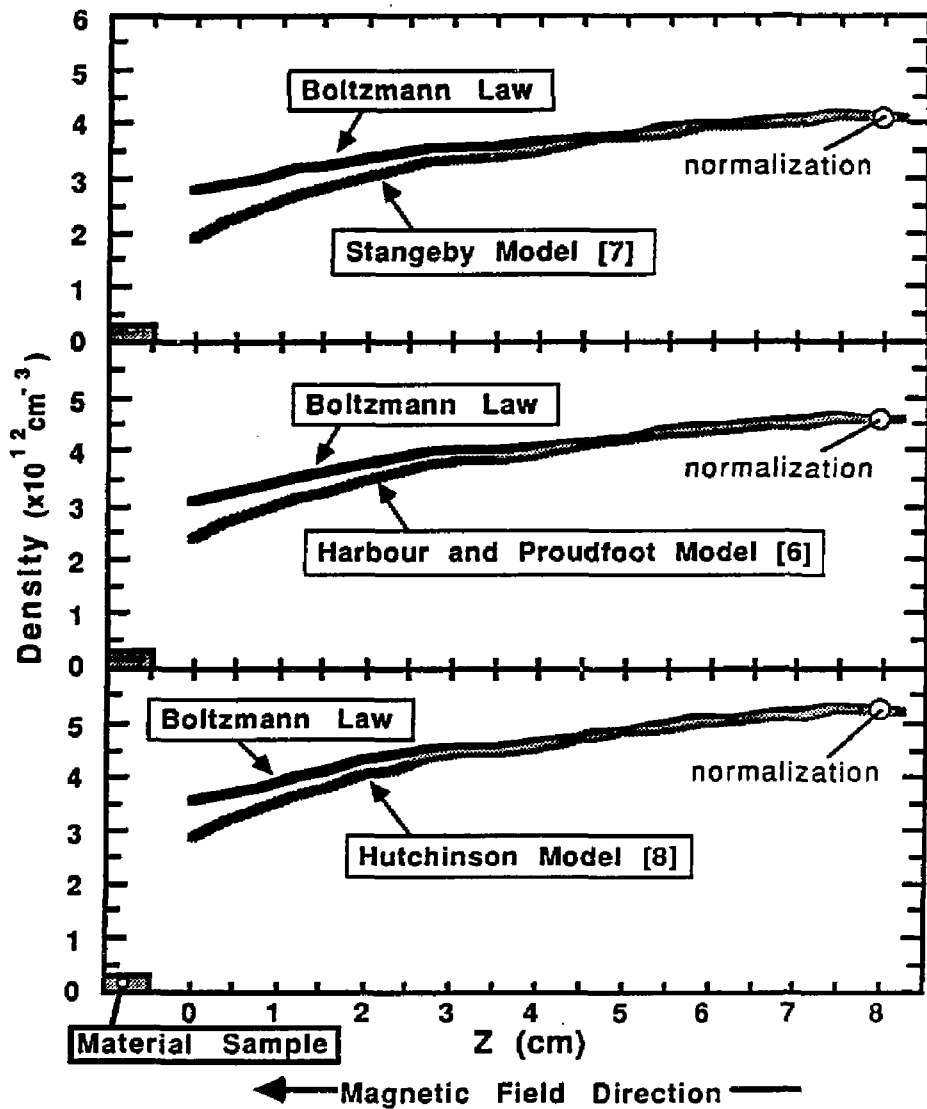


FIGURE 6

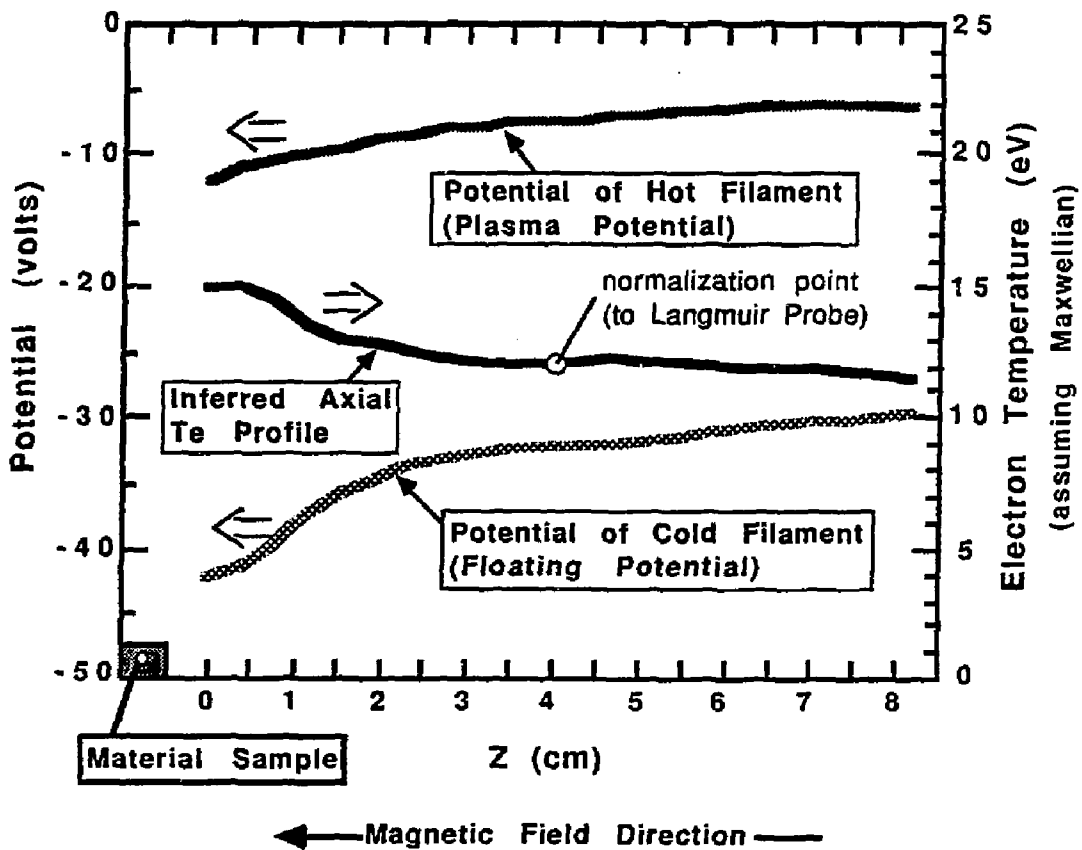


FIGURE 7

**EROSION AND REDEPOSITION BEHAVIOR
OF SELECTED NET-CANDIDATE MATERIALS
UNDER HIGH-FLUX HYDROGEN,
DEUTERIUM PLASMA BOMBARDMENT IN PISCES**

**E. Franconi*, Y. Hirooka, R.W. Conn,
W.K. Leung, B. LaBombard, and R.E. Nygren**

UCLA-PPG-1163

June, 1988

**Institute of Plasma and Fusion Research
Department of Mechanical, Aerospace, and Nuclear Engineering
University of California, Los Angeles
Los Angeles, California 90024**

***On leave from Associazione Euratom-ENEA sulla Fusione,
CRE Frascati, CP 65, 00044, Frascati, Rome, Italy**

**Presented at the 8th PSI meeting at Jülich, FRG, May, 1988.
(Submitted to the *Journal of Nuclear Materials*.)**

Erosion and Redeposition Behavior of Selected NET-candidate Materials
under High-Flux Hydrogen, Deuterium Plasma Bombardment in PISCES

E. Franconi*, Y. Hirooka, R.W. Conn,
W.K. Leung, B. LaBombard, R.E. Nygren

Institute of Plasma and Fusion Research
and
Department of Mechanical, Aerospace, Nuclear Engineering
University of California, Los Angeles
Los Angeles, CA 90024, USA

ABSTRACT

Plasma erosion and redeposition behavior of selected candidate materials for plasma-facing components in the NET-machine have been investigated using the PISCES-A facility. Materials studied include SiC-impregnated graphite, 2D graphite weaves with and without CVD-SiC coatings, and isotropic graphite. These specimens were exposed to continuous hydrogen or deuterium plasmas under the following conditions: electron temperature range from 5 to 35eV; plasma density range from 5×10^{11} to 1×10^{12} cm⁻³; flux range from 5×10^{17} to 2×10^{18} ions cm⁻² s⁻¹; fluence of the order from 10^{21} to 10^{22} ions/cm²; bombarding energies of 50 and 100eV; target temperature range from 300 to 1000°C. The erosion yield of SiC-impregnated graphite due to deuterium plasma bombardment is found to be a factor of 2 to 3 less than that of isotropic graphite materials. A further factor of 2-3 reduction in the erosion yield is observed in when redeposition associated with reionization of sputtered particle becomes significant. From post-bombardment surface analysis with AES, the surface composition in terms of the Si/C of SiC-impregnated graphite ratio is found to increase from 0.15 to 0.7 after hydrogen plasma bombardment to a fluence around 4×10^{21} ions/cm² at 350°C. However, the final surface composition appears to remain unchanged up to 4×10^{22} ions/cm², the highest fluence in the present study. Significant surface morphological modifications of SiC-impregnated graphite are observed after the high-fluence plasma exposure. Several structural problems such as coating-substrate adhesion have been pointed out for SiC-coated 2D graphite weave.

* On leave from Associazione Euratom-ENEA sulla Fusione,
CRE Frascati, CP 65, 00044 Frascati, Rome, Italy

1. INTRODUCTION

The plasma-facing components in the NET (Next European Torus) machine are expected to tolerate a heat flux of $10\text{-}40\text{ W/cm}^2$ and D-T plasma particle fluxes of the order of $10^{18}\text{ ions cm}^{-2}\text{s}^{-1}$ for long pulses up to 1000 sec [1]. Clearly, it is essential that candidate materials for these plasma-facing components be tested under similar high-flux and high-fluence hydrogen plasma bombardment. The PISCES-A facility [2] at UCLA allows us to investigate materials behavior under conditions relevant to those in NET.

With respect to materials selection, graphite is currently regarded as one of the most promising candidates because of its thermal properties and low atomic number. However, it is also true that graphite suffers from chemical erosion which leads to a formation of hydrocarbons [3]. This intrinsic weakness of graphite might in part be compensated by modification of surface characteristics. One possible modification is to impregnate or coat a porous graphite material with SiC, a material known to have a lower chemical erosion yield than graphite. In the present study, plasma bombardment experiments have been carried out for alternative materials to graphite as candidates for plasma-facing components in NET.

2. EXPERIMENTAL

2.1 Materials tested

The materials tested here include: (1) SiC-impregnated graphite (Schunk-Ebe GmbH) with a nominal composition of 33%SiC, 64%C, 3%Si; (2) 2D graphite weave (Schunk-Ebe GmbH); (3) SiC coated 2D graphite weave (Schunk-Ebe GmbH); and (4) isotropic graphite (Le Carbone Lorraine CL5890PT) which is currently used for the limiter tiles in the JET tokamak.

2-2. Plasma bombardment conditions

A schematic diagram of the PISCES-A facility is shown in Fig. 1. A disk specimen with a diameter of 2.5 cm was placed in continuous hydrogen or deuterium plasmas. A Langmuir probe was used to measure the plasma parameters. The plasma bombardment

conditions are: plasma density range from 5×10^{11} to 1×10^{12} cm^{-3} ; electron temperature range from 5 to 30eV; flux range from 5×10^{17} to 2×10^{18} $\text{ions cm}^{-2}\text{s}^{-1}$; fluence range from 10^{20} to 10^{22} ions/cm^2 ; bombarding energy range from 50 to 100eV. The specimen temperature was measured by a thermocouple and controlled in the range from 350 to 980°C. These conditions are believed to be relevant to those expected in NET during normal operation. More details of the PISCES-A facility and materials experiments can be found elsewhere [2-5].

These experimental conditions span a range where sputtered particles freely escape the plasma (referred to as the erosion regime) to where electron impact ionization is important and significant redeposition of sputtered particles occurs (referred to as the redeposition regime). The important parameter to determine these two regimes is the mean free path for electron impact ionization of the sputtered material. Details will be described later.

2-3. Post-bombardment analysis

Plasma-bombarded specimens were weighed to determine the weight loss for evaluation of the erosion yield. Typical weight loss observed here was from a few tens to about hundred milli gram, which is easily differentiated from any air-exposure effects. Also, these specimens were analyzed with AES (Auger electron spectroscopy) to determine the surface composition and with SEM (scanning electron microscopy) to observe the surface morphology.

3. RESULTS AND DISCUSSION

3-1. Basic considerations

It is known from our previous studies [2-5] that the ionization mean free path of sputtered particles plays an important role in determining the overall materials erosion behavior under plasma bombardment in the PISCES-A facility. Generally, the ionization mean free path of sputtered particles, λ , can be calculated using the relation:

$$\lambda = V_{av} / (n_e \langle \sigma v \rangle), \quad (1)$$

where V_{av} is the averaged velocity over the energy distribution of the desorbing particles, n_e is the plasma density and $\langle\sigma v\rangle$ is the rate coefficient for electron impact ionization. Here, the rate coefficient is evaluated from Lotz's formula [6]. Assuming a planer surface potential, the energy distribution needed to determine V_{av} is given by the relation [7]:

$$N(E) = E/(E+E_b)^3, \quad (2)$$

where E_b is the surface binding energy.

Resultant ionization mean free paths are listed in Table 1 for typical plasma parameters in the erosion and redeposition regimes. Because of the high surface binding energy, one should see a relatively long mean free path for physically sputtered carbon even under redeposition conditions. However, this effect will not significantly change the net erosion data to be discussed since chemical sputtering is considered to be the dominant erosion process at temperatures between 200 and 1000°C.

3-2. Experimental valuation of selected NET-candidate materials

The erosion yield of SiC-impregnated graphite and CL5890PT-graphite under deuterium plasma bombardment in the erosion regime at bombarding energies of 50 and 100 eV are shown in Fig. 2 as a function of surface temperature in the range from 350 to 1000°C. Corresponding data obtained from POCO-graphite (grade: HPD-1) from our previous work [9] are shown for comparison. The erosion yield data from CL5890PT-graphite and POCO-graphite are in relatively good agreement. One can also see that SiC-impregnated graphite exhibits a lower erosion yield than these isotropic graphite materials by a factor of 2 to 3. Similar data have been reported earlier, using graphite materials doped with SiC to a relatively low concentration of 4-5% [9,10]. The reduction of the erosion yield of SiC-doped graphite were interpreted by two possible mechanisms: (1) the virtual enrichment of silicon due to preferential removal of carbon from the surface; and/or (2) some catalytic effect of silicon as an enhanced hydrogen recombination site [10].

To clarify this point, SiC-impregnated graphite was bombarded with a hydrogen plasma up to a fluence of 4×10^{22} ions/cm² at a surface temperature of 350°C in the erosion regime. After a certain period of hydrogen plasma bombardment, the surface composition was analyzed. To avoid surface impurity effects, the post-bombardment AES analysis was conducted under 2 keV Ar⁺ bombardment.

The result of the surface analysis is shown in fig. 2. One can see that the surface composition in terms of the Si/C ratio changes rapidly as a function of bombardment fluence up to $3\text{-}5 \times 10^{21}$ ions/cm² and then reaches an equilibrium value. Apparently, chemical erosion removes carbon first from the surface. An equilibrium composition is then attained upon a material balance of Si/C for given conditions: erosion rate; and segregation rate from the bulk. The equilibrium surface composition is expected to be maintained unless plasma bombardment conditions change. In fact, the equilibrium composition has been found to remain unchanged up to 4×10^{22} ions/cm², the highest fluence in the present study. This fluence is equivalent to over 10,000 shots in existing tokamaks such as TFTR [11] and to about 100 shots in NET [1]. Also, the fluence above which the equilibrium surface composition was observed can be considered as the critical fluence, which is about 10 shots in NET, for the surface conditioning of this material.

The initial Si/C ratio of SiC-impregnated graphite before plasma bombardment is found to vary between 0.15 and 0.17 although the nominal ratio of this material is expected to be 0.25 from the vendor's data. This difference may be due to excess supply of carbon during the CVD-impregnation process. The equilibrium Si/C ratio after plasma exposure is found to be about 0.7. Thus, significant enrichment of Si on the surface is observed here. For comparison, the data from a virgin specimen of SiC-impregnated graphite are also shown in Fig. 2. The virgin specimen (see curve: C+SiC-1) yielded about a factor of 2 larger erosion rate, relative to a specimen with an equilibrated surface composition (see curve: C+SiC-2) at 350°C to a fluence of 4×10^{21} ions/cm², a typical fluence used for individual erosion yield measurements. For successive experiments at higher temperatures, no significant difference is observed, indicating that the surface composition is equilibrated.

It should be noted here that although the composition dependence on fluence has been investigated at 350°C, no corresponding data are available for higher temperatures at present. The equilibrium composition might depend on the surface temperature. However, it is also true that the erosion yield does not seem to depend strongly upon the concentration of SiC. In fact, we found a similar degree of reduction in the erosion yield using graphite impregnated with 33%SiC to the earlier data using graphite doped with 4-5% SiC. Therefore, we would rather deal with the present data, as measured, as an engineering benchmark.

The SiC-impregnated graphite specimen used for the high-fluence plasma bombardment experiment was analyzed with SEM and results are shown in Fig. 4. Due to physical and chemical sputtering, the surface morphology is significantly modified. However, no major cracks are observed, demonstrating good structural integrity.

Nevertheless, there may be a limit in the practical use of SiC-impregnated graphite since this material is extremely hard, brittle and hence non-machinable by ordinary tools.

Similar high-fluence plasma erosion experiments attempted for SiC-coated 2D graphite weave were not successful because the coatings flaked off in part or entirely. It is essential that the film-substrate adhesion be improved before this material is reconsidered as a NET-candidate. Also, weight loss measurements for the plasma-bombarded 2D graphite weave specimens were found to be influenced significantly by air exposure, i.e. moisture pickup, probably because of the low density structure (about 70-75% theoretical density). This is indicative of the possibility that one suffers significant outgassing if 2D graphite weave is placed in a vacuum system. For these reasons, the erosion yield data from 2D graphite weaves with and without SiC-coatings were not reproducible and are not reported here.

Shown in Fig. 5 are the erosion yield data of SiC-impregnated graphite and CL5890PT-graphite at bombarding energies of 50 and 100 eV at temperatures between 350 and 1000°C. One can see a significant energy dependence for each material. At these bombarding energies, SiC-impregnated graphite exhibits a lower erosion yield than isotropic graphite. Also, the erosion yield of SiC-impregnated graphite steeply decreases towards 1000°C. In our previous work [9], similar temperature dependence of the erosion yield was observed for POCO-graphite at an energy of 50 eV.

Redeposition experiments were carried out at a bombarding energy of 100eV at temperatures between 500 and 1000°C. Applying the probability of redeposition [4] for the mean free paths shown in Table 1, one expects about 2-3%, 50-60% and 80-90% redeposition for the cases of physically sputtered carbon, physically sputtered silicon and chemically sputtered deuterio-methane (CD₄), respectively. The net erosion yield data obtained under these conditions are shown in Fig. 6. The net erosion yields SiC-impregnated graphite and CL5890PT-graphite in the redeposition regime are found to be about a factor of 2-3 lower than those in the erosion regime. In-situ plasma spectroscopic experiments for more detailed investigation of preferential erosion-redeposition behavior of multi-component materials are under way.

4. SUMMARY AND AREAS TO BE INVESTIGATED IN FUTURE

High-flux, high-fluence plasma erosion and redeposition experiments have been conducted, using the PISCES-A facility for selected NET-candidate materials: SiC-

impregnated graphite; 2D graphite weaves with and without SiC-coatings; and isotropic graphite. The following results are obtained:

(1) In the erosion regime, SiC-impregnated graphite has about a factor of 2-3 lower erosion yield than isotropic graphite at energies of 50 and 100 eV. A further factor of 2 to 3 reduction in the net erosion yield has been observed for each material in the redeposition regime.

(2) The surface composition of SiC-impregnated graphite in terms of the Si/C ratio first increases from 0.15-0.17 to an equilibrium composition of 0.7 due to hydrogen plasma bombardment to a fluence of $3\text{-}5 \times 10^{21}$ ions/cm². The surface composition, once equilibrated, does not change as long as plasma bombardment conditions remain constant.

(3) After high-fluence hydrogen plasma bombardment, significant surface modifications are found for SiC-impregnated graphite. However, no major cracks are observed, indicating good structural integrity of this material.

(4) During high-flux plasma exposure, SiC-coatings on 2D graphite weave tends to flake off. The improvement of substrate-coating adhesion is necessary. Also, bare 2D graphite weave absorbs an appreciable amount of water vapor. One might expect significant outgassing in a vacuum system after air-exposure.

The importance of the data reported here lies in the general reduction of the erosion yield from the use of SiC as an additive to the host graphite structure. However, details of the role of SiC in reducing the erosion yield are still unclear. One might raise a question, for example, what the best composition of SiC is to minimize the erosion yield. There might be an optimized composition to retain the good machinability and thermo-mechanical properties of host graphite, and yet to minimize the erosion yield. To the best of our knowledge, there is no comprehensive data base to answer this question at present. Clearly, in evaluating these SiC-graphite composites as possible candidates for NET, additional data on their responses to plasma exposure will be needed both to guide the development of materials and to project the performance of components in NET made from such materials.

ACKNOWLEDGEMENT

The authors would like to express their sincere gratitude to J.Bohdansky and D.M.Goebel for illuminating discussions. Special thanks go to K.Andrews, J.Elverum and T.Sketchley for technical support. This work is supported by the Office of Fusion Energy, US Department of Energy under contract #DE-AT03-84ER52104.

REFERENCES

- [1] F.Englemann, M.Chazalon, M.F.A.Harrison et.al., J.Nucl.Mater. 145-147 (1987)154.
- [2] D.M.Goebel, G.A.Campbell and R.W.Conn, J.Nucl.Mater. 111&112(1982)457.
- [3] D.M.Goebel, Y.Hirooka, R.W.Conn et.al., J.Nucl.Mater. 145-147(1987)61.
- [4] Y.Hirooka, D.M.Goebel, R.W.Conn et.al., J.Nucl.Mater. 141-143(1986)193.
- [5] Y.Hirooka, D.M.Goebel, R.W.Conn et.al., Nucl.Instr. & Methods-B 23(1987)458.
- [6] W.Lotz, Zeitschrift fur Physik 216(1968)241.
- [7] M.W.Thompson, Philos. Mag. 18(1968)377.
- [8] W.D.Langer, Nucl. Fusion 22(1982)751.
- [9] D.M.Goebel, J.Bohdansky, R.W.Conn et.al., Nucl. Fusion (in press).
- [10] J.Roth, J.Nucl.Mater. 145-147(1987)87.
- [11] D.B.Heifetz, M.I.Baskes, H.F.Dylla and M.Ulrickson, J.Nucl.Mater. 145-147(1987)326.

FIGURE CAPTIONS

Fig. 1: A schematic diagram of the PISCES-A facility.

Fig. 2: Erosion yields of SiC-impregnated graphite and isotropic graphite materials (CL5890PT and POCO: HPD-1[9]) under deuterium plasma bombardment at an energy of 100 eV at temperatures between 350 and 1000°C in the erosion regime. The curves: C+SiC-1 C+SiC-2 are two series of erosion experiments starting with a virgin surface and an equilibrated surface, respectively (see text).

Fig. 3: Surface composition change in terms of the Si/C ratio of SiC-impregnated graphite during high-fluence hydrogen plasma exposure at an energy of 100 eV at a surface temperature of 350°C in the erosion regime.

Fig. 4: Scanning electron micrographs of SiC-impregnated graphite: (a) as-received; and (b) after high-fluence plasma bombardment up to a fluence of 4×10^{22} ions/cm² at 100 eV and at 350°C.

Fig. 5: The erosion yields of SiC-impregnated graphite and isotropic graphite (CL5890PT) under deuterium plasma bombardment at 50 and 100 eV at temperatures between 350 and 1000°C in the erosion regime.

Fig. 6: Comparison of the erosion yields of SiC-impregnated graphite and isotropic graphite (CL5890PT) under deuterium plasma bombardment in the erosion and redeposition regimes at an energy of 100 eV and at temperatures between 500 and 1000°C.

Table 1 Typical experimental parameters in the erosion and redeposition regimes.

PARAMETERS	EROSION	REDEPOSITION
Plasma flux (ions s ⁻¹ cm ⁻³)	1.0e18	2.0e18
Plasma density (cm ⁻³)	7.0e11	9.0e11
Electron temperature (eV)	5.0	35.0
MFP* for carbon (cm)	350	19
MFP* for silicon (cm)	45	5.5
MFP* for methane (cm)	20-35 (300-1000°C**)	1-3 (300-1000°C**)

* The mean free path for the first ionization by electron impact. The values are obtained from the Lotz's formula or data reported by Langer [8].

** The mean free path is calculated, assuming methane leaves with thermal energies given by the surface temperature.

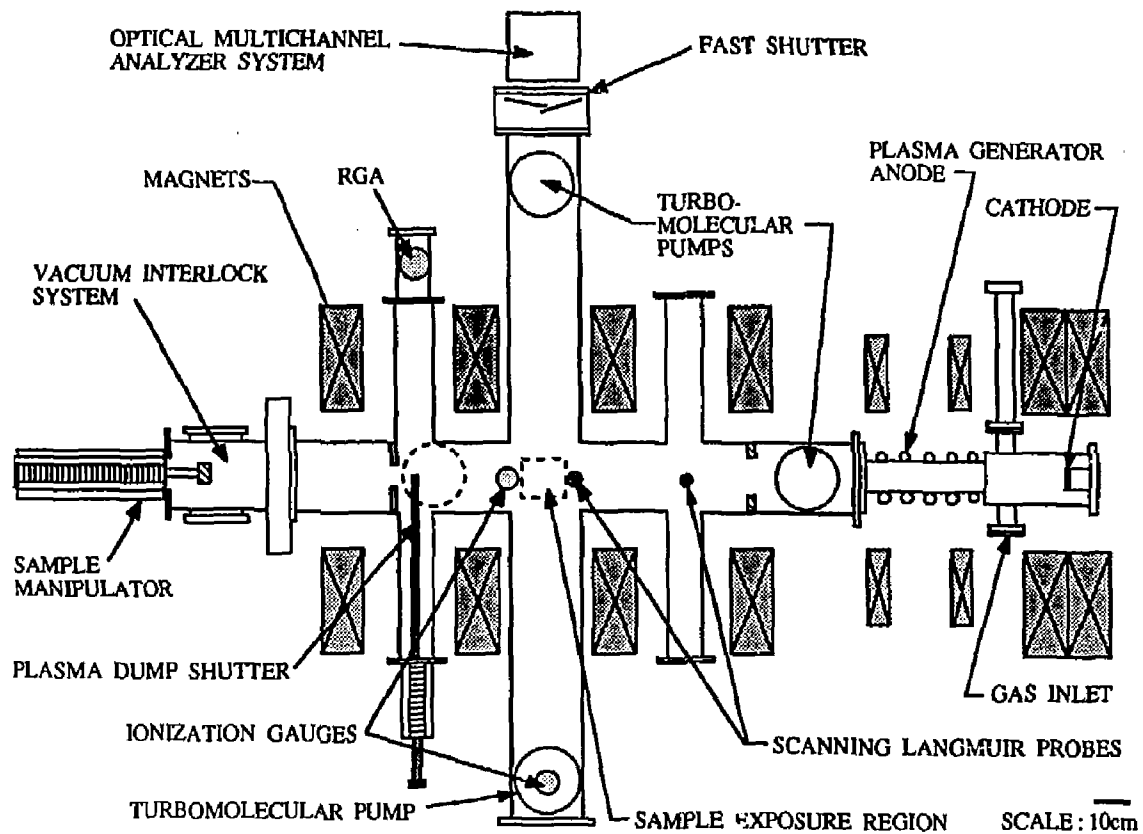


FIG. 1

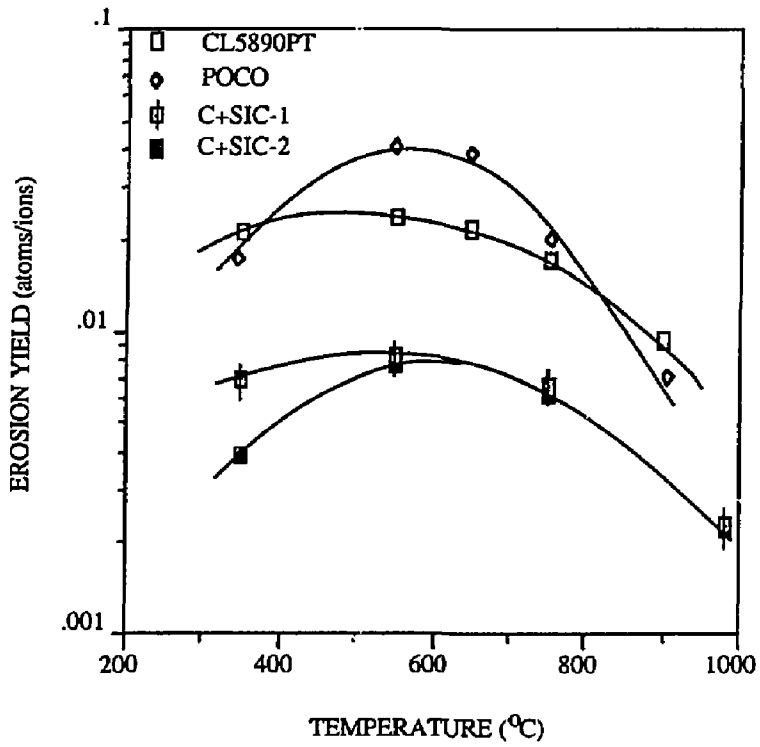


FIG. 2

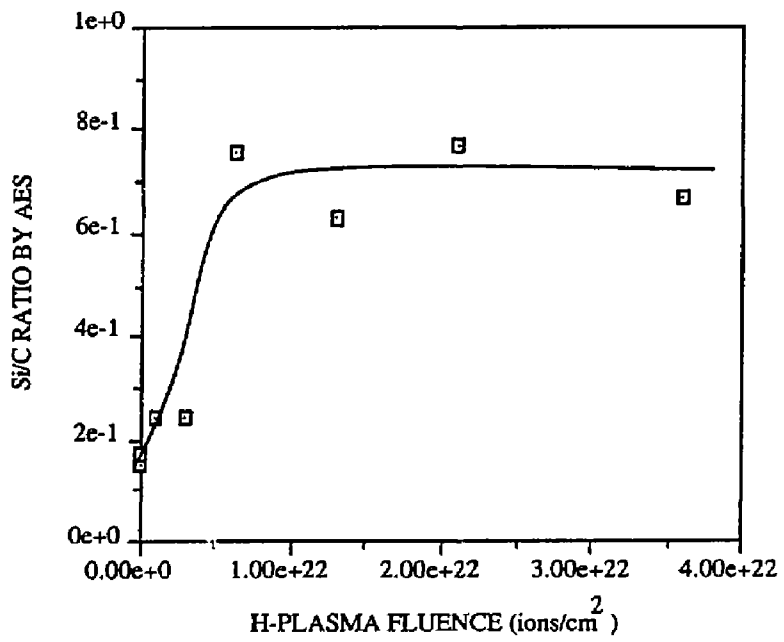
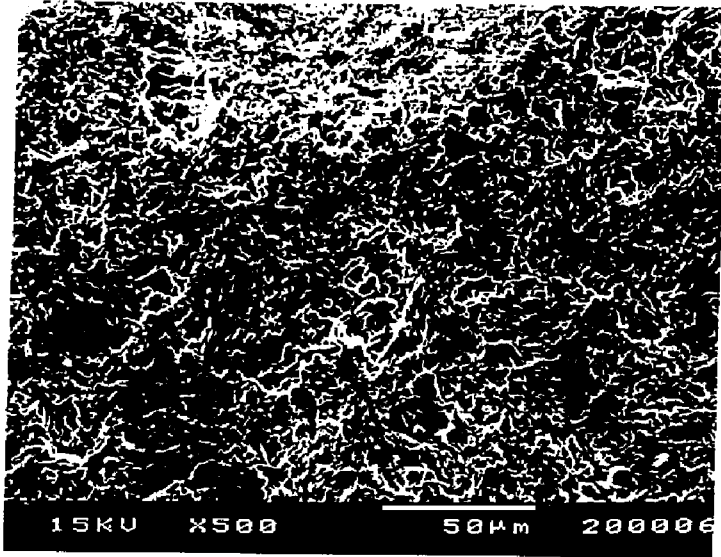
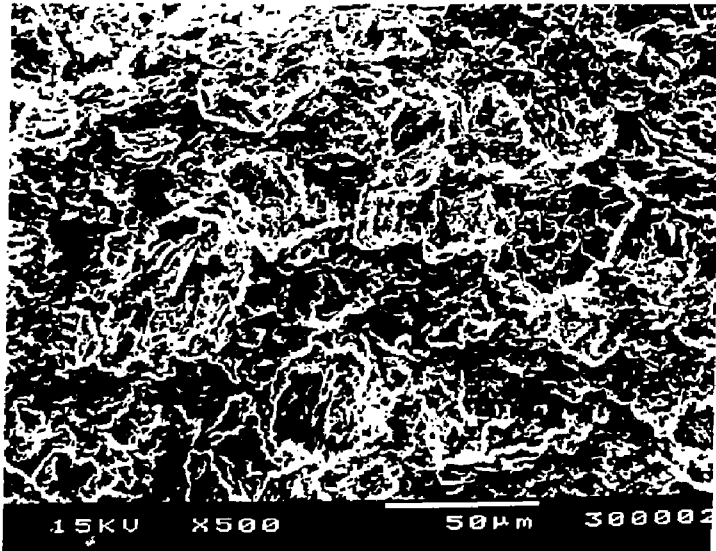


FIG. 3



(a)



(b)

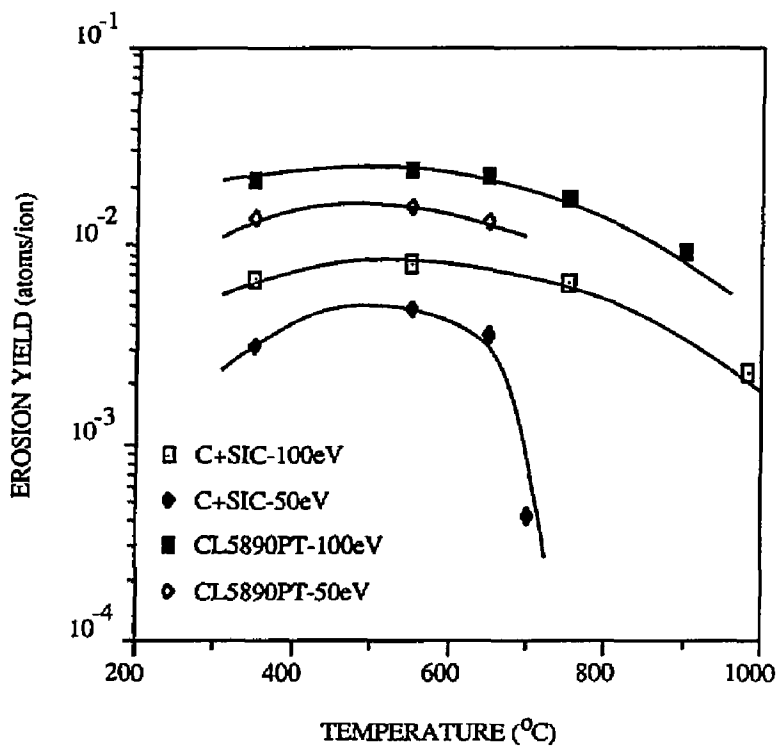


FIG.5

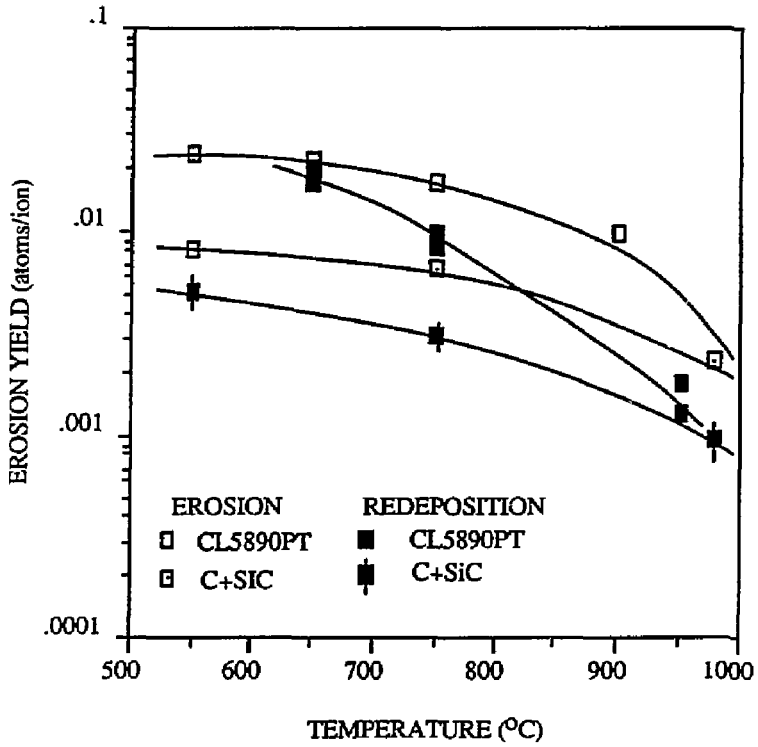


FIG.. 6

Boundary Asymmetries and Plasma Flow to the ALT-II Toroidal Belt Pump Limiter

W. J. Corbett¹, D. M. Goebel¹, R.W. Conn¹, R.T. McGrath²,
K.H. Dippel³, K.H. Finken³

¹ Institute of Plasma and Fusion Research, and Department of Mechanical, Aerospace and Nuclear Engineering, University of California, Los Angeles, CA 90024, U.S.A.

² Institut für Plasmaphysik, Kernforschungsanlage Jülich, Association EURATOM-KFA D-5170 Jülich, Fed. Rep. Germany

³ Sandia National Laboratories, Albuquerque, NM 87185, U.S.A.

ABSTRACT

The ALT-II toroidal belt pump limiter consists of 8 radially adjustable limiter blade segments located 45° below the outboard horizontal midplane of TEXTOR. An array of Langmuir probes has been installed in the plasma scoops to monitor radial decay lengths, electron/ion drift side asymmetries, and to measure total ion currents incident on the neutralizer plates. To complement these diagnostics, a pneumatic scanning double probe has been mounted at the outboard midplane to measure profiles in the scrape-off layer in to the limiter tangency point. Li-beam diagnostics on the top and bottom of TEXTOR are used to measure poloidal asymmetries. During Ohmic discharges, the electron temperature in the center of the scoops (3cm into the SOL) is 8-12eV, tending to decrease with rising line average density in the core. Corresponding edge plasma densities are in the range 2 to $5 \times 10^{11} \text{cm}^{-3}$. Recent probe measurements indicate that 10-50% more particle current is collected on neutralizer plates with flux tubes connected to the electron drift side on the outboard side of ALT-II. The primary reason for the asymmetric particle collection at the neutralizers is that particle flux e-folding lengths on the electron drift side are longer than on the ion drift side by up to a factor of 2, for non-detached plasmas. These measurements are confirmed by profiles obtained with the fast pneumatic scanning probe, and a Li-beam edge diagnostic¹ located in the bottom of TEXTOR. In this paper, measurements in the edge plasma behind ALT-II are reported to emphasize the role of scrape-off length asymmetries on particle collection by the ALT-II toroidal belt pump limiter.

I. Introduction

The design of toroidal belt pump limiters for recycling control in the tokamak edge plasma includes two important design criteria. First, convective power flow released from the plasma core must be evenly distributed over the limiter surface at tolerable levels for component reliability. Second, the thickness of plasma facing limiter components is minimized to obtain maximum particle collection at the neutralizer plates, and is typically designed to be about one particle e-folding length. The trade-off between these two criteria requires careful design of the limiter face for power handling, while minimizing the overall limiter blade thickness for optimum particle collection.

An additional requirement in belt limiter design concerns placement of the belt in the tokamak. Both power and particle flow asymmetries in the scrape-off layer have been detected at several poloidal locations with modular limiters²⁻⁴, and poloidally asymmetric edge plasma conditions have been clearly observed in the scrape-off layer of the Alcator-C tokamak⁵. Indeed, asymmetries in the plasma flow, and in particular asymmetries in the particle scrape-off length, directly impact placement of the limiter, power handling, and particle collection at the neutralizer plates.

In the following sections, we report on plasma flow asymmetries behind the Advanced Limiter Test^{6,7} (ALT-II) toroidal belt pump limiter in TEXTOR⁸. ALT-II is located 45° below the outboard horizontal midplane, and creates a toroidally symmetric bifurcation of the scrape-off layer plasma from tangency to the vessel wall. Differences in plasma flow to the inboard and outboard limiter scoops under the blades have been detected, and are correlated with scrape-off layer profile measurements from edge diagnostics located at the outboard midplane and bottom of TEXTOR. Standard discharge conditions are $I_p=340\text{kA}$, toroidal field $B_T=2.0\text{T}$, deuterium plasmas.

II. Probe Locations in the ALT-II Scrape-Off Layer

Each of the 8 ALT-II limiter blades is equipped with plasma collection scoops and a pump duct for particle exhaust. The limiter blades are covered with graphite tiles bolted to an Inconel baseplate to give an overall blade thickness of 1.7cm. Plasma flow behind the belt is intercepted

by graphite neutralizer blocks attached to the backside of the baseplates. As shown in Fig. 1, graphite scoops and a stainless steel plenum box are mounted over the neutralizer to reduce neutral gas backflow and duct gas to the pumps. The entrances to the plasma scoops are located at the edge of the shadow region cast by toroidally adjacent blades. In this way, efficient collection of the scrape-off layer particle flux is obtained, and a complete poloidal bifurcation of the scrape-off layer is made out to the TEXTOR liner. The scoop entrances measure 13.3 x 2.5cm, to accommodate 2-3 particle e-folding lengths in the radial direction for ohmic discharges. For the data presented here, the ion drift direction to ALT-II is from the bottom/inside of TEXTOR, and the electron drift direction is from the outboard side incident on the upper toroidal edge of the belt.

Particle currents to the neutralizer plates are measured with 'flux' probes biased into ion saturation. These probes extend radially from the baseplate to the bottom of the scoop. A profile-integrated measurement of ion current to the neutralizer plate is obtained by converting the probe current to a radial average flux and multiplying by the area of the scoop entrance. In addition to core efflux and pump flow measurements, the particle removal efficiency $\eta = \text{pump flow} / \text{scoop flow}$, and the ALT-II particle collection efficiency $\zeta = \Sigma(\text{scoop currents}) / \text{core efflux}$ can be estimated, independent of profile shape in the scrape-off layer.

Flux probes have been located in the scoops to monitor both flow asymmetry from above and below the belt, and toroidal uniformity around TEXTOR. An exception to this rule occurs when the ICRH antennas are inserted and particle flux on the electron side is partially intercepted by the graphite Faraday cage shields. Additional Langmuir probes measure local electron temperature and density. These probes are located in the center of the scoops, 3cm behind the limiter tangency radius.

Scrape-off layer profiles at the outboard horizontal midplane of TEXTOR are measured with a pneumatic scanning double probe. Langmuir probe measurements of plasma flow to the electron drift side scoops are correlated to scanning probe profiles, and compared with density profiles obtained with the Li-beam diagnostic located in the bottom of TEXTOR. Differences in plasma flow to the limiter scoops can then traced back to differences between scrape-off layer profiles on the inboard and outboard side of ALT-II.

III. SOL Plasma Flow to the ALT-II Limiter

A plot of the total ion current flowing to the neutralizer plates of several ALT-II blades located around the torus is displayed in Fig. 2a, with the limiter positioned at $a=44\text{cm}$. Plasma conditions across the poloidal extent of the scoop were measured by a set of Langmuir probes, and found to be constant. Typically, 2-5A ion currents flow to each scoop, with the outboard scoop currents exceeding inboard collection by 10-50%. The particle currents collected in the outboard scoops are nearly toroidally symmetric, averaging about 4.2A per scoop. Particle flow to scoops facing the ion drift side direction is also toroidally uniform, but reduced to an average value of 2.8A per scoop. The total current collected by the combined 8 ion drift side and 4 electron side scoops is about 40A. Typical core effluxes of 1.5 to 2×10^{21} have been measured with ALT-II as the main limiter in TEXTOR⁹, so that the particle collection efficiency $\zeta \approx 15\%$ for ohmic discharges with 12 scoops active.

Referring to Fig. 2b, local particle fluxes measured in the center of the scoops are also lower on the ion drift side of the belt. The ratio between the two fluxes is higher in this case, however, than the same ratio for the integrated currents to the neutralizer plates, indicating a difference in the scrape-off layer on opposite sides of the belt. On the inboard side, the scrape-off length for particle flux behind ALT-II is shorter than on the outboard side.

To clarify this result, an estimate for the decay length can be made from the integration of the flux profile from the limiter baseplate to the bottom of the scoop. We assume an exponential decay characteristic, with the local Langmuir probe measurement, Γ_{LP} , taken at the center of the scoop fixing the profile magnitude. The total scoop current is then given by,

$$I_{\text{scoop}}(\lambda) = \Delta\theta \lambda \Gamma_0 (1 - \exp(-\Delta_S/\lambda)) \quad (1)$$

where $\Delta\theta$ and Δ_S are the poloidal and radial extent of the scoop, and $\Gamma_0 = \Gamma_{LP} \exp(\Delta_{LP}/\lambda)$ is the particle flux at back of the baseplate. The total scoop current and flux to the center of the scoop are measured directly with probes on the ion and electron drift sides of the belt. Inserting probe locations measured during installation, we find the ratio between the scrape-off lengths

$\lambda_r(\text{Outside})/\lambda_r(\text{Bottom}) \sim 1.7$. Although the solution in λ is sensitive to both changes in the quantity $I_{\text{scoop}}/\Gamma_{\text{LP}}$ and deviations in the profile shape from exponential, the scrape-off length on the electron drift side is a factor of 1.4 to 2.0 longer than on the ion drift side. The result is a higher total particle current flowing to scoops facing the electron drift side of the belt.

A more precise evaluation of the particle flux scrape-off length is obtained utilizing a least squares fit of an exponential to the scanning probe profile. In Fig. 3 are displayed the electron temperature and particle flux profiles in the scrape-off layer plasma on the outboard horizontal midplane for the same shot. The radial locations of the limiter, scoop entrance, and Langmuir probes are indicated on this plot. An exponential fit to the profile yields a scrape-off length $\lambda_r \approx 1.0\text{cm}$. As shown in Fig. 4, this length is characteristic of values measured over a range of line average core densities with ALT-II as the main limiter, and is considerably shorter than the $\lambda_r = 1.5\text{-}2\text{cm}$ scrape-off length behind the ALT-I modular limiter¹⁰.

At the scoop center radius, $r=47\text{cm}$, the electron temperatures $T_e \approx 8\text{eV}$ and particle fluxes $\Gamma_{\parallel} \approx 110\text{m}^2/\text{cm}^2$ are well correlated between the scanning probe and the Langmuir probes located in the scoops. The length of the flux tube connecting the two measurement locations is about 3.5m, extending from ALT-II to the horizontal midplane. The total current to each of the electron drift side scoops can be estimated by integrating the scanning probe flux profile over the scoop entrance slot: $I_{\text{scoop}} = \iint \Gamma_{\parallel}(r) r d\theta dr \approx 3.8\text{A}$. This result is within 10% of the corresponding probe measurements taken in the electron drift side scoops.

A comparison between density profiles obtained with the scanning probe and the Li-Beam edge diagnostic in the bottom of TEXTOR is given in Fig. 5. Both diagnostics have equal connection lengths ($L=3.5\text{m}$) to the ALT-II limiter. The 0.9cm density decay length measured below ALT-II is less than the $\lambda_n = 1.35\text{cm}$ decay length measured above the belt by a factor of 1.5. This factor is comparable to the ratio for particle flux decay lengths calculated from Langmuir probe data taken in the scoops as described above.

Since heat flux measurements on ALT-II show up to 2 times higher power deposition on the ion drift side¹¹, and from direct measurements of 2-3 times higher particle fluxes from the ion drift direction on the ALT-I limiter¹⁰, a flow asymmetry to ALT-II favoring the ion side is known to exist near the tangency point. The combined effects of this particle flux asymmetry at

tangency, and the variation in scrape-off length above and below the ALT-II limiter can be used to explain the scoop current asymmetry detected with Langmuir probes.

To demonstrate this effect, the ratio of currents to the ion and electron drift sides is calculated with the following simple model for scrape-off layer particle flow to the ALT-II limiter scoops. Above the belt, plasma flows from a region with a relatively long particle flux scrape-off length, $\lambda_{\Gamma} \approx 1.0\text{-}1.2\text{cm}$. If the temperature decay length λ_T is approximately symmetric, then the flux scrape-off lengths will be in the same ratio as the density scrape-off lengths. We take the ratio between particle collection rates in oppositely directed scoops:

$$\frac{I_E}{I_I} = \frac{1}{2} \frac{\lambda_E e^{(-\Delta_B/\lambda_E)} [1 - e^{(-\Delta_S/\lambda_E)}]}{\lambda_I e^{(-\Delta_B/\lambda_I)} [1 - e^{(-\Delta_S/\lambda_I)}]} \quad (2)$$

Here, the subscripts 'E' and 'I' refer to the electron and ion particle drift directions, from above and below ALT-II. The factor of $\frac{1}{2}$ accounts for the particle flow asymmetry at the limiter tangency point. Using the value $\lambda_{\Gamma} = 1.0\text{cm}$ above the belt, and assuming the flux decay length below the belt is reduced by the factor 1.5, we find $\lambda_{\Gamma}(\text{below}) = 0.7\text{cm}$. Thus, from Eq. 2 the ratio for the integrated particle currents collected in the scoops is $I_e/I_{ion} = 1.4$, in good agreement with the flux probe data shown in Fig. 2. The measured ratio by the probes of 1.5 is probably higher due to the tendency for the profile to deviate from a pure exponential at the scoop radius on the electron drift side. In summary, both the preferential particle flow in the ion drift direction at the limiter tangency radius, and the particle flux scrape-off length asymmetry above and below the belt, are necessary to explain the Langmuir probe particle collection measurements in the scoops behind ALT-II.

IV. Conclusions

Probe measurements in the shadow of ALT-II have been used to detect an asymmetry in the structure of the scrape-off layer above and below the belt limiter. More plasma is incident on neutralizer plates with flux tubes connecting to the outboard side of TEXTOR where the particle flux scrape-off lengths are longer. The particle flux decay lengths measured with the scanning

probe lie in the range 1-1.2cm, with the shortest values occurring at higher line average densities when the edge temperature is low. Neutralizer plates with flux tubes connecting to the bottom/inside of the tokamak receive 10-50% less flux due to a decrease in the characteristic decay lengths. This effect is partially compensated by an ion flow asymmetry favoring the ion drift direction. The physical mechanisms behind the particle flow asymmetry at tangency and the poloidal variation in scrape-off lengths are presently under investigation.

For these experiments, ALT-II was operated with 8 ion side scoops and 4 electron side scoops, and had an overall collection efficiency for core efflux of 15-20%. During the next operating period, 3 additional scoops will be added on the electron drift side to raise collection efficiencies up to 20-25% in ohmic discharges. With the scheduled addition of 3-4MW ICRH plus 2.6MW NBI auxiliary power input to the plasma core, the characteristic scrape-off lengths are expected to increase behind ALT-II. In the range of interest, $\lambda_r \approx 1-2\text{cm}$, the particle collection efficiency scales almost linearly with λ_r , and collection efficiencies of the order 25-35% are anticipated. Since ALT-II typically pumps 25% of the collected current⁸, the pump limiter will remove up to 10% of the core efflux.

Acknowledgements

The authors would like to thank the TEXTOR Team, especially Dr. Y.T. Lie for providing Li-beam data, and would like to acknowledge the technical assistance of K. Andrews, B. Becks, V. Low, A. Hiller, K. Sheedy and T. Sketchley.

* Work supported by the U.S. Department of Energy under contract #DE-F603-85ER51069 and Association Euratom-KFA.

References

1. Y. T. Lie, et al., in: Proc. Int. Conf. on Plasma Physics, Lausanne, Vol. 2 (1984) 320.
2. K. H. Dippel, et al., Plasma Physics and Controlled Nucl. Fusion Research (Proc. 10th Intl. IAEA Conf.), London (1984), Vol. 1, IAEA Vienna (1985).
3. R. Budny, et al., J. Nucl. Mat. 121 (1984) 294.
4. P. K. Mioduszewski, et al., J. Nucl. Mat. 145&146 (1987) 210.
5. B. LaBombard, B. Lipschultz, Nuclear Fusion 27, No. 1 (1987) 81.
6. R. W. Conn, et al., J. Nucl. Mat. 121 (1984) 350.
7. J. Koski, et al., J. Nucl. Mat. 121 (1984) 309.
8. G. H. Wolf, et al., J. Nucl. Mat. 122&123 (1984) 1124.
9. D. M. Goebel, et al., these proceedings.
10. D. M. Goebel, et al., Plasma Physics and Controlled Fusion 29, No. 4 (1987) 473.
11. K. H. Finken, et al., these proceedings.

Figure Captions

1. Backside view of ALT-II limiter blade showing scoops, neutralizer plate, plenum box, and probe locations.
- 2a. Toriodally uniform currents to the neutralizer plates behind ALT-II, with 50% more particle collection on the electron drift side.
- 2b. Particle flux measured at the scoop centers on the ion and electron drift sides of the belt.
3. Electron density and particle flux profiles in the scrape-off layer measured on the horizontal midplane. Positions of the particle collection slot and Langmuir probes are indicated.
4. Comparison between density profiles measured above and below ALT-II. Density profiles on the outboard side are more broad than on the inboard side.
5. Scanning probe density and particle flux scrape-off lengths measurements as a function of line averaged core density.

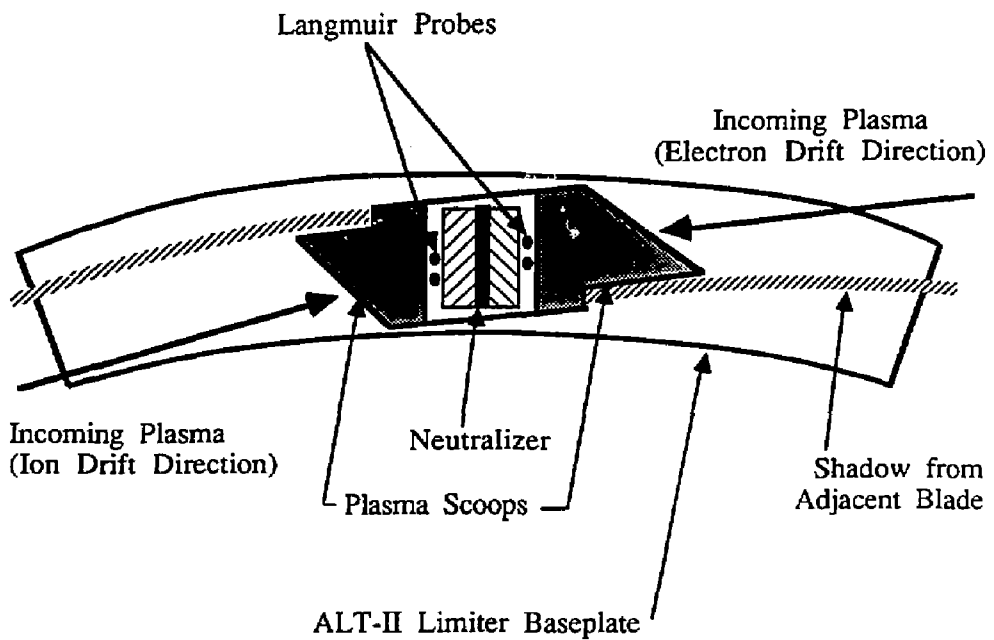


Figure 1

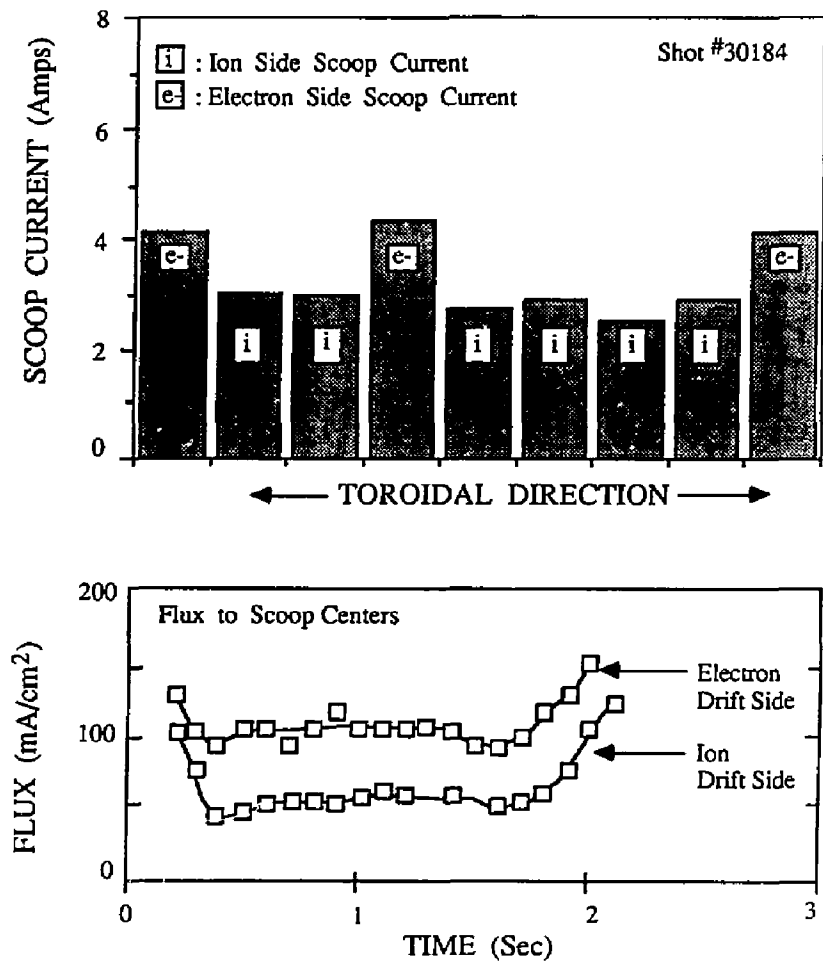


Figure 2

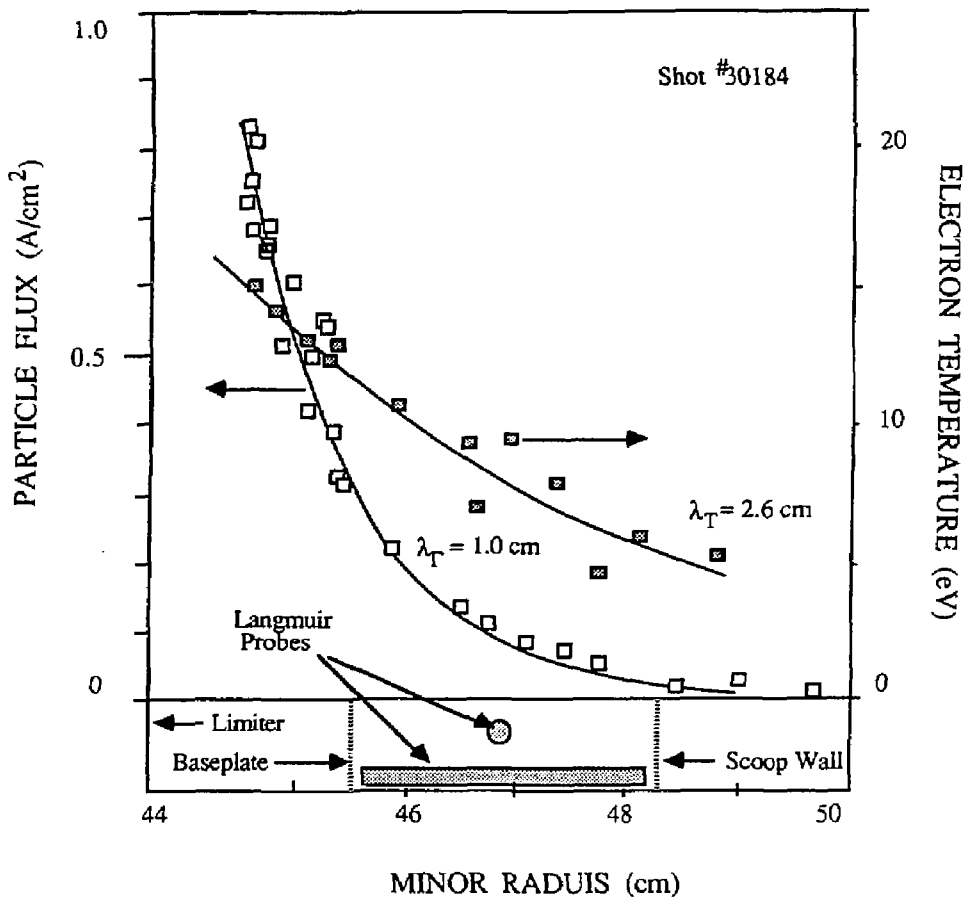


Figure 3

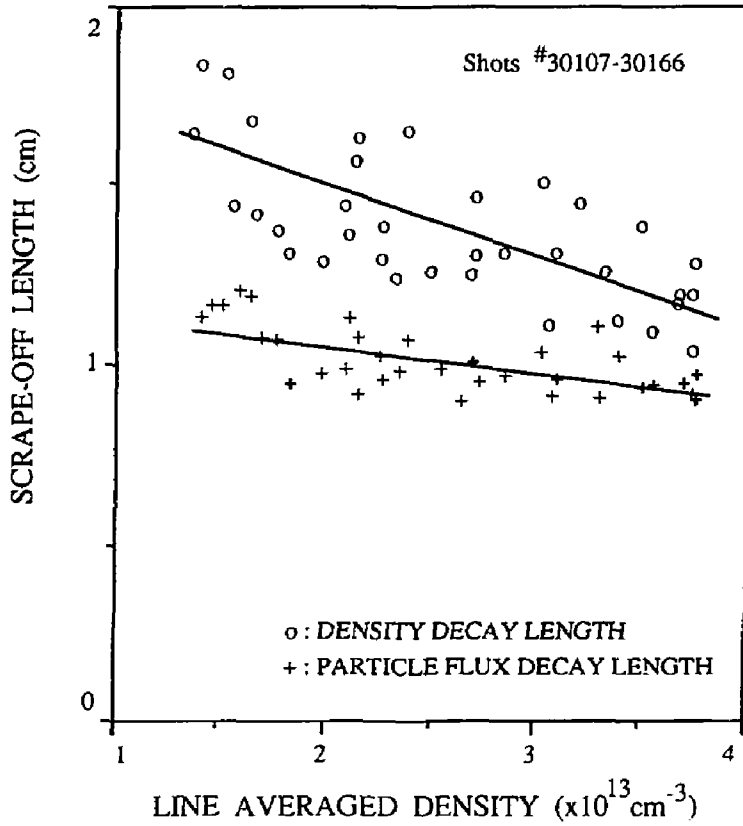


Figure 4

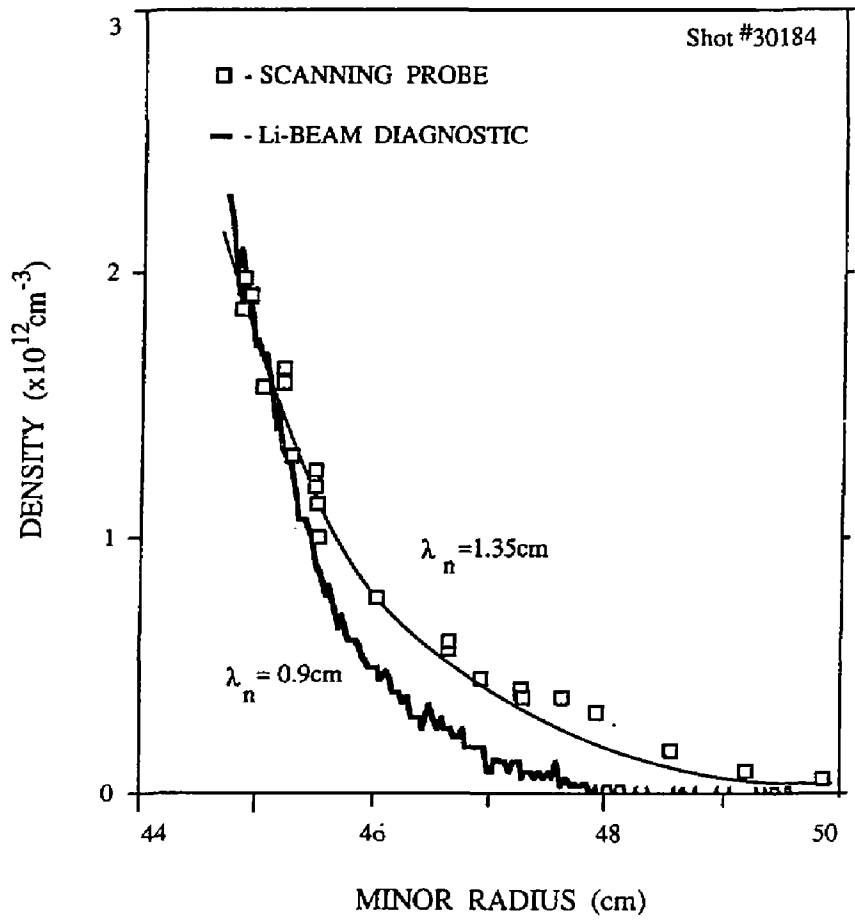


Figure 5

ALT-II Toroidal Belt Pump Limiter Performance in TEXTOR

D.M. Goebel¹, R.W. Conn¹, W.J. Corbett¹, K.H. Dippel², K.H. Finken²,
W.B. Gauster³, A. Hardtke², J.A. Koski³, W. Kohlhaas², R.T. McGrath³,
M.E. Malinowski⁴, A. Miyahara⁵, R. Moyer¹, A. Sagara⁵, J.G. Watkins³,
G. Wolf², the TEXTOR Team², and the ICRH Team⁶

¹ Institute of Plasma and Fusion Research, and Department of Mechanical, Aerospace and Nuclear Engineering, University of California, Los Angeles, CA 90024, U.S.A.

² Institut für Plasmaphysik, Kernforschungsanlage Jülich, Association EURATOM-KFA D-5170 Jülich, Fed. Rep. Germany

³ Sandia National Laboratories, Albuquerque, NM 87185, U.S.A.

⁴ Sandia National Laboratories, Livermore, CA 94550, U.S.A.

⁵ Institute of Plasma Physics, Nagoya University, Nagoya Japan

⁶ Ecole Militaire/Koninklijke Militaire School, Association EURATOM-Belgian State B-1040 Brussels, Belgium

ABSTRACT

The Advanced Limiter Test (ALT-II) is a toroidal belt pump limiter in the TEXTOR tokamak. ALT-II is composed of 8 blade segments which form an axisymmetric toroidal belt of 3.4m^2 exposed surface area, located on the outside of the torus at 45° below the horizontal midplane. Ohmic plasma operation with ALT-II as the main limiter is characterized by a line-averaged density range of 5×10^{12} to $5.5 \times 10^{13} \text{ cm}^{-3}$ at $B_T = 2\text{T}$ and $I_p = 340\text{kA}$, $Z_{\text{eff}} = 1.1$ to 2 and typically 40 to 95% of the power radiated depending on the plasma density. ICRH heating of the plasma with up to 2.6MW of incident power has been achieved, which modifies the scrape-off layer (SOL) and the pump limiter performance. The recycling coefficient in TEXTOR is normally close to one, but helium RG conditioning and baking of the limiter at 400°C is found to lower the recycling coefficient to 0.8 for the order of 10 shots. Measurements by arrays of probes in the SOL and thermocouples in the limiter tiles indicate the flow to the limiter is toroidally symmetric (taking field ripple into account) and poloidally asymmetric. Poloidal asymmetries result in different power and particle fluxes to the ion and electron drift sides of the limiter. The density and power scrape-off lengths are on the order of 1-2 cm and significantly longer on the outside of the torus (electron drift side). In spite of the flow asymmetry favoring the ion drift side near the tangency point, the longer e-folding lengths on the electron side in the SOL result in equal or

higher particle collection by the electron side. The probe arrays indicate that during ohmic heating a total of 15 to 20% of the core efflux is incident on the neutralizer plates located in scoops beneath the blades. More particles are collected during ICRH auxiliary heating due to changes in the e-folding lengths and shorter particle confinement times. Based on particle removal experiments with pumping on one blade, the total exhaust efficiency of the limiter if pumped at all eight blades is 5 to 10%.

1. Introduction

The ALT-II pump limiter^{1,2} is an axisymmetric toroidal belt installed in the TEXTOR tokamak³ with the objectives of optimizing plasma performance and studying the physics of particle removal, recycling and impurity control with large area limiters in tokamaks. The plasma quality and confinement performance of tokamaks has been shown to depend critically on the edge plasma characteristics and recycling. Tokamaks with magnetic divertors⁴ have demonstrated a modification of the edge profiles and enhanced confinement. The conditioning of the inner graphite bumper-limiter in TFTR to produce transient low recycling has resulted in improved confinement during neutral beam fueling and heating⁵. Modular pump limiters have been investigated⁶⁻⁸ to provide continuous density and impurity control by reducing the recycling at the plasma boundary. The ALT-I program in TEXTOR⁹⁻¹¹ studied the particle and heat removal capabilities of several modular pump limiter geometries. While increasing the number of modular limiters can provide high power removal through power sharing, such as the system planned for Tore Supra¹², the particle removal capability of the limiter system does not increase in proportion to the number of limiters. This is because direct shadowing of the pump limiter entrances can occur with multiple modular limiters.

With a toroidal belt, the limiter surface is made large to distribute the heat, and the shadowing of particle collection regions is alleviated by uniformly placed neutralizer plates. In addition, the leading edge of the entrance slot is oriented in the toroidal direction, which reduces the heat flux when compared to a modular pump limiter where the leading edge is inherently perpendicular to

the field lines. Thus the toroidal belt pump limiter is more relevant for particle control in high power fusion plasmas. ALT-II is designed to exhaust 5 to 10% of the core efflux by active pumping to investigate the physics of particle removal and recycling control in a toroidal pump limiter geometry. Conditioning of the limiter surface can also be used to further reduce the recycling by graphite-surface pumping with the tiles.

In this paper, the first results from ALT-II experiments are reported. After a description of the belt pump limiter configuration, the plasma performance and recycling conditions achieved on the limiter are presented. The difference in the scrape-off layer (SOL) between the belt limiter and modular limiters as they affect particle removal, and the heat distribution on the blades, are discussed. Finally, the particle removal capability of ALT-II in ohmic and ICRH discharges is presented based on pumping experiments at two of the blades.

2. Experimental arrangement

The ALT-II limiter consists of eight radially moveable blades forming an axisymmetric toroidal belt located 45° below the outside horizontal midplane. The plasma facing surface of each blade is covered by shaped graphite tiles¹³ bolted to an inconel base plate. The blades are 150cm long and 28cm wide, representing about 3.4m² of graphite area exposed to the plasma. The belt is designed to collect up to 4MW of power for 3sec, and each blade is curved in the toroidal and poloidal directions to distribute the incident heat loads. The tiles and base plate together are only 1.7cm thick to optimize the number of particles that diffuse behind the front surface and flow to the collection scoops under the limiter. Two segments of the belt limiter are shown installed in TEXTOR in Fig.1. Each blade is supported by 2 worm-and-screw driven jacks¹⁴, each capable of 5cm of motion for blade positioning and alignment. The jacks are mounted on the liner and connected by a linkage system to motors outside the vacuum system.

Each blade is equipped on the underside with a localized particle collection region and vacuum ducting to a pumping unit. Pumps are currently installed on only two of the blades. A view of the vacuum system at blade #2 is shown in a poloidal cut of TEXTOR in Fig.2. Neutral gas

produced by plasma striking the neutralizer plate flows through vacuum ducting to a pumping system consisting of Zr-Al getter pumps and a turbomolecular pump. The Bayard-Alpert ionization gauge on each pumping system can monitor the neutral density either at the pumps or at the neutralizer plate by opening the proper vacuum valves. Since the ionization gauge measures the pressure between the two pumps, the real pumping speed of the system is difficult to obtain. The particle removal rate of each blade system is calibrated by injecting calibrated gas flows into the vacuum-elbow section in front of the getters with the valve to TEXTOR closed, and measuring the indicated pressure by the gauge for each flow rate. The effective pumping speed of each system is estimated to be on the order of 4000 l/sec.

To decrease the backflow of gas from the neutralizer plate to the plasma, graphite scoops are installed to form a channel in which the plasma flows toward the plates. A view of the underside of two blades, as seen from the bottom, is given in Fig.3. Four of the blades are equipped with scoops which accept particles only from the ion drift direction. For comparison, the other four blades have scoops in both the ion and electron drift directions. Therefore, ALT-II at present has eight ion side scoops and four electron side scoops. The scoops have inside dimensions of 2.5cm in the radial dimension and 13.5cm in the poloidal direction. However, the area of the plasma which flows into each scoop is determined by poloidal shadowing from the scoops and neutralizer plates on the adjoining blades. This situation is also shown schematically in Fig.3. The poloidal extent of the scoops and neutralizer plates is chosen such that the plates extend at the design q over the full poloidal projection of the belt and collect all of the particles flowing in the SOL under the blade. In fact, the plates are positioned poloidally to provide a small shadow in the plasma in which the blade supports are placed.

Standard conditions in the tokamak during ALT-II operation in deuterium are: $n_e = 1$ to $5 \times 10^{13} \text{cm}^{-3}$, $B_T = 2.0 \text{T}$, $I_p = 340 \text{kA}$, $R_0 = 1.75 \text{m}$, $a = 44$ to 46cm , liner temperature = 150°C . Plasma current of up to 480kA , toroidal fields of 2.6T , and liner temperatures of 400°C have been used. TEXTOR is normally carbonized¹⁵ before plasma operation by utilizing deuterated methane in either deuterium or helium RG discharges. The wall conditioning has been further

improved by helium rf-assisted glow discharge (RG) cleaning immediately before plasma shots, which reduces the amount of deuterium and oxygen in the carbonized layer. The SOL flux, density and temperature are measured by several diagnostics in the edge¹⁶. The scanning probe¹⁷ is a pneumatically driven double probe which scans a distance of 15 cm, moving from behind the TEXTOR liner to near the limiter tangency point in a time of about 0.1sec. After each shot the probe characteristics are automatically fitted, and profiles of the ion flux, density, and electron temperature plotted. The scanning probe is located on the horizontal midplane of TEXTOR, which is normally on the electron drift side of ALT-II. An array of 21 probes¹⁸ is positioned under the blades to provide local SOL information in the scoops. Finally, the Li-beam diagnostics^{19,20} on the top and bottom of TEXTOR are used to determine the poloidal symmetry of the density and electron temperature, and their respective scrape-off lengths.

3. Plasma operation on ALT-II

Conditioning of the 3.4m² of limiter surface area was achieved by extensive baking at 400°C, RG cleaning in hydrogen, deuterium and helium, and carbonization¹⁵ of the limiter and liner surfaces. Plasma performance was strongly affected by the conditioning procedure used in the machine. After standard RG conditioning and carbonization in deuterium, the plasma density range was examined during operation on ALT-II. Line averaged plasma densities below 5x10¹²cm⁻³ were routinely obtained without hard X-ray production from run-away electrons due to the large area graphite surface. Inspection of the blades and tiles after operation failed to find any localized damage. The density limit with this conditioning procedure at the standard machine conditions described above was found to be about 4x10¹³cm⁻³, which is the same as that found during operation on the poloidal limiters. The operation space of the machine on the Hugill diagram was found to be similar with ALT-II as that achieved on the poloidal limiters³ with the standard conditioning procedure. The radiated power varied from 50 to 100%, increasing with the plasma density to detachment²¹. The recycling coefficient, *R*, during these shots was always approximately equal to one.

The energy confinement time has been improved in many machines above the L-mode scaling²² through a modification of the recycling in the boundary.^{4,5,23} In an attempt to reduce the hydrogen inventory and release by ALT-II and the limiter in TEXTOR, the carbonization procedure was performed in a He RG discharge with a limiter temperature of 150°C. RG discharge cleaning in He was also performed for 15min before plasma shots. During plasma discharges, the recycling coefficient was found to remain near one, and the density was difficult to control. However, the oxygen level in the machine was reduced by a factor of about 4 compared to the D conditioning procedure, which resulted in an extended density limit over that previously achieved in TEXTOR to $5.5 \times 10^{13} \text{cm}^{-3}$. The energy and particle confinement times, τ_E and τ_p respectively, are plotted in Fig.4 versus the line averaged plasma density when ALT-II is the limiter, for the two conditioning cases. The values of τ_p were obtained from the scanning probe data, as will be described later. The decrease in oxygen and resulting lower Z_{eff} (~ 1.5) resulted in increased energy and particle confinement times, a higher density limit, and a reduction in the radiated power by 10 to 20% at any given density.

Low recycling operation was achieved with ALT-II by repeating the carbonization and RG discharge cleaning techniques in helium, but including heating of the limiter to 400°C for four hours before shots. The line averaged core density versus time for the fifth shot of the day is shown in Fig.5. Heavy gas puffing was required to raise the density, and the plasma density decayed rapidly once the gas was turned off. The effective particle containment time, defined by $\tau_p^* = \tau_p / (1-R)$, where R is the recycling coefficient,^{6,7} is evaluated from the time decay of the density. The value of τ_p^* decreased from a normal value of 2 to 5sec to 0.6sec with the strong pumping by the limiter and walls. The value of R was also reduced from near 1 to about 0.8. This low recycling condition lasts for approximately 10 shots, during which time the recycling coefficient gradually increases again toward one. It is possible that the He conditioning technique left mostly weakly bound hydrogen on the limiter surfaces, which was removed by the high temperature outgassing. The limiter and walls would then gradually fill up from the hydrogen

bombardment from the discharge. An additional 15 to 30 min of He RG discharge was observed to reduce the recycling temporarily, but was not as effective as the high temperature baking.

The low recycling condition produced by this conditioning procedure featured very low impurity levels. Z_{eff} in ohmic discharges, determined from the soft X-ray continuum, was reduced from a standard level of between 1.5 and 2 to a lowest value of 1.4 in deuterium and 1.1 in hydrogen at a line averaged density of about $2 \times 10^{13} \text{cm}^{-3}$. From spectroscopic measurements in the plasma, the oxygen level decreased by a factor of 4 to 5 compared to the standard conditioning procedure, which resulted in an increased density limit and a decrease in the lowest radiated power to about 40% of the input power. As the recycling increased from shot to shot, the oxygen level also increased to its previous values. This behavior of a saturation in the recycling and increasing oxygen levels as a function of the number of shots did not occur when the carbonized layer was doped with boron.²⁴

4. Belt limiter operation

The effect of operation with a full toroidal belt limiter, compared to modular limiters, is to reduce the average connection length of the flux tubes in the torus, which reduces the SOL density and particle decay lengths. This is illustrated in Fig.6, where the density and electron temperature profiles from the scanning probe are given for the case of a single blade of ALT-II positioned at a plasma minor radius of 44cm and the remaining 7 blades forming an effective belt positioned at 47.5cm. The scanning probe is not "shadowed"²⁵ by any of the limiters or the belt in the tokamak because the collection length of the very small probe tip is only 1-2m, and the distance along a field line to the belt is 3.5m. For the SOL region with only a single blade from 44 to 47.5cm, the e-folding length is found to be greater than 4cm. At the position of the belt limiter (47.5cm), the average connection length is reduced and the e-folding lengths fall to the characteristic values ($\approx 1.6\text{cm}$) found with the belt.

The density e-folding length in the SOL, λ_{n0} , can be simply described⁷ by

$$\lambda_{ne} = \left(\frac{D_{\perp} L}{f c_s} \right)^{\frac{1}{2}} \quad (1)$$

where D_{\perp} is the perpendicular diffusion coefficient, L is the flux tube connection length, $c_s = [k(T_e+T_i)/M_i]^{1/2}$ is the acoustic sound speed. $T_{e,i}$ are the electron and ion temperatures respectively, M_i is the ion mass, and f is the fraction of the sound speed that the plasma flows at over the length of the flux tube. The belt limiter always connects to itself after approximately q rotations around the torus. The average connection length over which plasma is collected by the flux tube and flows toward the toroidal belt limiter is then roughly $2\pi q R_0/2$, where q can be estimated from $q_{cyl}(r) = r B_T/R_0 B_p$, where r is the radius of the limiter, B_T is the toroidal field, B_p is the poloidal field, and R_0 is the major radius of the torus. For a deuterium plasma in TEXTOR with $R_0 = 175\text{cm}$, $q(a) = 3.2$, $D_{\perp} = (1/3)D_{Bohm} = 2.7 \times 10^3 \text{ cm}^2\text{sec}^{-1}$, $T_e = T_i = 30\text{eV}$, and $f = 0.3$, Eq.1 predicts that λ_{ne} is equal to 1.78cm, in good agreement with the data from Fig.6 for the belt.

The fact that the toroidal belt limiter always connects to itself suggests that the average connection length for flux tubes at a given poloidal angle is the same for every toroidal angle. Likewise, the average connection length for flux tubes at a given toroidal angle is the same for every poloidal angle. This picture suggests a toroidally symmetric scrape-off layer plasma with uniform e-folding lengths. In fact, the 21 probes arrayed in the scoops indicate that the ion flow to the belt is toroidally symmetric if the toroidal field ripple is taken into account. The toroidally uniform SOL and short density e-folding lengths with ALT-II result in 10 to 90% of the core efflux incident on the blade²⁶. The connection length with a modular limiter system depends on the specific flux tube being considered and the mapping of that tube to the individual limiters. For non-integer values of q , the flux tube may never intersect the limiter, the connection length is very long, and the e-folding lengths increase as seen in Fig.6. The longer λ_{ne} with modular limiters resulted in significantly higher liner fluxes compared to operation with ALT-II²⁶.

The heat flux to the belt was studied with infrared camera views of two blades²⁷. In Fig.7a, an infrared image of blade #2 is shown near the end of a 3 second ohmic discharge. The maximum

temperature rise on the tiles during this discharge was 25°C, which is typical of ohmic discharges. The individual graphite tiles can be seen along with mounting screws. The direction of the toroidal field and plasma current in TEXTOR are such that the plasma flowing in the ion drift direction passes along the bottom of the torus and strikes the lower toroidal edge of the belt, coming from the lower right corner of the image in Fig.7a.. Likewise, the plasma flow in the electron drift direction crosses the outside (large major radius) of the torus and strikes the top toroidal edge of the belt.

The ion side of the blade is seen in the figure to receive a higher heat flux. This is due to an asymmetry in the particle and power flow directions previously observed in TEXTOR^{11,28}, and a major radius misalignment of the belt due to thermal expansion of the heated liner. At a liner temperature of 150°C, a horizontal outward displacement of the magnetic axis by 3-5mm is required to align the system. For a properly aligned system, the flow asymmetry results in up to 3 times more flux on the ion drift side compared to the electron side at densities below $2 \times 10^{13} \text{cm}^{-3}$, decreasing to almost equal fluxes at high density. Also apparent from the figure is the toroidal variation in the heat flux due to field ripple. The ripple causes the tiles at the center and ends of each blade, located between two adjacent toroidal field coils, to contact the plasma first and receive higher heat and particle fluxes.

Finally, note that each tile gets much hotter on one side than on the other, and that the right side of the bottom tiles and left side of the top tiles are hotter. While the base plates of the blades have both toroidal and poloidal curvature, the tiles are poloidally curved and toroidally flat. Analysis of the edge region magnetic field structure¹² shows that there are slight differences in the vector addition of the toroidal and poloidal fields on the left and right side of each tile. Since the field lines are nearly tangent to the tile surfaces, small differences in the vector algebra affect the exact incident angle and produce variations in the incident heat fluxes of a factor of five across the face of each tile. The inversion of the hot side from top to bottom of the blade is due to an overall sign change of the poloidal component of the flow.

Shown in Fig.7b are calculated values for the incident heat flux onto the ALT-II tiles for the ohmic discharge discussed above. Included in the calculation are the full three-dimensional geometry of the blades, tiles and magnetic field structure in the TEXTOR edge. The radial dependence of the power flux is described using a scrape-off length of 1.0cm, and symmetric ion/electron side flows are assumed. The bottom to top (ion/electron side) asymmetry shown in the figure is caused by the 5mm misalignment of the magnetic axis with the toroidal axis of the blade due to the expansion of the liner. The effects of magnetic ripple and the asymmetric loading on the individual tiles, as discussed above, can be clearly seen in the analytical results.

5. Pump limiter performance

Particles in the SOL that diffuse beyond the 1.7cm of blade thickness flow along the field lines to the collection scoops and can be pumped by the vacuum system. Any objects inserted into the SOL intersect the particles flowing toward the scoops, reduce the particle e-folding length, and decrease the collection by the limiter. This behavior is shown in Fig.8, where the total current into the scoops calculated from an integration of the flux probe data is plotted for a series of shots where the limiter was moved. Note that there are 8 ion drift side scoops and only 4 electron drift side scoops. Initially, the belt was positioned at 46cm, the ICRH antenna was located at 47cm, and the scoops collected about 30A of ions. Moving the belt to 44cm then provides a 1.3cm gap between the blades and antenna for particles to flow into the scoops, and the total current to the scoops increases to about 40A. The increase occurs primarily on the electron drift side due to the fact that the antenna shadows that side of the blades.

The shadowing of the scoops is well predicted by a mapping of the magnetic field lines¹² in the SOL. The TEXTOR torus is unfolded in Fig.9 and drawn in terms of poloidal and toroidal angles with the positions of the eight ALT-II blades and the two ICRH antennae indicated. The field line shown is mapped from the blade toward the electron drift side scoop of blade #2, and is intersected by antenna #2 close to the blade. This shadowing of the electron drift side scoops by the antennae causes the behavior shown in Fig.8. The degree of shadowing is proportional to the

connection length to the obstruction. Close objects like the antenna (within 1 toroidal turn) cause a 50 to 100% reduction in the collected current. Other limiters in the SOL over 3 toroidal turns away ($L > 30\text{m}$) have been observed to reduce the scoop collection by 10 to 20%. Shadowing effects from these remarkably long connection lengths mapped to the blades suggest that rotation of the plasma is not a significant process in TEXTOR. In addition, poloidal diffusion cannot greatly exceed the radial diffusion in the boundary or the shadow would be filled.

The particle removal capabilities of ALT-II have been investigated with the pumps at blades #2 and 6. The particle removal rate of each blade for ohmic discharges is shown in Fig.10 for a core density scan. Blade #2 removes more than twice the amount of #6, and the total amount increases with the core density. This pumping difference between the blades exists because #2 has both ion and electron side drift scoops, and collects more ions than blade #6. As seen in Fig.10, the ion drift side current collection by the two blades is roughly the same. The electron drift side scoop collects more ions than the ion side because the particle e-folding length on the outside of the torus is found to be a factor of 1.5 to 2 times higher than on the bottom of the torus^{16,17}. The higher collection by the electron side scoop results in more than twice the current to blade #2. At equal radii of 44cm, the total ion collection by the present configuration of ALT-II with 12 scoops is about equal to the modular ALT-I,²⁷ with an actual value of 40 to 50A for ohmic discharges. It is planned to increase the ALT-II collection capabilities by an additional 30% during the next machine opening by adding three more electron side scoops.

The pumping response of the ALT-II system is linear with the incident flux, in contrast to the results from ALT-I²⁹. The removal efficiency, defined as the ratio of the pumping rate to the ion current into the scoops, is plotted in Fig.10 and shown to be about 25% for both blades for these shots. The removal efficiency typically ranges between 25 and 30% for ALT-II operation. The removal efficiency for ALT-II is roughly half that reported for the modular ALT-I¹⁰, due to the long vacuum ducting to the pumps and lower pumping speeds per blade for ALT-II.

The reason that the total removal rate increases with core density and that the removal efficiency is constant is apparent from the SOL profiles. In Fig.11, the density and iron

temperature profiles from the scanning probe for two values of the core density are shown. While the density e-folding length decreases as the core density increases, the magnitude of the SOL density is found to increase proportionally to the core density. Extrapolating the scanning probe data to the tangency point, one can find $n_e(a)$. This value of the edge density is approximately linear with the line average plasma density. The increase in SOL density and localized modifications in the profiles (toward non-exponential) produce higher particle collection by the scoops at higher core densities. The scoops collect particles in the SOL only beyond 45.7cm, where the plasma density is below $5 \times 10^{11} \text{cm}^{-3}$. This low plasma density results in negligible plasma neutral interactions in the scoops, and a constant removal efficiency²⁹. The T_e profile is observed to flatten in the SOL as the core density increases, and the values of T_e can be reduced to below 10eV. This behavior appears to be a continuous transition toward detached plasmas as the core density rises, where the T_e profile gradually becomes very flat and cold and the density profiles are modified.

To evaluate the exhaust efficiency of ALT-II, defined as the limiter removal rate by the pumps divided by the core efflux, it is necessary to know the core efflux. The number of particles diffusing past the last closed flux surface²⁸, assuming exponential scrape-off lengths, is given for each side of the belt by

$$\Gamma_T = \int_0^\theta d\theta \int_0^a \Gamma(a) \exp(-(r-a)/\lambda_\Gamma) r dr, \quad (2)$$

where θ is the one turn poloidal projection of the toroidal belt limiter, $\Gamma(a)$ is the parallel flux at the tangency point, λ_Γ is the particle flux e-folding length, r is the radius, and a is the limiter radius. The poloidal projection of the toroidal belt is $2\pi/q(a)$, and Eq.2 is integrated to give

$$\Gamma_T = \kappa \frac{2\pi}{q(a)} \Gamma(a) \lambda_\Gamma (a + \lambda_\Gamma), \quad (3)$$

where κ is a factor included for the amount of current to the ion and electron drift sides of the belt. For ohmic discharges, κ is found from an evaluation of the the Li-beam profiles on the ion

side and the scanning probe profiles on the electron side to be about equal to two. Any non-exponential flux profiles must be directly integrated to determine the core efflux from the SOL diagnostics.

Once the core efflux is known, it is possible to define a global particle confinement time:

$$\tau_p = \frac{N}{\Gamma_T} = \frac{q(a) \bar{n}_e V}{2\pi\kappa \Gamma(a) \lambda_T (a + \lambda_T)} \quad (4)$$

where N is the total number density in the tokamak, \bar{n}_e is the line averaged density, $V=2\pi^2Ra^2$ is the plasma volume, and $q(a)$ is set to 3.25 for proper matching of the scoops to the field lines. Once the scaling of the particle confinement time is known with \bar{n}_e or with ICRH power, the core efflux is easily determined. From Fig.4, τ_p is found to be linearly proportional to \bar{n}_e , and the core efflux is thus approximately constant during a density scan. From the scanning probe data during ALT-II operation, the total core efflux is about $1.6 \times 10^{21} s^{-1}$. This agrees well with the values from previous TEXTOR measurement using ALT-I²⁸ or the poloidal limiters³⁰.

The present configuration of ALT-II with 12 scoops collects 40 to 50A of ions during ohmic discharges, which is 15 to 20% of the core efflux derived above. An estimate of the total potential exhaust efficiency of ALT-II can be made using the collected current at blade #2, as shown in Fig.10. Adding three electron side scoops will increase the collection efficiency of the belt to 9A per two-sided blade, or up to 26.5%. If pumps are installed at all eight blades, and the removal efficiency remains between 25 and 30% at every blade, then the total exhaust efficiency of ALT-II will be in the range of 5 to 10%.

6. Operation with ICRH auxiliary heating

The ICRH heating system³¹ installed in TEXTOR has two pairs of antennae³² located 180° toroidally apart and on the outside-top of the torus. During operation with ALT-II, up to 2.6MW of ICRH power³³ has been coupled into TEXTOR. The ICRH auxiliary heating leads to a

significant modification in the plasma boundary, and in the particle removal performance of the pump limiter. In Fig.12, the plasma density, ICRH power, ion and electron side probe fluxes, and particle removal rates are shown for a shot with 1.4MW of ICRH power coupled to the plasma. With the recycling coefficient close to 1 before ICRH in this shot, desorption of hydrogen and oxygen from the walls by the ICRH results in a rapid core density increase, followed by a plasma disruption at the end of ICRH pulse. The pumping by ALT-II is observed to increase during ICRH heating, resulting in a two-fold increase in the pumping by blade #2 for this shot. This behavior is due to a change in the particle fluxes to the blades and a modification in the SOL with ICRH.

In general, the flux of particles to the ion drift side scoop of blade #2 is found to increase in proportion to the ICRH power level. The scanning probe and ALT-II probes indicate that this flux increase is due to a reduction in global τ_p with auxiliary heating. As shown in Fig.4, τ_p follows τ_E in the ohmic phase in TEXTOR, and this behavior continues during ICRH heating when τ_E decreases as described by L-mode scaling³³. However, the flux to the electron side probe does not follow this trend, and can even decrease with ICRH power. To explain this effect, the electron side SOL n_e and T_e profiles from the scanning probe during 1.33MW of ICRH power are shown in Fig.13. The ICRH heating modifies the boundary by reducing the n_e and T_e e-folding lengths and increasing the plasma density near the tangency point. Further in the SOL, the density is reduced because of the shorter e-folding length, but the profile is flattened and local bumps in n_e and T_e observed. The plasma production and increased T_e deep in the SOL could be attributed to localized power deposition in the edge by parametric instabilities³⁴, and may explain the localized sputtering and metal impurity production previously observed during ICRH in TEXTOR³⁵.

In spite of an increase in the core efflux and the tangency point density with ICRH, the particle collection in the blade #2 electron drift side scoop decreased for this shot due to the profile modifications which resulted in lower edge densities. At higher ICRH powers, the flat density profiles and large density bumps in the SOL can result in increases in the electron side

scoop particle collection if the bumps occur at the same radius as the scoops. Electron side scoops that do not map to the active antenna regions tend to behave in the same manner as the ion side scoops. Since the SOL modifications are not observed by the ion drift side probes, it is likely that the perturbations are somewhat local (within 1-2 toroidal turns) and related to the antennae.

If the increased removal rates with ICRH were due only to τ_p changes with auxiliary heating, then the exhaust efficiency of the pump limiter with heating would be unchanged because the removal efficiency is nearly constant. The modifications in the SOL on the outside midplane due to the ICRH antennae tend to reduce the collection by the electron side scoops at low power and increase it at high power. The exhaust efficiency of ALT-II with ICRH auxiliary heating will then depend on the details of the boundary modifications, but is expected not to change dramatically based on the present work.

7. Conclusions

Plasma operation in TEXTOR with ALT-II and improved conditioning techniques features an enlarged operating density range of 5×10^{12} to $5.5 \times 10^{13} \text{ cm}^{-3}$ at standard toroidal field and plasma current, $Z_{\text{eff}} = 1.1$ to 2 and typically 40 to 95% of the power radiated depending on the plasma density. ICRH heating of the plasma with up to 2.6 MW of incident power has been achieved. The ICRH heating increases the pump limiter particle removal rate by a reduction of τ_p , but does not significantly change the exhaust efficiency of ALT-II. Strong modification of the SOL by ICRH heating is observed in the profiles of the density and electron temperature, which can affect the pumping rate of the limiter. The recycling coefficient with ALT-II can be reduced to about 0.8 for the order of 10 shots by helium RG conditioning and baking of the limiter at 400°C. The flow to the limiter is toroidally symmetric if the field ripple is taken into account, and poloidally asymmetric. The density and power scrape-off lengths are on the order of 1-2 cm and significantly larger on the outside of the torus (electron drift side). The particle and power flow asymmetry is higher on the ion drift side near the tangency point at lower

densities, and becomes more balanced as the density increases. The longer e-folding lengths on the electron drift side in the SOL result in equal or higher particle collection by the electron side scoops, compared to the ion side scoops. The probe arrays indicate that a total of 15 to 20% of the core efflux is incident on the neutralizer plates during ohmic heating in the present configuration, which will be increased to over 25% by the addition of more electron side scoops. Based on particle removal experiments with pumping at one of the two-sided blades, the total exhaust efficiency of the limiter if pumped at all eight blades is 5 to 10%. This exhaust rate equals the design values of the system^{1,2}.

Acknowledgments

The authors would like to thank J.Banks, G.Brown, S.Grotz, C.Stickelman, M.Schumacher, T.Uchikawa, and R.Watson, for their efforts in the engineering design and fabrication of ALT-II, and K.Andrews, G.Gunner, A.Hiller, V.Low, K.Sheedy, T.Sketchely, and A.Verberkmoes for technical support of the ALT-II program.

* Work supported by the U.S. Department of Energy under contract #DE-F603-85 ER 51069.

References

1. R.W.Conn, D.M.Goebel, S.P.Grotz, et al., J.Nucl.Mat. 121 (1984) 350.
2. J.A.Koski, R.D.Boyd, S.M.Kempka, et al., J.Nucl.Mat. 121 (1984) 309.
3. K.H.Dippel, H.L.Bay, G.Bertschinger, et al., J.Nucl.Mat. 145-147 (1987) 3.
4. F.Wagner, et al., Phys.Rev.Lett. 49 (1982) 1408.
5. H.F. Dylla, these proceedings.
6. P.K. Mioduszewski, J.Nucl.Mat. 111&112 (1982) 253.
7. R.W. Conn, J.Nucl.Mat. 128&129 (1984) 407.
8. D.M. Goebel, Fusion Technology 10 (1986) 761.
9. R.W.Conn, S.P.Grotz, A.K.Prinja, et al., Proc. 10th Symp. on Fusion Tech.(SOFT) Jülich, Vol.1 (Pergamon Press, New York, 1983) p.497.
10. A.E.Pontau, S.E.Guthrie, M.E.Malinowski, et al., J. Nucl. Mat. 128&129 (1984)434.
11. K.H.Dippel, K.H.Finken, S.E.Guthrie, et al., Plasma Physics and Controlled Nucl. Fusion Research (Proc. 10th Intl. IAEA Conf., London 1984), Vol. 1, IAEA Vienna (1985).
12. R.T.McGrath, C.C.Klepper, T.Uckan, P.Mioduszewski, "A Model for Diffusion in the Tokamak Edge Region and Application to the Modular Pump Limiters on Tore Supra", to be published in Fusion Technology, 1988.
13. R.T.McGrath, Sandia Report #SAND86-0615, June 1986.
14. G.W. Brown, Fusion Technology 10 (1986) 795.
15. J. Winter, J.Nucl.Mat. 145-147 (1987) 131.
16. A.Pospieszczyk, F.Aumayr, H.L.Bay, et al., these proceedings.
17. D.M.Goebel, W.J.Corbett, R.W.Conn, et al., Proc.15th EPS, Dubrovnik Yugoslavia, May 16-20, 1988.
18. W.J. Corbett, D.M.Goebel, R.W.Conn, et al., these proceedings.
19. Y.T.Lie, K.Hoethker, W.Bieger, K.Kadota, Proc. Intl. Conf. on Plasma Physics, Lausanne (1984) 320.
20. A.Pospieszczyk, G.Ross, Proc.14th EPS, Vol. III-1280, Madrid Spain, June 22-26, 1987.

21. U.Samm, H.Bay, P.Bogen, et al., "Properties of Detached Plasmas", KFA Jülich Report #Jül-2123, ISSN #0366-0885 (1987).
22. S.M.Kaye and R.J.Goldston, *Nuclear Fusion* 25 (1985) 65.
23. S.Sengoku, these proceedings.
24. J.Winter, H.G.Esser, V.Philipps, et al., these proceedings.
25. P.Stangeby, *J.Phys.D*, 18 (1985) 1547.
26. U. Samm, these proceedings.
27. K.H.Finken, J.G.Watkins, R.T.McGrath, et al., these proceedings.
28. D.M.Goebel, G.A.Campbell, R.W.Conn, et al., *Plasma Physics and Controlled Fusion* 29 (1987) 473.
29. G.A.Campbell, D.M.Goebel and R.W.Conn, UCLA Report #PPG-958, 1986.
30. U.Samm, et al., Proc. IEEE Conf.Plasma Sci., Austin, Texas, Nov. 1985, IEEE Journal of Plasma Science (1986).
31. G.Van Oost, V.P.Bhatnager, T.Delvigne, et al., *Fusion Technology* 12 (1987) 449.
32. A.M.Messian, J.M.Beuken, L.DeKeyser, Proc.15th EPS, Dubrovnik Yugoslavia, May 16-20, 1988.
33. A.M.Messian, V.P.Bhatnager, T.Delvigne, et al., *Plasma Physics and Controlled Fusion*, 28, 71 (1986).
34. R. VanNieuwenhove and G.Van Oost, "Observation of Harmonic and Parametric Decay Instabilities During ICRH Heating on TEXTOR", Proc.15th EPS, Dubrovnik Yugoslavia, May 16-20, 1988.
35. B.Schweer, et al., Proc.13th Europ. Conf. Cont. Fus. and Plasma Heating, Schliersee, (1986).

Figure Captions

1. Photograph of two blades segments of the ALT-II toroidal belt limiter installed in TEXTOR.
2. Poloidal cross section of TEXTOR showing the vacuum ducting from the ALT-II blade to the getter and turbomolecular pumps. The ionization gauge can measure the pressure either in the neutralizer region or by the pumps.
3. Bottom view of two of the blades showing the scoops and the flux tubes that map
4. Energy and particle confinement times during an ohmic density scan with TEXTOR operating on the ALT-II limiter. The He RG conditioning and carbonization provides a higher density limit and confinement times compared to the standard conditioning procedure.
5. Line averaged core density and gas feed pulse versus time after carbonization and conditioning of ALT-II in a He RG discharge, and baking of TEXTOR at 400°C. The strong pumping by the limiter and walls results in a low particle containment time and rapid decrease of the density with time after the gas feed is turned off.
6. Scrape-off layer density and electron temperature profiles from the scanning probe for the condition of one ALT-II blade located at 44cm and seven blades positioned at 47.5cm. The shorter average connection length with the toroidal belt compared to a modular limiter result in shorter density and temperature e-folding lengths.
- 7a. An infrared camera image of an ALT-II blade near the end of a 3s ohmic discharge. The maximum temperature rise recorded for this shot was about 25°C.
- 7b. Heat flux incident on the ALT-II blade calculated using a three-dimensional model of the blade tiles and magnetic field structure in TEXTOR. Maximum loading is 50W/cm² for this ohmic discharge.
8. Total current collected by the 12 ALT-II scoops from an integration of the flux probe data. As the limiter is moved from a radius of 46 to 44cm, the shadowing of the scoops by the ICRH antenna at 47cm is reduced and the collected current increases. The increase is greatest for the electron drift direction scoops because the obstruction (the antenna) is located on the electron drift side of the belt.

9. Magnetic field line tracing in TEXTOR with the toroidal and poloidal angles of the torus shown unfolded. The plot traces a flux tube starting from the belt and ending at the electron drift side scoop of blade #2 in the upper right hand corner. The plasma flowing from the stagnation point near the middle of the flux tube toward the scoop can be intersected by the ICRH antenna relatively close to the blade.
10. Particle removal rate by the pumps at two blades, total current into each scoop, and removal efficiency during a density scan. The two-sided collection by blade #2 results in higher pumping rates because the electron side scoop collects up to 50% more current and the removal efficiency is the same for both blades.
11. Density and electron temperature profiles from the scanning probe for low and high line-averaged density shots with ALT-II as the primary limiter. As the core density increases, the edge density rises and the electron temperature drops. The density e-folding length is also observed to decrease as the core increases, while the temperature profile flattens.
12. Effect of 1.8MW ICRH power coupled to the plasma on the line averaged density, probe currents into the scoops and pumping rate at blade #2. The ion drift side scoop current increases due to a decrease in the global particle confinement in the machine with auxiliary heating. The electron drift side current is decreased due to modification of the scrape-off by the ICRH. The pumping rate of the blade shows a two-fold increase with ICRH heating at this power.
13. Scrape-off layer density and electron temperature profiles from the scanning probe during 1.33MW of ICRH power coupled to the plasma. The auxiliary heating increases the edge density and temperature, and decreases the e-folding lengths close to the tangency point. The production of density and electron temperature bumps deep in the profiles may be related to metal impurity production observed during ICRH heating.



TEXTOR ALT-II

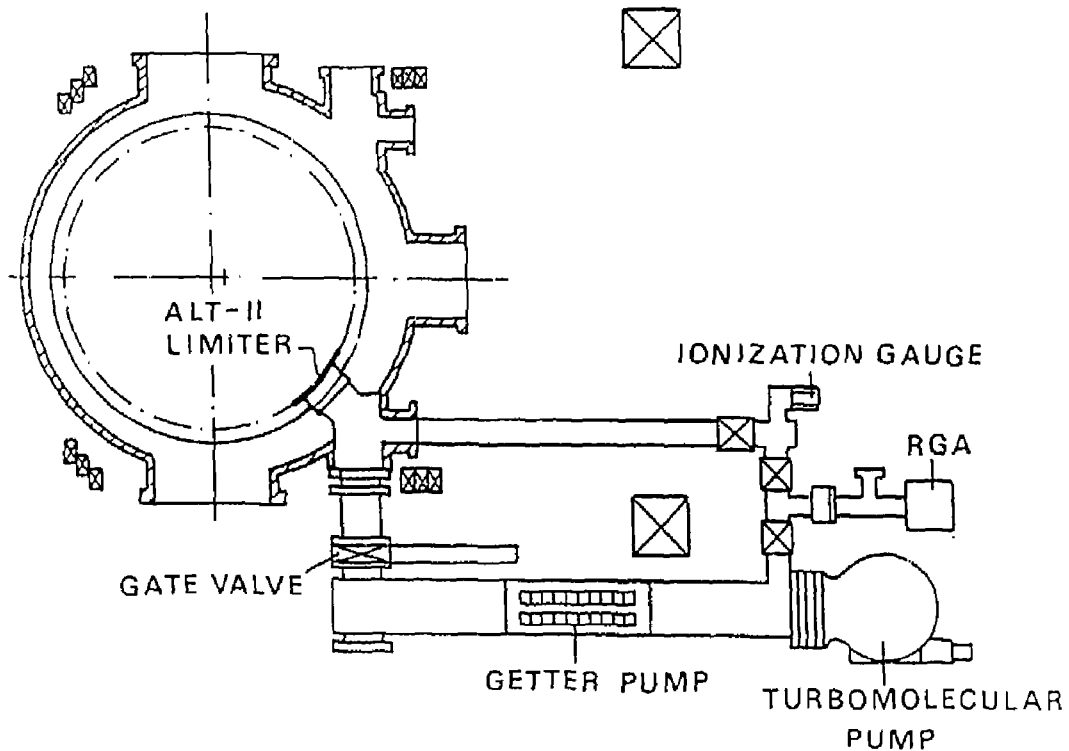


Figure 2

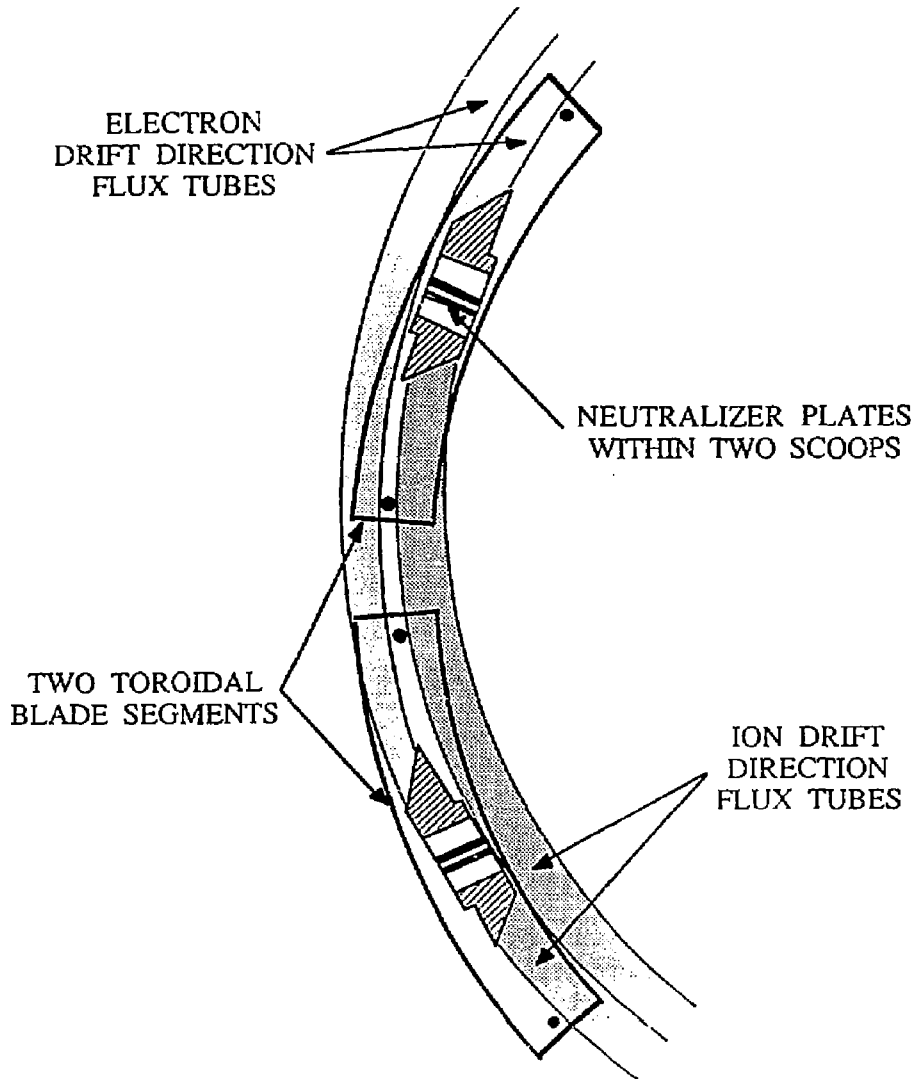


Figure 3

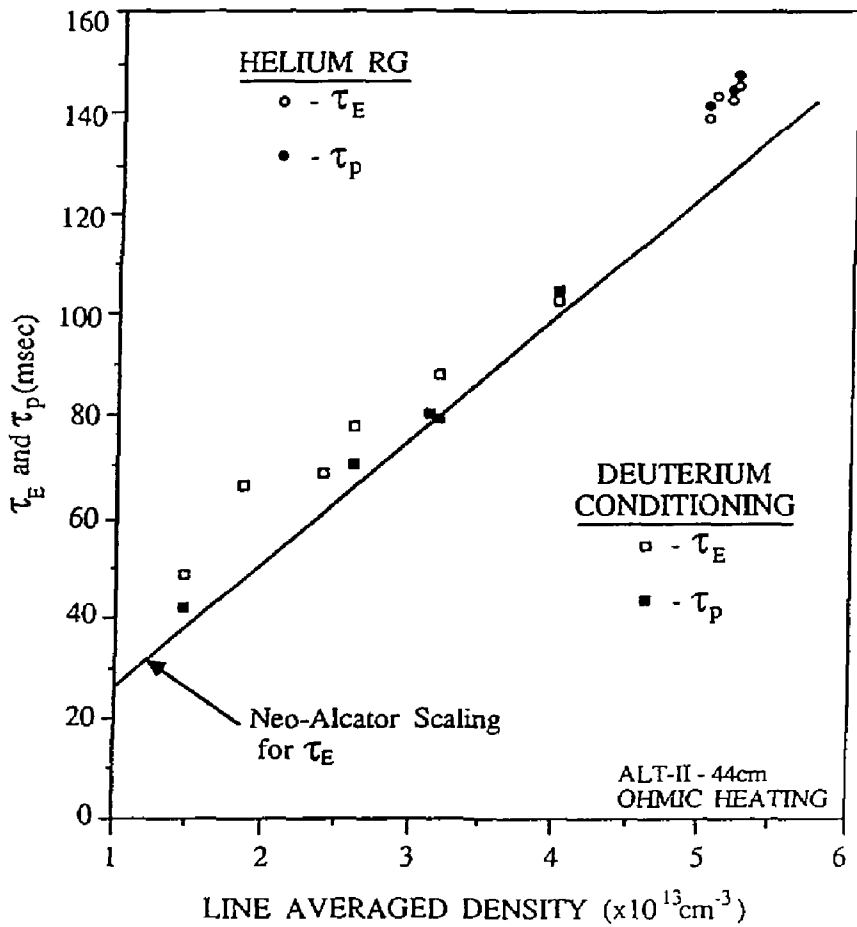


Figure 4

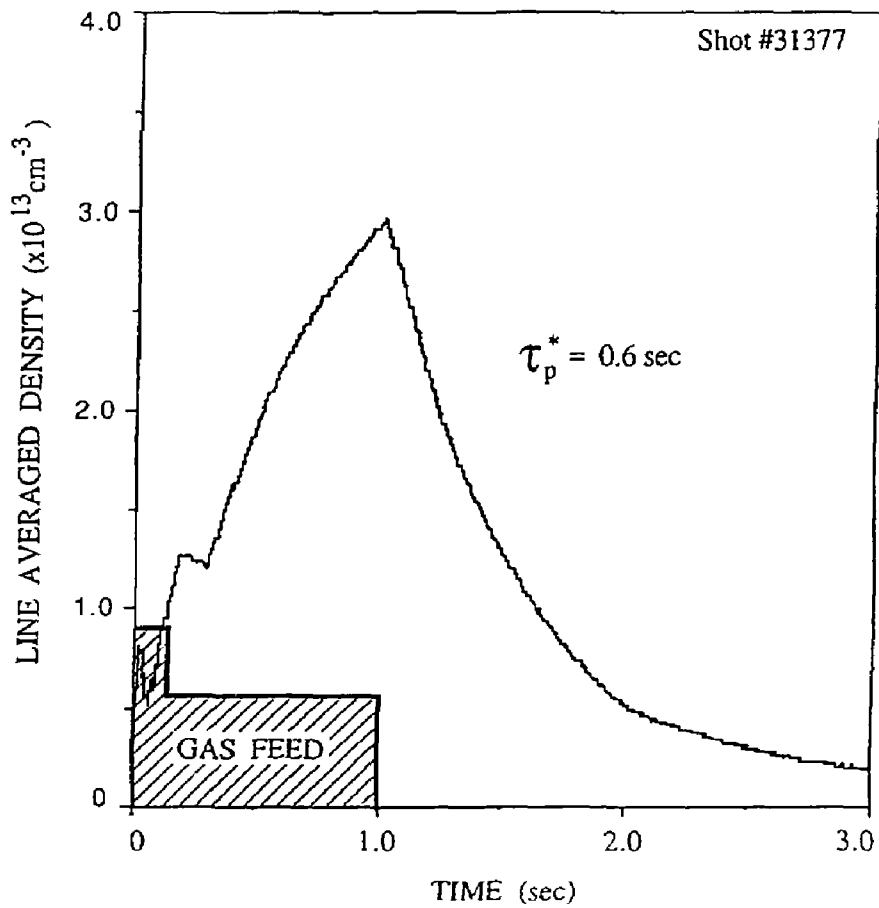


Figure 5

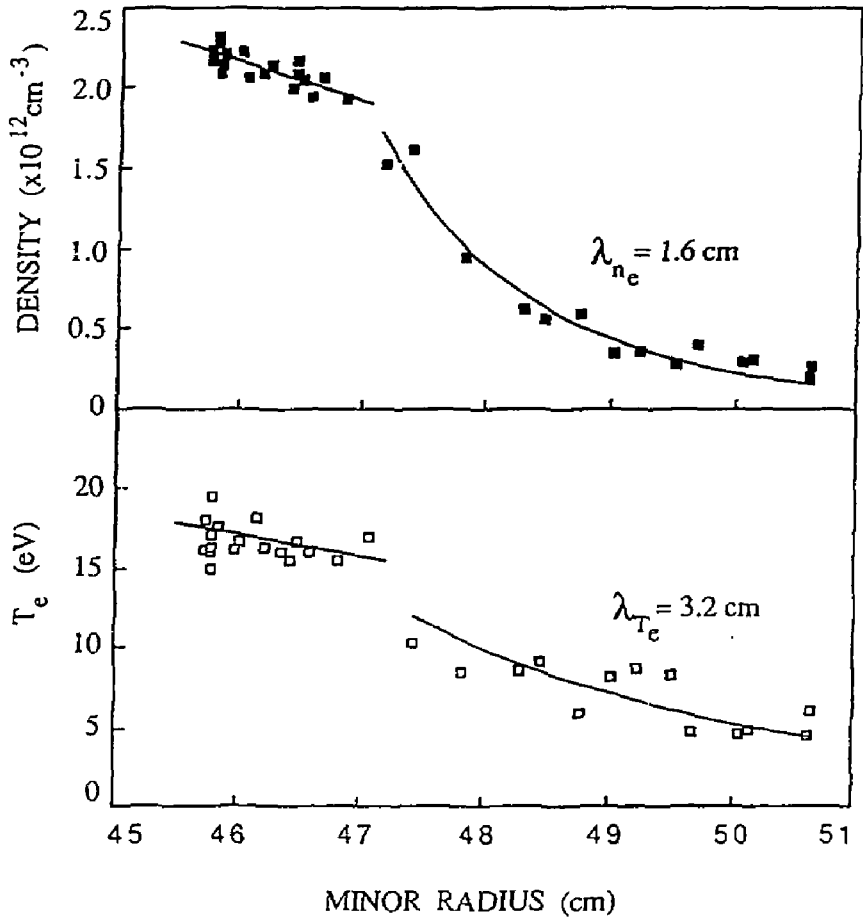
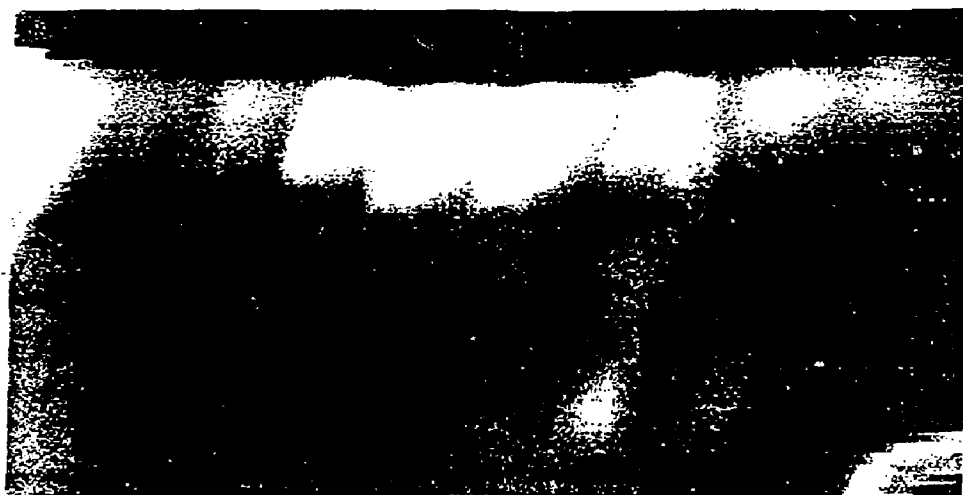
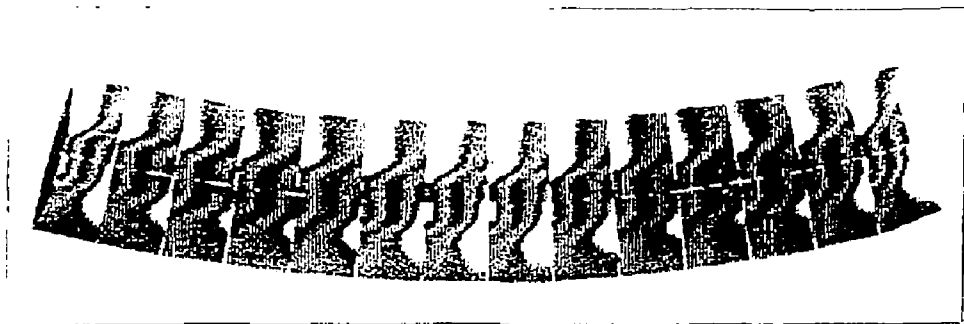


Figure 6



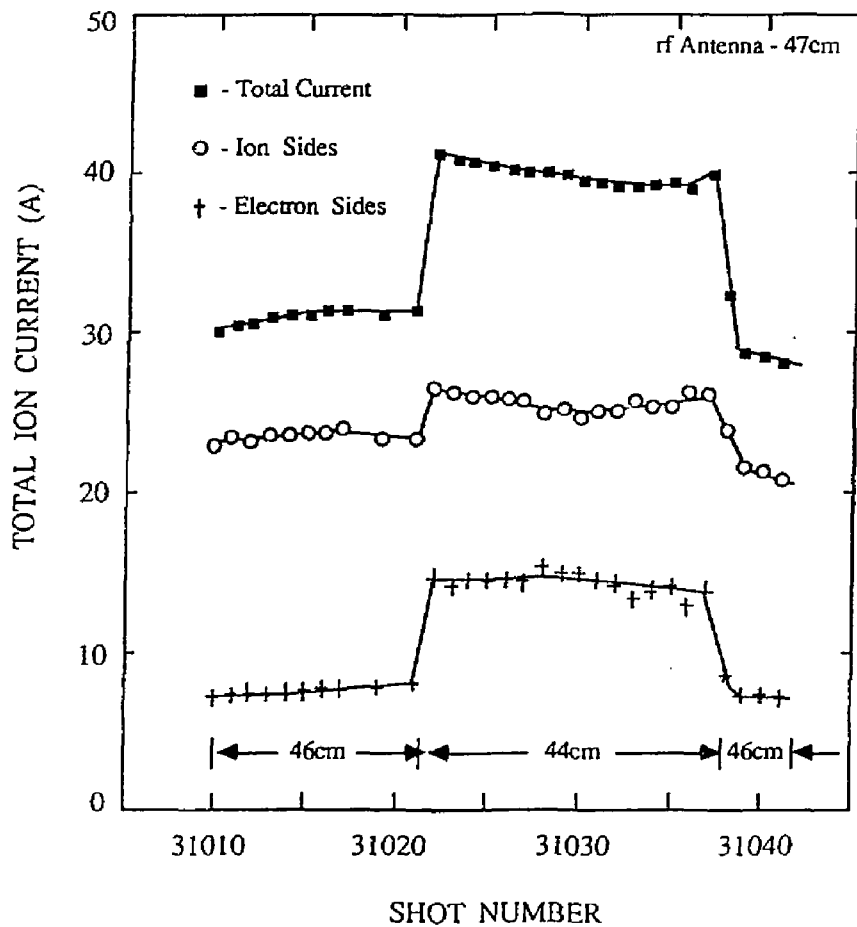


Figure 8

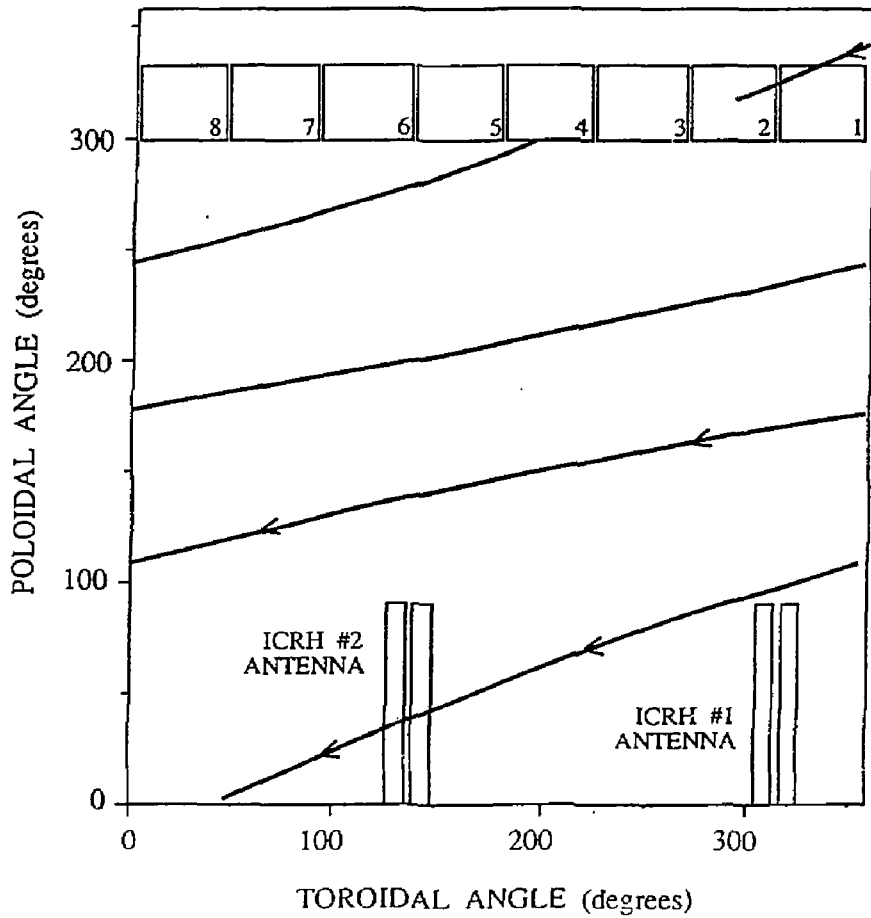


Figure 9

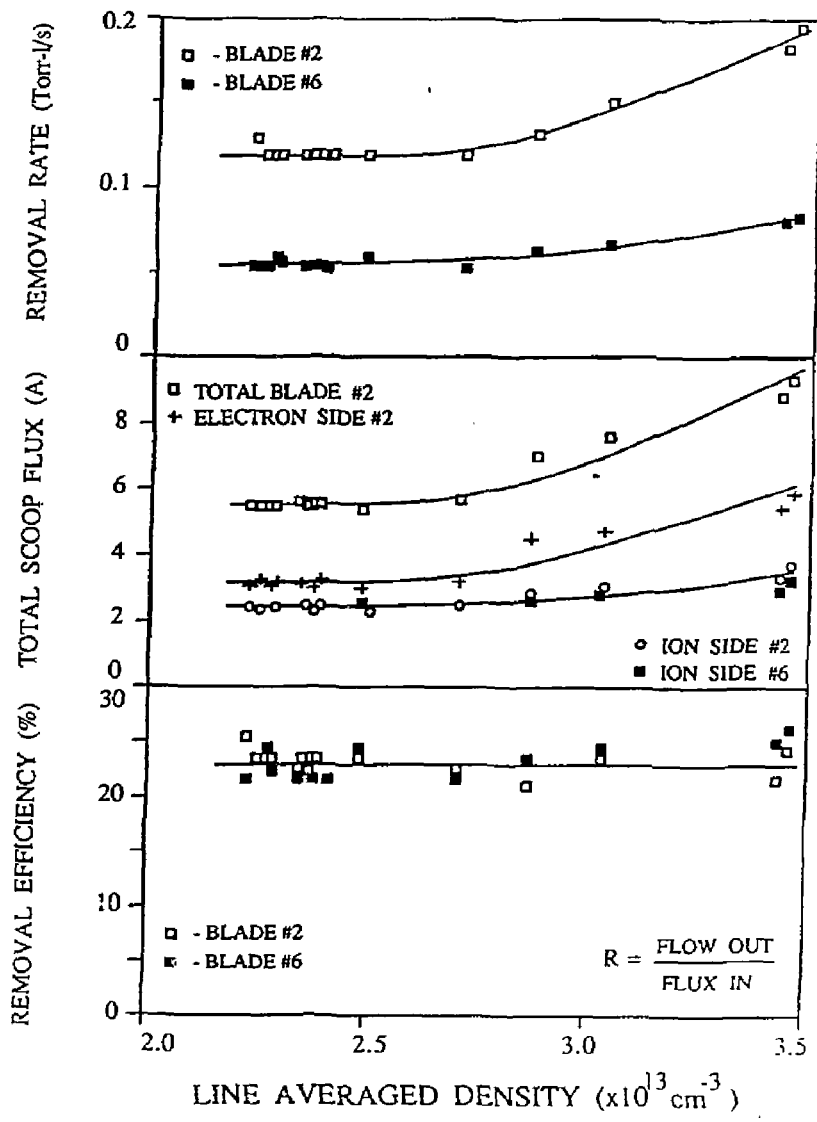


Figure 10

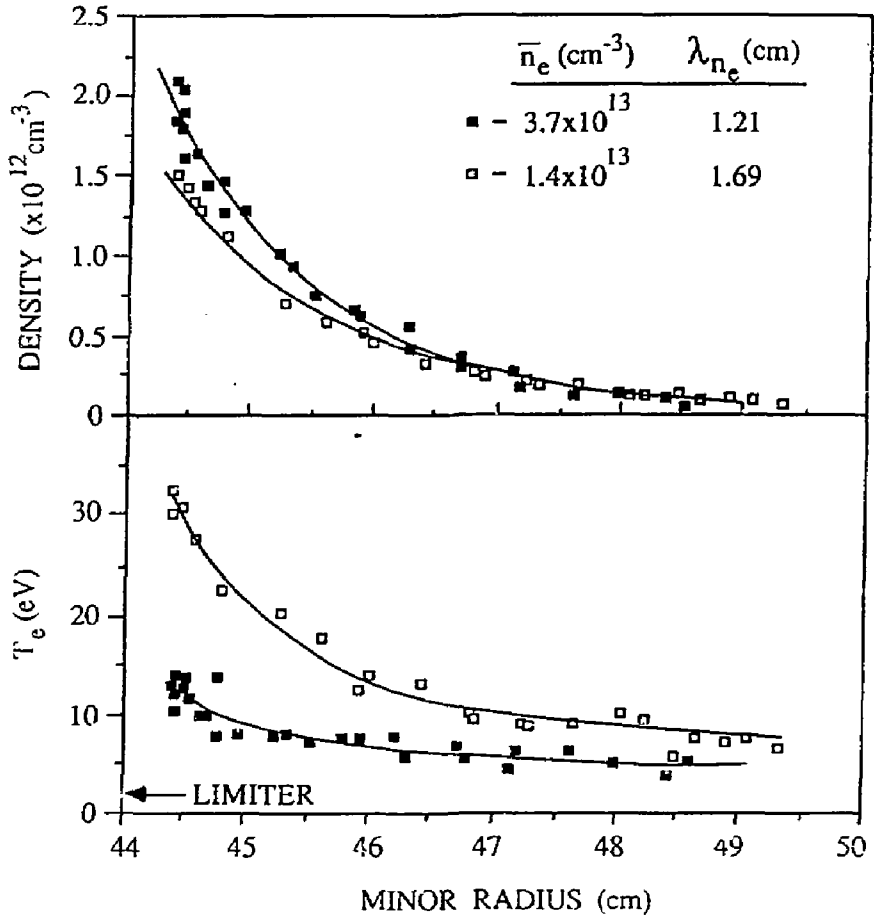


Figure 11

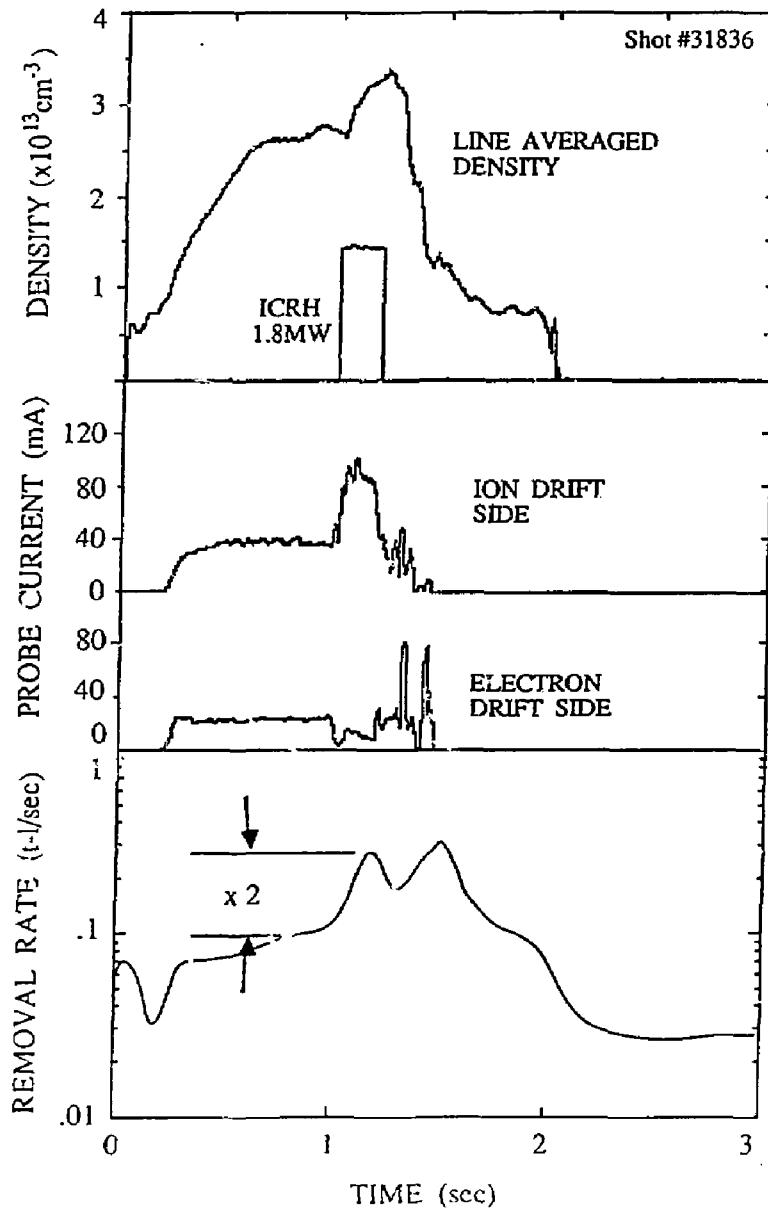


Figure 12

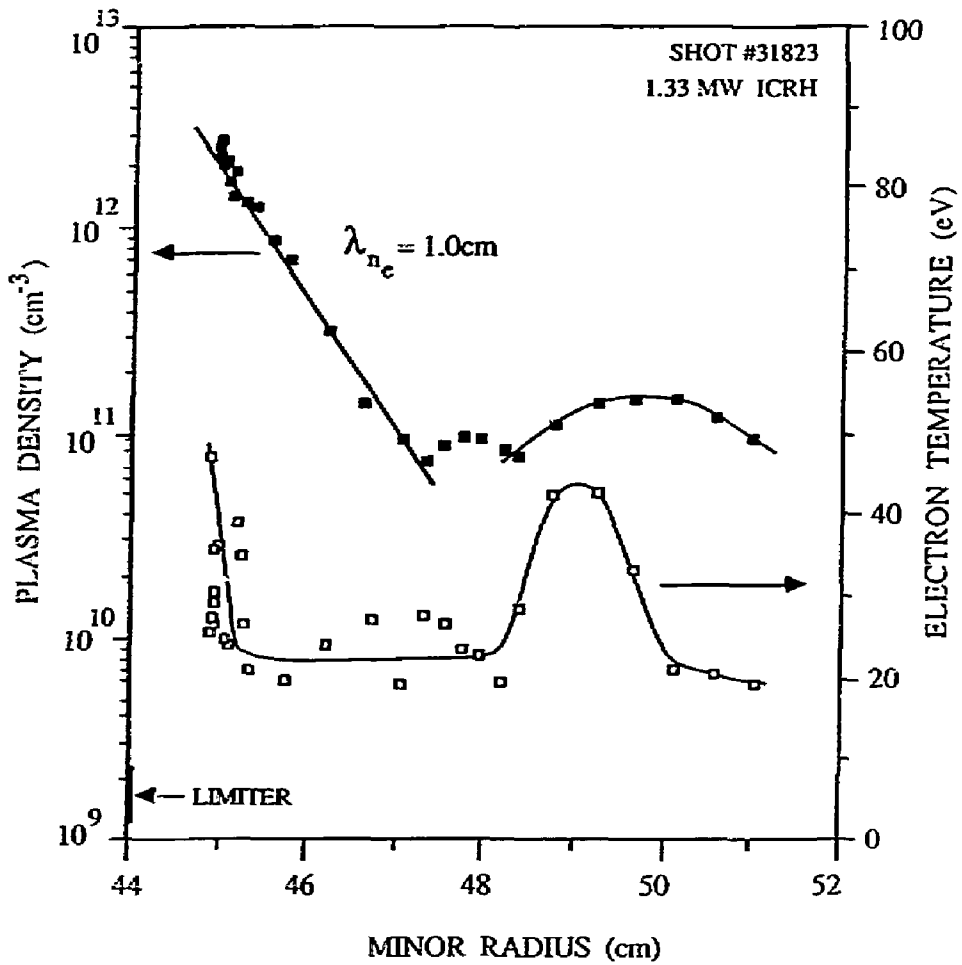


Figure 13

Abstracts of Recent Overview Papers

1. Y. Hirooka, W.K. Leung, R.W. Conn, D.M. Goebel, B. LaBombard, R. Nygren, *Hydrogen Pumping and Release by Graphite under High Flux Plasma Bombardment* (available as UCLA PPG 1123 January 1988, accepted for publication in J. Vac. Sci. & Tech. - A)
2. W.K. Leung, Y. Hirooka, R.W. Conn, D.M. Goebel, B. LaBombard, R. Nygren, *An In-situ Spectroscopic Erosion Yield Measurement with Applications to Sputtering and Surface Morphology Alterations* (available as UCLA-PPG 1163 July 1988, accepted for publication in J. Vac. Sci. & Tech. - A.)
3. D.M. Goebel, R.W. Conn, W.J. Corbett, K.H. Dippel, K.H. Finken, W.B. Gauster, A. Hardtke, J.A. Koski, W. Kohlhaas, R.T. McGrath, M.E. Malinowski, A. Miyahara, R. Moyer, A. Sagara, J.G. Watkins, G. Wolf, the TEXTOR Team, and the CRH Team, *ALT-II Toroidal Belt Pump Limiter Performance in TEXTOR*
4. W.J. Corbett, D.M. Goebel, R.W. Conn, R.T. McGrath, K.H. Dippel, K.H. Finken, *Boundary Asymmetries and Plasma Flow to the ALT-II Toroidal Belt Pump Limiter*

Boundary Asymmetries and Plasma Flow to the ALT-II Toroidal Belt Pump Limiter

W. J. Corbett¹, D. M. Goebel¹, R.W. Conn¹, R.T. McGrath²,
K.H. Dippel³, K.H. Finken³

¹ Institute of Plasma and Fusion Research, and Department of Mechanical, Aerospace and Nuclear Engineering, University of California, Los Angeles, CA 90024, U.S.A.

² Sandia National Laboratories, Albuquerque, NM 87185, U.S.A.

³ Institut für Plasmaphysik, Kernforschungsanlage Jülich, Association EURATOM-KFA D-5170 Jülich, Fed. Rep. Germany

Keywords: tokamak, toroidal pump limiter, scrape-off profiles, asymmetries

ABSTRACT

The ALT-II toroidal belt pump limiter is constructed with 8 radially adjustable limiter blade segments located 45° below the outboard horizontal midplane of TEXTOR. An array of Langmuir probes installed in the plasma scoops measures the total ion current to each neutralizer plate, including asymmetries in flow incident from above and below the belt. Recent measurements indicate that 10-50% more current is collected by neutralizers with flux tubes connecting to the electron drift side, on the outboard side of ALT-II. The source of the particle collection asymmetry is deduced from profile measurements in the scrape-off layer (SOL). On the outboard midplane, a scanning double probe measures $\lambda_n=1.4\text{cm}$, while profiles obtained with a Li-beam diagnostic located at the bottom of TEXTOR show $\lambda_n=0.9\text{cm}$. The primary source of the asymmetric particle collection at the neutralizers is therefore the difference in e-folding lengths between the electron and ion drift sides. In this paper, we report on measurements in the SOL behind ALT-II to emphasize the role of asymmetric decay lengths on particle collection by the ALT-II toroidal belt pump limiter.

Hydrogen Pumping and Release by Graphite under High Flux Plasma Bombardment

Y.Hirooka, W.K.Leung, R.W.Conn, D.M.Goebel, B.Labombard, R.Nygren

Institute of Plasma and Fusion Research
Department of Mechanical, Aerospace and Nuclear Engineering
University of California, Los Angeles
Los Angeles, California 90024

K.L.Wilson

Physical Research Division
Sandia National Laboratories
Livermore, California 94550

ABSTRACT

Inert gas (helium or argon) plasma bombardment has been found to increase the surface gas adsorptivity of isotropic graphite (POCO-graphite), which can then getter residual gases in a high vacuum system. The inert gas plasma bombardment was carried out at a flux $\approx 1 \times 10^{18}$ ions $s^{-1} cm^{-2}$ to a fluence of the order of 10^{21} ions/cm² and at temperatures around 800 °C. The plasma bombarding energy was varied between 100 and 200 eV. The gettering speed of the activated graphite surface is estimated to be as large as 25 liters $s^{-1} cm^{-2}$ at total pressures between 10^{-6} and 10^{-7} torr. The gettering capacity estimated is 0.025 torr-liter/cm² at room temperature. The gettering capability of graphite can be easily recovered by repeating inert gas plasma bombardment. The activated graphite surface exhibits a smooth, sponge-like morphology with significantly increased pore openings, which correlates with the observed increase in the surface gas adsorptivity.

The activated graphite surface has been observed to pump hydrogen plasma particles as well. From calibrated H-alpha measurements, the dynamic hydrogen retention capacity is evaluated to be as large as 2×10^{18} H/cm² at temperatures below 100 °C and at a plasma bombarding energy of 300 eV. The graphite temperature was varied between 15 and 480 °C. Due to the plasma particle pumping capability, hydrogen recycling from the activated graphite surface is significantly reduced, relative to that from a pre-saturated

surface. A pre-saturated surface was also observed to reproducibly pump a hydrogen plasma to a concentration of 9.5×10^{17} H/cm². The hydrogen retention capacity of graphite is found to decrease with increasing temperature. At temperatures between 450 and 480 °C, the hydrogen retention estimated for the activated surface and pre-saturated surface is 7.9×10^{17} H/cm² and 2.7×10^{17} H/cm², respectively. A transient pumping mechanism associated with the sponge-like surface morphology is conjectured to explain the large hydrogen retention capacity. Hydrogen release behavior under helium and argon plasma bombardment was also investigated, and the result indicated the possibility of some in-pore retrapping effect. The effective plasma impact desorption cross sections are evaluated in the plasma bombarding energy range from 15 to 300 eV. A significant fraction (70-80%) of pre-implanted hydrogen was observed to release under inert gas plasma bombardment to a fluence of 6×10^{19} ions/cm². The graphite surface, once saturated, can be reactivated via plasma-impact hydrogen desorption, regardless of the helium and argon bombarding energy examined here.

An In-situ Spectroscopic Erosion Yield Measurement with Applications to Sputtering and Surface Morphology Alterations

W. K. Leung, Y. Hirooka, R. W. Conn, D. M. Goebel, B. Labombard, R Nygren
Mechanical, Aerospace and Nuclear Engineering Department and Institute of Plasma and Fusion
Research, University of California, Los Angeles, USA

Abstract

An in-situ spectroscopic erosion yield measurement is developed and used to monitor material surface erosion during bombardment by a plasma. The experiments are performed in a plasma that has the characteristics of a fusion tokamak boundary plasma but the technique is applicable to many processes where plasma erosion is important. Erosion yield of materials bombarded in a high flux (up to 10^{18} ion/cm²/s) plasma environment has been previously studied using weight loss measurements. In the present study, the sputtered flux from a material is monitored by the line emission intensities of atoms eroded from the surface. The line intensities can be used to infer erosion yields after proper calibration. The method agrees well with results from weight loss measurements. Earlier work established that the material surface structure can substantially influence the erosion yield. When a change of surface morphology (e.g. cone formation) occurs, weight loss methods cannot be used to determine the erosion yield. However, the in-situ erosion measurement is suitable and is used to investigate the relation between the on-set of morphology changes and alternations in erosion yield during plasma bombardment. Experiments are reported for copper, as an example of a pure material, and stainless steel, as an example of an alloy system. The formation of surface cones is observed only when both the sample temperature is above a critical value and surface impurities exist. If the source of impurities is removed, or the sample temperature is lowered below the critical value, a surface rough with cones will be returned to a smooth state.

JVST Accepted for publication

ALT-II Toroidal Belt Pump Limiter Performance in TEXTOR

D.M. Goebel¹, R.W. Conn¹, W.J. Corbett¹, K.H. Dippel², K.H. Finken²,
W.B. Gauster³, A. Hardtke², J.A. Koski³, W. Kohlhaas², R.T. McGrath³,
M.E. Malinowski⁴, A. Miyahara⁵, R. Moyer¹, A. Sagara⁵, J.G. Watkins³,
G. Wolf², the TEXTOR Team², and the ICRH Team⁶

¹ Institute of Plasma and Fusion Research, and Department of Mechanical, Aerospace and Nuclear Engineering, University of California, Los Angeles, CA 90024, U.S.A.

² Institut für Plasmaphysik, Kernforschungsanlage Jülich, Association EURATOM-KFA D-5170 Jülich, Fed. Rep. Germany

³ Sandia National Laboratories, Albuquerque, NM 87185, U.S.A.

⁴ Sandia National Laboratories, Livermore, CA 94550, U.S.A.

⁵ Institute of Plasma Physics, Nagoya University, Nagoya Japan

⁶ Ecole Militaire/Koninklijke Militaire School, Association EURATOM-Belgian State B-1040 Brussels, Belgium

ABSTRACT

The Advanced Limiter Test (ALT-II) is a toroidal belt pump limiter in the TEXTOR tokamak. ALT-II is composed of 8 blade segments which form an axisymmetric toroidal belt of 3.4m² exposed surface area, located on the outside of the torus at 45° below the horizontal midplane. Ohmic plasma operation with ALT-II as the main limiter is characterized by a line-averaged density range of 5x10¹² to 5.5x10¹³ cm⁻³ at B_T = 2T and I_p=340kA, Z_{eff} = 1.1 to 2 and typically 40 to 95% of the power radiated depending on the plasma density. ICRH heating of the plasma with up to 2.6MW of incident power has been achieved, which modifies the scrape-off layer (SOL) and the pump limiter performance. The recycling coefficient in TEXTOR is normally close to one, but helium RG conditioning and baking of the limiter at 400°C is found to lower the recycling coefficient to 0.8 for the order of 10 shots. Measurements by arrays of probes in the SOL and thermocouples in the limiter tiles indicate the flow to the limiter is toroidally symmetric (taking field ripple into account) and poloidally asymmetric. Poloidal asymmetries result in different power and particle fluxes to the ion and electron drift sides of the limiter. The density and power scrape-off lengths are on the order of 1-2 cm and significantly longer on the outside of the torus (electron drift side). In spite of the flow asymmetry favoring the ion drift side near the tangency point, the longer e-folding lengths on the electron side in the SOL result in equal or

higher particle collection by the electron side. The probe arrays indicate that during ohmic heating a total of 15 to 20% of the core efflux is incident on the neutralizer plates located in scoops beneath the blades. More particles are collected during ICRH auxiliary heating due to changes in the e -folding lengths and shorter particle confinement times. Based on particle removal experiments with pumping on one blade, the total exhaust efficiency of the limiter if pumped at all eight blades is 5 to 10%.

PISCES PAPERS

Y. Hirooka, D.M. Goebel, R.W. Conn, G.A. Campbell, and W.K. Leung¹, K.L. Wilson, W. Bauer, R.A. Causey, and D.H. Morse², J. Bohdansky³ *Materials Surface Modification by Plasma Bombardment Under Simultaneous Erosion and Redeposition Conditions*, Nuclear Instruments and Methods in Physics Research, 1987.

W.K. Leung, Y. Hirooka, R.W. Conn, D.M. Goebel, B. LaBombard, R. Nygren¹ *An In-situ Spectroscopic Erosion Yield Measurement with Applications to Sputtering and Surface Morphology Alterations.*, Journal of Vacuum Science & Technology -A.

D.M. Goebel, Y. Hirooka and T.A. Sketchley¹ *Large-area Lanthanum Hexaboride Electron Emitter*, Rev. Sci. Instrum, Sept. 1985.

Y. Hirooka, D.M. Goebel, R.W. Conn, G.A. Campbell, and W.K. Leung¹, K.L. Wilson, W. Bauer, R.A. Causey, A.E. Pontau,² J. Bohdansky³ A.R. Krauss, D.M. Gruen and M.H. Mendelsohn⁴, *Erosion and Redeposition Experiments in the PISCES Facility*, Journal of Nuclear Materials, 1987.

Y. Hirooka, R.W. Conn, D.M. Goebel, B. LaBombard, R. Lehmer, W.K. Leung, R.E. Nygren and Y. Ra¹ *Deuterium Pumping and Erosion Behavior of Selected Graphite Materials Under High Flux Plasma Bombardment in PISCES*, 8th Annual Conference on Plasma Surface Interactions in Controlled Fusion Devices, Julich, May 1988.

B. LaBombard, R.W. Conn, Y. Hirooka, R. Lehmer, W.K. Leung, R.E. Nygren, Y. Ra, G. Tynan¹, *Presheath Profiles in Simulated Tokamak Edge Plasmas*, April 1988.

Y. Hirooka, W.K. Leung, R.W. Conn, D.M. Goebel, B. LaBombard, R. Nygren¹, and K.L. Wilson² *Hydrogen Pumping and Release by Graphite Under High Flux Plasma Bombardment*, J. Vac. Sci & Tech. - A, Jan. 1988.

G. Tynan, D.M. Goebel, R.W. Conn¹, *Measurement of Parallel Ion Energy Distribution Function in PISCES Plasma*, Aug. 1987.

Y. Hirooka, R.W. Conn, and D.M. Goebel¹, *Quasi-Thermodynamic Prediction of Hydrogen Reemission Behavior From Titanium Films*, Journal of Nuclear Materials, 1985.

Y. Hirooka, D.M. Goebel, R.W. Conn, W.K. Leung and G.A. Campbell¹, *Materials Erosion and Redeposition Studies at the PISCES Facility - Net Erosion Under Redeposition*, Journal of Nuclear Materials, 1986.

Y.Hirooka, R.W. Conn, D.M. Goebel, B. LaBombard, R. Lehmer, W.K. Leung, R.E. Nygren, Y. Ra¹. *Deuterium Pumping and Erosion Behavior of Selected Graphite Materials under High Flux Plasma Bombardment in PISCES*

D.M. Goebel and R.W. Conn *Observation of Enhanced Particle Removal Rates in Pump Limiter Simulation Experiments*, Journal of Nuclear Materials, 1984.

D.M. Goebel, G. Campbell, and R.W. Conn¹. *Plasma Surface Interaction Experimental Facility (PISCES) For Materials and Edge Physics Studies*, Journal of Nuclear Materials, 1984.

R.W. Conn¹. *Plasma-Materials Interactions (PMI) and High-Heat-Flux (HHF) Component Research and Development in the U.S. Fusion Program*, Oct. 1986.

- 1 Institute of Plasma and Fusion Research, UCLA
- 2 Sandia National Laboratories, Livermore, CA
- 3 Max-Planck-Institut fur Plasmaphysik, FRG
- 4 Argonne National Laboratory, Argonne, IL
- 5 Oak Ridge National Laboratory, Oak Ridge, TN
- 6 Canadian Fusion Fuels Technology Project
- 7 Plasma Physics Laboratory, Princeton University
- 8 Institute of Plasma Physics, Association Euratom-KFA Juelich, F.R.G.
- 9 Sandia, Albuquerque
- 10 Ecole Royale Militaire, Brussels, Belgium

ALT-I and ALT-II

D.M. Goebel, G.A. Campbell, R.W. Conn, W.K. Leung¹, K.H. Dippel, K.H. Finken⁸, G.J. Thomas, A.E. Ponteau², *Langmuir Probe Measurements in the TEXTOR Tokamak During ALT-I pump Limiter Experiments*, Plasma Physics and Controlled Fusion, 1987.

D.M. Goebel, R. W. Conn, W.J. Corbett¹, K.H. Dippel, K.H. Finken⁸, W.B. Gauster⁹, A. Hardtke⁸, J.A. Koski⁹, W. Kohlhaas⁸, R.T. McGrath⁹, M.E. Malinowski², A. Miyahara, R. Moyer, A. Sagara, J.G. Watkins, G. Wolf, the TEXTOR Team, and the ICRH Team, *ALT-II Toroidal Belt Pump Limiter Performance in TEXTOR*, Journal of Nuclear Materials, 1988

R.W. Conn, D.M. Goebel, S.P. Grotz, A.K. Prinja, R.F. Schafer¹, D.B. Heifetz⁷, W.B. Gauster, J.A. Koski⁹, *An Advanced Pump Limiter Experiment of Large Toroidal Extent - ALT II*

R.W. Conn, D.M. Goebel, W.K. Leung, G.A. Campbell, B. LaBombard, A.K. Prinja¹, W. L. Hsu, G.J. Thomas², K.H. Dippel, K.H. Finken, R. Reiter, et al⁸, T. Delvigne, P. Descamps, F. Durodie, et al.¹⁰, *ALT-I Pump Limiter Behaviour and Edge Plasma Flows During Biasing and ICRF Heating in the TEXTOR Tokamak*

Advanced Limiter Test - II Design Study, (see 1, 2, 5, 6, 7, 8, 9, 10, below.)

D.M. Goebel, R.W. Conn, G.A. Campbell, W.K. Leung, K.H. Dippel, K.H. Finken, G.H. Wolf,¹ G.J. Thomas, A.E. Pontau, W. Hsu² *ALT-I Pump Limiter Experiments*, 1987

D.M. Goebel, G.A. Campbell, R.W. Conn, W.K. Leung¹, K.H. Dippel, K.H. Finken⁸, G.J. Thomas, A.E. Ponteau², *Langmuir Probe Measurements in the TEXTOR Tokamak During ALT-I pump Limiter Experiments*, Plasma Physics and Controlled Fusion, 1987.

D.M. Goebel, R. W. Conn, W.J. Corbett¹, K.H. Dippel, K.H. Finken⁸, W.B. Gauster⁹, A. Hardtke⁸, J.A. Koski⁹, W. Kohlhaas⁸, R.T. McGrath⁹, M.E. Malinowski², A. Miyahara, R. Moyer, A. Sagara, J.G. Watkins, G. Wolf, the TEXTOR Team, and the ICRH Team, *ALT-II Toroidal Belt Pump Limiter Performance in TEXTOR*, Journal of Nuclear Materials, 1988

R.W. Conn, D.M. Goebel, S.P. Grotz, A.K. Prinja, R.F. Schafer¹, D.B. Heifetz⁷, W.B. Gauster, J.A. Koski⁹, *An Advanced Pump Limiter Experiment of Large Toroidal Extent - ALT II*

R.W. Conn, D.M. Goebel, W.K. Leung, G.A. Campbell, B. LaBombard, A.K. Prinja¹, W. L. Hsu, G.J. Thomas², K.H. Dippel, K.H. Finken, R. Reiter, et al⁸, T. Delvigne, P. Descamps, F. Durodie, et al.¹⁰, *ALT-I Pump Limiter Behaviour and Edge Plasma Flows During Biasing and ICRF Heating in the TEXTOR Tokamak*

- 1 Institute of Plasma and Fusion Research, UCLA
- 2 Sandia National Laboratories, Livermore, CA
- 3 Max-Planck-Institut für Plasmaphysik, FRG
- 4 Argonne National Laboratory, Argonne, IL
- 5 Oak Ridge National Laboratory, Oak Ridge, TN
- 6 Canadian Fusion Fuels Technology Project
- 7 Plasma Physics Laboratory, Princeton University
- 8 Institute of Plasma Physics, Association Euratom-KFA Juelich, F.R.G.
- 9 Sandia, Albuquerque
- 10 Ecole Royale Militaire, Brussels, Belgium